NASA Contractor Report 4092

Application of Satellite Data to Tropic/Subtropic Moisture Coupling

Aylmer H. Thompson and James P. McGuirk

CONTRACT NAS8-35182
SEPTEMBER 1987

NASA

NASA Contractor Report 4092

Application of Satellite Data to Tropic/Subtropic Moisture Coupling

Aylmer H. Thompson and James P. McGuirk
Texas A&M University
College Station, Texas

Prepared for
George C. Marshall Space Flight Center
under Contract NAS8-35182

National Aeronautics
and Space Administration

**Scientific and Technical
Information Office**

1987

TABLE OF CONTENTS

Application of Satellite Data to Tropic/Subtropic Moisture Coupling

James P. McGuirk and Aylmer H. Thompson

Final Report

1. INTRODUCTION AND SUMMARY.

a. Accomplishments:

The goal of the proposed research was to define a common tropical disturbance (which we have named a moisture burst), to describe its synoptic appearance, and to place it in the context of the tropical general circulation. Because moisture bursts usually develop over the tropical oceans, they are poorly observed by the operational data network. Therefore a second, but equally important, goal was to develop quantitative methodology, based on satellite derived data, to observe synoptic systems like moisture bursts. We focused on three case studies during the First GARP Global Experiment (FGGE) of 1979 so that we would also have some special conventional data available.

This introduction summarizes, the accomplishments of three years of research effort. More detail is provided in the enumeration of findings in sections 2-6, and more detail still in the documentation listed in section 7. Section 8 recommends future tasks. In accord with the two general goals, the major accomplishments fall in two broad classes: new findings of atmospheric phenomena; and documentation of data and technique development:

1. Phenomena. We have developed an objective definition of moisture bursts which describes a specific class of tropical atmospheric system. This definition has been utilized to prepare a climatology of moisture bursts over the tropical eastern North Pacific Ocean. The climatology is based on cloud imagery and upon 850 and 200 mb streamline

analysis. The typical behavior and temporal variation of moisture bursts have allowed them to be interpreted in terms of the tropical general circulation. Three dimensional fields of numerous variables were prepared for three case studies, two in January 1979 and one in May 1979. These case studies describe many structural elements of moisture bursts: the evolution of moisture distribution and its transport into midlatitudes; the development and intensification of the subtropic jet; the development of a mid-latitude or subtropical trough to the northwest of moisture bursts, and the concomitant intensification of frontal-like features; the interaction of larger and smaller scale waves with moisture bursts; and the distribution of horizontal winds. Of special interest was the lack of moisture burst activity associated with the 1982-83 El Niño. One major shortcoming was the lack of data to diagnose divergence and the vertical motion field. Because of this type of data sparsity, we have only begun to consider the causes of moisture bursts.

2. Data technique development. The scope of the project was set by identifying two short case study periods and investigating all available data over the tropical Pacific (rather than looking at long time periods and a restricted range of data types). Several problems were identified in the official FGGE archive at the World Data Center in Asheville. The most serious were associated with the archiving of cloud drift winds and TIROS radiance soundings, and with the moisture analysis.

The quantitative satellite channel radiance data were found to be at least as useful as any other data type. Statistical analysis revealed quality synoptic scale signal. EOF analysis indicated that the two most reliable signals, averaged over the whole Pacific domain, were tropospheric averaged temperature and moisture signals. These two numbers

distribution of higher order EOFs, and relations between channel data and conventional data explained over 80% of the total variability of satellite channel data. Closer inspection of individual channel horizontal structure functions, the distribution of higher order EOFs, and relations between channel data and conventional data provided convincing evidence that nearly every channel contains useful information in synoptically active regions. In fact, the satellite moisture channel data generally verify the less certain ECMWF moisture and dynamic analyses. Decomposition of channel data into eigenvectors was a useful synoptic technique, and the statistically derived eigenvectors could usually be interpreted physically. A regression technique was developed to convert TIROS observations in cloudy regions and NOAA 5 observations to full "bogus" TIROS observations; large areas devoid of complete satellite data could then be filled in. The satellite channel data, both in individual mappings and in EOF form, were used successfully to assist in the diagnosis of moisture bursts.

b. Fulfillment of proposed task statement:

In our proposal, two separate work statements were enumerated: The first was a list of four scientific objectives pertaining to moisture bursts. They were stated as:

1. Complete a diagnostic study of moisture bursts.
2. Develop a theoretical model of moisture bursts, with emphasis on the cause of moisture bursts.
3. Use theoretical studies to estimate the role of moisture bursts in the tropical general circulation.
4. Relate the moisture burst to the STJ and to downstream effects.

We have satisfied objectives (1) and (3), although better analysis techniques will result in commensurate better understanding. (2) was

overly ambitious and probably exceeds our capability based on currently available data. This conclusion is one of the hard truths learned in this data analysis. We have made progress on (4), but felt that more intense study of the moisture burst origin region would be more fruitful than downstream studies, which could be approached with conventional data; we have outlined a study of downstream effects in a new proposal.

A more appropriate statement of accomplishments is the following procedure/task statement, taken directly from the proposal submitted in May 1981:

Procedure/Task Statement:

1. Assemble data--IIb and IIIb (Accomplished).
2. Prepare maps of data availability (Accomplished).
3. * Merge the data for case studies (Accomplished).
4. * Relate the satellite information to conventional data (Accomplished).
5. Diagnose the moisture burst (Accomplished).
6. Begin preparation of a theoretical model of a moisture burst (Accomplished).
7. Test the model (Premature).
8. Prepare a quantitative description of a moisture burst (Partially Accomplished).
9. Establish a chronology of moisture bursts (Accomplished).

*Tasks (3) and (4) involved far more effort than was initially anticipated. A number of problems discovered in the data have not been solved to date. These problems are not unique to this research. Six and one half years after the FGGE observational year, the ECMWF has still not completed the final three dimensional analysis (III c) envisioned in the early

planning documents of FGGE.

On the other hand, the time spent on these tasks was worthwhile. We have identified a number of useful techniques of satellite data analysis which will be developed under new contract. We have also defined more precisely the synoptic information content of quantitative satellite data over the tropical oceans.

Tasks (6) and (8) have not been accomplished in a way to make (7) feasible. Although we have deduced much quantitative information on burst structure, the limits of data analysis in this region of the atmosphere precludes definitive conclusions. Further technique development will result in further quantitative understanding of moisture bursts.

In the remainder of this report, we elaborate on these accomplishments. We conclude with some remarks on future work.

2. DATA DEVELOPMENT.

Moisture bursts must be studied in the data-sparse regions where they occur. Our philosophy was to investigate all possible forms of data to minimize, as far as possible, the problems of insufficient data. This philosophy required us to restrict the number of days chosen for the study. In retrospect, the work would have been reduced tremendously if we had restricted, rather, the kinds of data we utilized, and examined these data over much larger time intervals. Each data type had its own format, its own distribution and error characteristics, its own information content and its own "best" analysis technique. Merging disparate data types is a task still in its infancy. The current prescribed procedure is optimal interpolation, a procedure which may not be optimal at all for synoptic diagnosis in data-sparse tropical regions.

a. Data:

Satellite data, conventional data and analyses were used. Imagery was obtained from a number of NOAA sources and from Marshall Space Flight Center (MSFC). Channel radiance data were obtained from the FGGE archive at World Data Center A (Asheville, NC). ECMWF III(b) gridded fields and II(b) observations were obtained from the archives of the National Center for Atmospheric Research (NCAR). Finally, hard copy analyses were obtained from publications of ECMWF and NOAA's Geophysical Fluid Dynamics Laboratory (GFDL).

The following tabulation summarizes the data sets we utilized:

1. Satellite Imagery. Daily GOES full disk visible imagery; 6-hourly GOES full disk infrared imagery; 30-minute GOES full disk infrared imagery in the form of time-lapse motion pictures; color enhanced Pacific sector GOES infrared imagery; full disk water vapor imagery from GOES (VAS)

for a pilot study of 1982 moisture bursts.

2. Published Analyses. Daily ECMWF and GFDL 200 and 850 mb streamline and isotach analyses for tropical and subtropical regions; daily data distribution maps from ECMWF; moisture analyses, incorporating TIROS moisture data for a few days in January 1979 (from GLA).

3. Gridded III(b) data. u, v, h, q, p_0 and T available on a 1.875° lat/lon grid (these fields were consolidated onto a 3.75° lat/lon grid, to minimize computations and to agree better with data resolution); winds were also recomputed into irrotational and nondivergent components.

4. II(b) Satellite observations. Brightness temperatures for 26 TIROS N radiance channels, including HIRS, MSU and SSU channels (these were available twice daily, with HIRS channels missing in overcast regions; horizontal spacing for soundings is approximately 250 km); retrieved layer-average temperature and moisture profiles (SATEMS) for each of these soundings; a smaller set of channel brightness temperatures from the VTPR instrument on NOAA 5.

5. II(b) Conventional observations. Single station/level observations from islands, ships and North America; constant level balloons; and aircraft; temperature, moisture and wind profiles from radiosonde, dropsonde, pibal and special FGGE scientific shipsondes.

In spite of this considerable collection of data, observations within the overcast cloud of moisture bursts were still infrequent. Only sporadic soundings were favorably located. VTPR and HIRS infrared observations were not recorded. Low level cloud drift winds could not be obtained, and only a few appropriate upper level clouds could be tracked. The region is not crossed by a common shipping route. Islands do not exist where, meteorologically, they are needed most.

b. Discrepancies and data irregularities.

The following is a list of irregularities in acquired data, unexpected missing data, and other anomalies in the various data archives. The purpose is to document those previously unknown problems we encountered in the generally high-quality FGGE archive, and also to point out possible limitations in the interpretation of our subsequent data analysis.

1. The satellite sounding data obtained from NCAR formed a highly abridged set. It contained only about 10% of the available soundings and was not appropriate for synoptic analysis. To date, neither NCAR personnel nor we ourselves have discovered who prepared this set and why.

2. The complete TIROS N data set obtained from World Data Center A was, in a sense, too complete. It contained over twice as many soundings as the ECMWF claimed were available. The problem was twofold. First, a complete set of retrievals and brightness temperatures was prepared erroneously. When a new set was prepared properly, these soundings were added to the existing set and erroneous soundings were not deleted. Incomplete documentation remains a problem. The second source of excess soundings was the U.S. Special Effort, which computed a high-density set of satellite retrievals for additional studies. Documentation constraints leave the source of these data unclear. Care must be taken to separate good from bad when using this set.

3. A surprising number of missed TIROS N passes existed through our study region during the first Special Observing Period. Had we known this beforehand, we might have selected different case studies. On the other hand, we selected the most interesting appearing moisture bursts during SOP 1. Several swathes of satellite data are missing during the

crucial initiation stage of the first, and strongest, moisture burst.

4. Two problems were belatedly discovered pertaining to the individual channel radiance data:

i) Brightness temperatures for channel 10, the boundary layer moisture channel, were computed incorrectly in the preprocessing. Although this defect can be repaired, it requires reprocessing at NOAA from the very first step and has not been attempted.

ii) After subjecting the channel data to EOF analysis, it became obvious that at least one of the eigenvectors represented a signal related to limb-darkening. At large scan angles left-looking and right-looking measurements are oppositely biased. This bias can be removed from our data, but we have not yet done so.

5. Several files of cloud drift winds, in the FGGE archive, are incorrectly identified as GOES Indian Ocean data, a geometric impossibility. These data are of lower quality than the GOES cloud drift winds and their source has yet to be identified.

6. A serious problem exists with the ECMWF moisture analysis. An erroneous parameter used in the analysis cycle caused the systematic exclusion of all tropical moisture soundings. Secondly, a decision was made to exclude satellite moisture channel information in the III(b) analysis; given the problem with channel 10, this decision was fortunate. However, the result of these two developments was that no upper air moisture data were available for the III(b) moisture analysis. It was therefore based on only weakly varying, and sporadic, surface data, and on model integrations.

c. Verification:

A number of data intercomparisons were conducted to both verify and

merge data of different type and quality. This task was necessary, in general, to qualify the use of satellite channel data for tropical synoptic diagnostics. The key results are summarized.

1. SATEMS (retrieved layer-averaged temperature profiles). These soundings are computed routinely for initialization of numerical forecast models. It was not clear a priori that they could be used for quantitative synoptic analysis. Comparisons of vertically-oriented cross sections of radiosonde and SATEM data along the west coast of North America were discouraging. Over a period of several days of strong frontogenesis associated with a moisture burst, almost no synoptic signal could be detected in the SATEM sections. Based on this result, no further use was made of the SATEM profiles in our research; rather, we opted for analysis and interpretation of individual channel brightness temperatures.

2. Winds. A number of wind comparisons were made with various data sets:

i) On synoptic scales, spatially coherent differences exist between III(b) winds and cloud drift winds. It remains unclear whether these coherent differences are unutilized information or spatially correlated error.

ii) Subjective analysis of all wind observations resulted in streamline and isotach analysis quite different from ECMWF analyses, particularly in the upper troposphere and during the time of most rapid moisture burst development. Apparently, optimal interpolation does not make full use of available data in active, data-sparse regions; the reason, most likely, is that stronger emphasis is placed on minimizing potential error.

iii) Analysis of low level radiosonde winds, observed from ship,

strongly suggests only weak correspondence between surface and 850 mb winds. Wind shear is almost independent of wind direction. Therefore, extrapolation of cloud drift winds downward or ship winds upward, as done in optimal interpolation, will not carry a strongly reliable signal in synoptically active regions. This problem is particularly acute in the investigation of moisture bursts. Data availability along the axis of the case study moisture bursts is only about one observation per 3.75°lat/lon box per five days.

iv) Histograms of differences between co-located cloud drift winds and ECMWF analyzed winds indicate signal-to-noise ratios approaching 1 in moisture burst regions.

v) Systematic errors in the coded wind direction in all constant level balloon data resulted in their exclusion from our analysis.

3. Moisture.

Moisture, as certainly one of the most significant meteorological variables, but difficult to measure, analyze and interpret, received most of our analysis attention, especially given the lack of data input to the ECMWF moisture analysis.

i) Intercomparisons were made between III(b) moisture estimates, raob moisture measurements, and the satellite moisture channel observations for co-located data at the nominal level of the satellite weighting function maximum. Correlation between the three sets was poor. However, for moist soundings (relative humidity greater than 50%), correlation coefficients exceeded 0.7 for all sets tested. Near dry soundings (relative humidity less than 30%), both III(b) and satellite observations spanned the entire observed range.

ii) Maps were made of temporal standard deviation of moisture

channel data for the nine-day case study period. The same calculations were made using III(b) data. The patterns matched very closely, with maximum variability occurring along the moisture burst axis.

iii) Using these same data, correlation coefficients were computed between III(b) and gridded moisture channel data at each grid point. Although there were large regions where the correlation was statistically significant, 25% of the gridpoints possessed correlations of the wrong sign; that is, III(b) saying wet, and satellite dry, or vice versa. The only encouraging feature of the maps was that the regions of agreement were generally those along the moist, synoptically active moisture burst axis. [As an aside, these same calculations were carried out for III(b) temperature analyses and corresponding temperature sensing channels, and the results were much more satisfactory; satellites detect temperature variation better than they detect moisture variation.]

iv) Summarizing these results, we conclude that the ECMWF analysis yields surprisingly realistic moisture fields in synoptically active tropical systems--surprising in that no upper level moisture data went into the analysis. This realism implies that the dynamics of the ECMWF model are doing a credible job over the data-sparse eastern tropical Pacific.

3. SATELLITE STATISTICS.

The following sections summarize three analysis methodologies developed to utilize satellite channel radiance data: Empirical Orthogonal Functions (EOF), horizontal structure functions, and individual channel analysis. The approach consists of both technique development and interpretation.

a. Bogus channel data:

Before these techniques could be implemented, regions devoid of satellite data had to be eliminated, insofar as possible. These regions existed between adjacent satellite passes, in regions where passes were missed for one reason or another, and in overcast regions where only microwave and upper atmospheric infrared channels were available. Response surface regression with a full quadratic model was used to predict missing channels from available predictor channels. In the first two types of regions, VTPR channels from NOAA 5 were regressed onto TIROS N channels; in the third region, infrared channels were predicted from available TIROS N channels.

1. Some confidence existed that meaningful differences could be detected between clear and cloudy regions, because nearly all TIROS channels available in cloudy regions were found to possess mean brightness temperatures different than clear sky means, with a statistical confidence exceeding 99%. These differences are larger in equatorial regions than in subtropical regions.

2. Regressions from TIROS N are superior to those from NOAA 5 in most channels. The significant exceptions to this superiority are the better predictions of the moisture channels by the NOAA 5 VTPR channels. An explanation is unknown at this time; NOAA 5 has some moisture detection

capability in a channel at 18 micrometers, but if this channel is not responsible, this result must be spurious. The major reasons for the superiority of TIROS N information are the deteriorated condition of NOAA 5 and the existence of colocation errors in time and space with respect to TIROS locations.

3. TIROS N reconstructions were most successful in the thermal channels in the 4.4 micrometer band, where better than 90% explained variance was achieved. The worst channels were the water vapor channels, where only about 40% of the variance was explained. Explained variance in other channels was about 80-90%. The regression was robust and could be applied equally well to non-calibration periods.

4. NOAA 5 reconstructions were also successful in the 4.4 micrometer band and in the 90 and 700 mb microwave channels, as well; nearly 90% of the variance of these channels was explained. As previously mentioned, about 70% of the moisture channel variance was explained. The NOAA 5 regression was not robust. Behavior was superior within the calibration set, and rms errors were much larger when the regression equations were applied to independent data.

5. The bogusing procedure increased the available data significantly: TIROS N regressions in cloudy regions increased the available data by 25%. NOAA 5 regressions added yet another 35% increase.

6. Map comparisons at synoptic times and time series at specific latitudes showed marked improvement in data coverage and resulting signal, using the bogus data. Performance was best in regions where TIROS N passes were missing. One unresolved problem is the existence of "bull's eyes" introduced by bogus data. These are caused mostly by VTPR regressions. A smoothing procedure will be developed to remove these anomalies. Some

bull's eyes, however, are realistic. These are due to precipitation and cloud water effects in the microwave channels of soundings retrieved from cloudy regions. Care must be taken not to smooth these extrema.

b. Empirical orthogonal functions:

The highly correlated nature of the TIROS individual channels can be used to advantage through EOF decomposition; sets of individual channels can be collected into eigenvectors which more efficiently represent the data. These eigenvectors are interpreted physically. The amplitudes of each eigenvector can be mapped in the horizontal and can also be interpreted physically.

1. Eigenvectors 1 and 2.

i) Eigenvector 1 is, unambiguously, a tropospheric - average temperature signal. It explains nearly 65% of the total field variance of the TIROS data set. It varies insignificantly from time period to time period.

ii) Eigenvector 2 is, unambiguously, a tropospheric moisture signal. Associated with this signal is a weak boundary layer thermal signal, such that, when the atmosphere is moist, the boundary layer is warm. The variance explained varies between 12 and 18%. Occasionally, this eigenvector is not number two, depending on synoptic condition.

2. Higher order eigenvectors.

Eigenvectors 3 through 5 are unique, but their relative order varies from time period to time period. The principal channel contributors are the moisture channels, the microwave channels, and two window channels. One of the eigenvectors represents spurious scan angle bias, particularly in the tropopause level channels; it accounts for 3 to 5% of the variance. The other two channels are interpreted, alternatively, as either cloud and

precipitation effects in the presence of strong convection, or as corrections to eigenvector 2 (wet regions that occasionally have cold boundary layers, for example).

3. Principal Components (Spatial Patterns).

i) PC 1 accurately describes synoptic features such as fronts and cold troughs. It seems to be more accurate than individual channels and to describe more fine scale detail than is incorporated in the ECMWF analysis.

ii) PC 2 accurately delineates the moisture associated with the moisture bursts of the case studies. Time evolution can be followed easily. Moisture variability along the burst axis can be resolved. Moisture variation along the ITCZ is easily detected, as is the Pacific dry zone in the extreme eastern Pacific.

iii) At first examination, it can be concluded erroneously that only two significant degrees of freedom are contained in the entire 26 channel TIROS data set, based solely on variance explained. Inspection of the higher order (lower variance) principal components suggest that there are more physically-significant eigenfunctions and degrees of freedom. PC 3 through 5 compress most of their signal into the synoptically active regions and into land/sea contrast along the coast of North America. Variable lapse rate, precipitation cores, and high liquid water content can be identified along the moisture burst axis and within the ITCZ.

iv) Items (ii) and (iii) above suggest the possibility of constructing a "moisture burst function", a collection of several eigenvectors and typical amplitudes which reproduce the significant structure of moisture bursts.

v) The EOF analysis has been verified against individual

channel mappings and against cloud imagery and radiosonde time and space sections. Often, the principal components can distinguish subtle differences in moisture content and distribution. Although individual channel mappings are similar to PC mappings (they must be), there are significant differences near some of the relative extrema. Detailed examination should uncover additional structural detail within moisture bursts.

c. Channel data:

Most of the significant channel data results have been discussed already under separate headings. We emphasize that maps of individual channel brightness temperatures generally provide more detail than equivalent III(b) analyses, particularly in the moisture and microwave channels. Features which are not apparent in III(b), such as the split jet which appears in the May 1979 case study, appear readily in the upper level moisture channel. Regions of intense rising motion (convective cores) appear as isolated cold cores in the microwave window channel. Comparisons of Hovmöller-type diagrams for TIROS and III(b) moisture variables show significant differences in moisture distribution in the vicinity of moisture burst origin regions; there is more intense spatial variation in the channel data, and a definite wet bias to the east of the burst cloud axis compared to a slight III(b) wet bias to the west of the burst. This last item has repercussions regarding source of moisture for moisture bursts.

d. Structure functions:

For each TIROS N channel, the correlation coefficient was computed as a function of the separation distance between pairs of observations. The plot of this correlation as a function of separation distance gives a measure of the horizontal coherence measured by each channel, and is called

the horizontal structure function. These functions varied widely depending on absorber, geographic region and synoptic condition. Because of the differences in structure functions between the many channels, it is concluded that the TIROS observation set possesses a number of degrees of freedom, in spite of the high inter-channel correlation.

1. Variation by absorber.

i) The most significant difference between channels is explained by sensitivity to moisture. Across the whole domain, the water vapor channels had the smallest correlation, or integral length scale (the area under the structure function curve). Channels insensitive to water vapor – most microwave channels and infrared channels in the 14 micrometer band – had the largest integral length scale. Infrared channels in the 4.4 micrometer band, which are somewhat sensitive to water vapor, are intermediate.

ii) In subtropical regions, where water vapor is not a strong factor for upwelling radiation, the integral length scale or correlation was stratified by nominal elevation of the weighting function: The higher in the atmosphere a channel's weighting function peaked, the larger was the integral length scale. The physical implication is that atmospheric length scales in the subtropics are larger in the upper troposphere and decrease uniformly toward the surface.

iii) Microwave channels peaking at the surface and tropopause were anomalous. The surface channel, which is sensitive to varying ocean emissivity and to cloud and precipitation effects, had the smallest integral length scale of all channels in all conditions; its magnitude was sometimes less than 500 km. The integral length scale for the tropopause channel was small for an upper atmospheric channel; this anomalous behavior

is thought to be caused by scan angle bias, which plagued this channel.

iv) Excepting the microwave channel, window and near-surface channels generally had the largest integral length scales. Thus, if the scales of surface thermal anomalies are reflected in the near surface integral length scales, atmospheric synoptic scale events respond on different length scales than the surface forcing.

2. Variation by geographic region.

The correlation data were stratified by latitudinal band to separate equatorial and subtropical behaviors. This stratification had, as a necessary consequence, the effect of emphasizing east-west variations at the larger scales. In a 15° wide belt, meridional variations with scales larger than about 1000 km are not sensed.

i) Structure functions in the subtropical strip (15-30°N) followed trends established for the entire region fairly closely, except the integral length scales were smaller; the large correlation associated with the north-south temperature contrast was poorly sampled. The integral scale of the water vapor channel was smallest. Structure functions for most channels became negative between 1500 and 2000 km, indicating wave-type activity at about this same length scale.

ii) In the equatorial strip, 15°N-10°S, structure functions were markedly different. All thermal channels were much smaller, with integral length scales of about half their subtropical values. The largest integral length scale occurred in water vapor channels. They exceeded subtropical thermal length scales by about 50% and subtropical moisture scales by about 50% as well. Stratospheric integral scales are very small, suggesting substantial tropical tropospheric contributions. Finally, negative correlations are generally absent, indicating weaker equatorial wave

behavior.

3. Synoptic variations.

Structure functions were computed for two different days, each with very different synoptic behavior. Integral scales for the thermal and surface/window channels were about 20% smaller for the case of weaker synoptic activity. Larger differences existed for thermal channels sensitive to water vapor, even though the differences in the water vapor channels themselves were not nearly so great. It is clear that more synoptic variability comparisons need to be made.

4. DEFINITION AND CLIMATOLOGY.

Moisture bursts, which have been known to exist for at least 25 years, have only recently been evaluated quantitatively. This section summarizes moisture burst definition and the mean behavior of moisture bursts over the northeastern Pacific. Considerable development work preceded an objective definition of the synoptic scale event. This definition was utilized to develop a climatology of moisture burst occurrence, and to extend this occurrence record to the atypical El Niño/Southern Oscillation event of 1982-83. A subset of this climatology, based on infrared imagery, was utilized to develop a circulation climatology at upper and lower tropospheric levels.

a. Moisture burst definition

An objective definition was developed so that moisture bursts could be identified and quantified nearly uniquely from unenhanced infrared imagery.

1. Definition. A moisture burst is defined as a continuous band of upper- and mid-level clouds, at least 2000 km in length, which crosses 15°N. Bursts are defined to begin at the first evidence of poleward progression of a cloud mass out of the inter-tropical convergence, or the southward movement of a frontal cloud band south of 15°N. Both of these types are included because, after initiation, these two kinds of events are indistinguishable. Moisture bursts are defined to end when the cloud band becomes shorter than 2000 km, or when it no longer crosses 15°N.

2. Motivation of Definition. This definition was formulated to capture a specific class of similar-appearing events, which it did. The essential characteristics of these events, from a morphological point of view, are that they are synoptic in time and length scale (they last, on average, 4.5 days), and that they represent tropic/extratropic interaction.

Physical mechanisms are not emphasized in the definition because they are not well known and are not objectively detectable in satellite imagery. If other data had been used in the definition, such as water vapor imagery, a slightly different definition would have resulted.

b. Climatology:

1. Distribution. About 10 moisture bursts per month develop randomly between 160°E and 120°W during the northern hemisphere cool season. The longitudinal distribution over the course of a six-month cool season is nearly uniform. These conclusions are based on observation of 180 moisture bursts over three six-month cool seasons. Only the area between 160°E and South America was examined for this study, though the bursts occur in other areas also.

2. Extratropic Interaction. Nearly 60% of moisture bursts are confined to the subtropics south of 35°N, although 10% of them cross 55°N.

3. El Niño Behavior. During El Niño and summer seasons, when the Hadley circulation is strong, moisture burst frequency decreases significantly. During the 1982-83 ENSO event, burst activity decrease 40%. Bursts were not observed at all in the strongly convective zone over the warm ocean anomaly that propagated eastward across the Pacific. Burst activity was anomalously strong east of 120°W, where bursts are normally infrequent.

c. Circulation:

Forty moisture bursts were identified to form a composite of upper (200 mb) and lower (850 mb) circulation patterns from ECMWF wind analyses.

1. Trough. An upper level trough within 2000 km to the northwest of a moisture burst is a ubiquitous feature with all bursts. It does not always precede the burst, but always intensifies as the burst

develops. The trough commonly, but not always, propagates eastward with the burst cloud mass. In fact, one typical mechanism of burst cessation is the over-running of the cloud band by the trough.

2. Winds. In all cases there is also a strengthening of the southwesterlies along the moisture burst axis. In equatorial areas, this jet is not well documented, but along the burst axis, it is generally interpreted as the subtropical jet.

3. Low-level features. A number of typical equatorial features are associated with the low-level circulation beneath moisture burst cloud masses: easterly waves, cols, and equatorial-crossing vortices. Unfortunately, different operational analyses identify different synoptic features for the same burst. For the forty-burst climatology, nearly 50% were associated with cols, 35% with wavelike features, and about 15% with no particular disturbance. When disturbances are present, the cloud mass usually has its origin in anticyclonically curving flow to the east of the wave axis or col confluence line. These lines normally are aligned with the long axis of the cloud mass.

5. SYNOPTIC CASE STUDIES.

Additional insight into the structure and behavior of moisture bursts was sought by using case studies of individual bursts. Cases selected include two consecutive winter bursts (20-29 January 1979) and a spring burst (13-17 May 1979). These cases were selected because of the better data coverage available form the Special Observing Periods of the FGGE.

a. Evolution of a moisture burst:

The following lists several of the features characteristic of the evolutionary behavior of the moisture bursts:

1. About two-thirds of the bursts develop from an impulse having a near-equatorial origin; the remainder are associated with a cold outbreak or frontal impulse. An upper jet current develops and intensifies over and west of the origin region and develops a distinct perturbation which increases in amplitude as the burst develops. There is evidence in the first January case and in the May case that the jet develops out of the near-equatorial region. As its amplitude increases it merges with the strong winds (subtropical jet?) of the associated subtropical or middle latitude upper trough. This is not simply an intensification of equatorward (southward) moving extratropical features (although this evolution does take place with some moisture bursts).

2. There is often evidence of cross-equatorial flow at both upper and lower levels with the development of the moisture burst. Even without cross-equatorial flow, strong meridional winds characteristically occur in the origin region.

3. The cloud axis and the upper trough axis approach each other as the cloud band widens to the north and elongates northeastward.

4. Dissipation of bursts is usually, but not always, triggered

by cessation of the deep tropical convection associated with their origin.

The downstream consequences and developments of moisture bursts were not examined in detail for reasons stated in the first chapter. We point out that there are significant cases of extensive rainfall and/or cyclogenesis over Mexico or the southern United Stated as moisture bursts intrude on those regions.

b. Moisture distribution:

Conclusions about the moisture distribution associated with moisture bursts are sensitive to the particular observing system. This shortcoming must be corrected. Nonetheless, the following may be stated:

1. Moisture fields as developed dynamically in the ECMWF analysis scheme appear reasonable and imply that the synoptic-scale dynamical development is a relevant mechanism in establishing vertical motion in moisture bursts. These analyses suggest that the primary source of moisture is large-area-averaged vertical motion within the ITCZ. Downstream, the moisture bursts cease looking like ITCZ systems.

2. The rawinsonde data available suggest that there is strong convection underneath the moisture burst clouds throughout a significant portion of the length of the system; thus the cloud mass is not simply advected. Also, it is unclear whether the moisture source is to the west, the east or the south of the origin region.

3. Moisture distributions in the May case and water vapor channel imagery in a number of cases suggest that the moisture burst may be a merging of both tropical and extratropical disturbances. This merging is suggested as well in temperature fields determining from radiosonde data.

4. Not only are moisture bursts regions of high moisture content; they are regions of high moisture variability as well. These

signals are often undetected in the tropical boundary layer.

c. Baroclinity, jet structure and wind distribution:

1. 24-h thermal variations. Temperatures, both in the lower and upper troposphere, show significant interdiurnal variations during moisture bursts, occasionally exceeding 10K per day. These changes imply strongly baroclinic mechanisms. Probably less than half of the baroclinity can be attributed to the equatorward surges of middle-latitude air.

2. Frontogensis and Jet Acceleration. One consequence of the baroclinity is the strong upper winds associated with the burst. Even though the baroclinity associated with the bursts is much weaker than that of middle latitudes, speeds often exceed 30 m/sec, with directions significantly different from 270°. This jet often develops to the south of what would customarily be identified as the subtropical jetstream. In nearly 1/3 of moisture bursts, the jet is swept southward with a frontal system and usually undergoes further acceleration.

3. Smaller Scale Features. The moisture bursts of the eastern Pacific Ocean occur above the low-level easterlies. Patches of strong westerlies can occur west of the origin region. Transient easterly waves have been observed to migrate through the origin region as well; the cause-effect relation of these waves is uncertain. High amplitude temperature anomalies (10K) have been detected in the upper troposphere. Complex horizontal and vertical profiles of wind seem relevant.

6. PROCESSES AND BUDGETS.

Only preliminary efforts have been attempted to ascertain cause with respect to moisture bursts and effect mechanisms. Most of this work has been limited to FGGE III(b) data.

a. Moisture:

Attempts to estimate moisture fluxes and budgets associated with moisture bursts of the eastern North Pacific Ocean area met with mixed success. Two calculations, one based on the FGGE II-b data (radiosondes and dropwindsondes) and the other on the FGGE III-b data set (the gridded analyses) were employed. Conclusions based on the results and their comparisons follow:

1. Calculations of water vapor flow across latitude lines (the northward and southward fluxes) provided a fair representation of reality, especially when based on the dropwindsonde data (however, there is concern regarding the accuracy of dropsonde moisture profiles). The fluxes across various segments of the latitude circle usually match what would be expected from the synoptic behavior of the atmosphere in the vicinity of the moisture burst.

2. Water vapor flow into, or out of, small volumes does not seem to be well represented by either form of data. The FGGE III-b analyses likely are the poorer data for synoptic investigations because the data analysis procedures tend to be biased toward the climatological structure where data are scarce, as is always the case in the area being investigated.

3. The results also may be biased because of the questionable accuracy of the initial data. This is particularly true with the moisture analyses of the FGGE III-b set because of problems with the handling of

moisture by the analysis model used.

The results obtained from the moisture budget study are probably the least satisfying and least reliable product of our efforts. Generally, confidence of even the correct sign of the flux convergence is lacking. On the other hand, this is where the satellite-derived information may prove to be most valuable. By no means do we consider our efforts toward evaluation of these moisture budgets to be completed.

b. Mass budget/vertical motion:

1. Surface Pressure. Fields of surface pressure were analyzed to determine system movement and mass changes associated with synoptic development. Although the data are noisy, time series represent a coherent view of an intensifying low pressure system that moves slowly to the east northeast.

2. Mass budget. The same analysis was repeated with surface pressures computed kinematically from the vertically integrated divergence. An incoherent noisy field resulted. Over the entire study region, a bias in divergence existed such that a large systematic pressure increase should have been observed across the domain; it was not.

3. Kinematics. Finally, the 850 and 200 mb winds were split into non-divergent and irrotational components. Although the gross pattern of velocity potential fit the cloud top brightness temperature pattern, synoptic scale correspondence was lacking. The upper level center of divergence, supposedly associated with the evolving moisture burst, did not occur in even the correct hemisphere. Moisture channel brightness temperatures, used as an alias for rising motion, did no better than the kinematic analysis, although patterns were similar. Part of the problem of deducing divergence from mean wind patterns is that the divergent component

of the wind tends to align itself with the mean wind (or non-divergent part); thus divergence seems to be caused more by speed changes than by directional changes. The streamline pattern, therefore, will carry little useful information pertaining to divergence.

c. Momentum budget:

1. Zonal winds. As moisture bursts develop, the vertically and zonally integrated zonal wind increases magnitude significantly throughout the domain from 30°N to 10°S. Two westerly maxima are observed, one at 23°N and the other at about 4°N. This momentum increase seems to propagate weakly from the northern boundary at 30°N to the equator.

2. Boundary layer winds. Although observations are poor, the moisture burst stratifies boundary layer winds and shear into four different behaviors, including a strong equatorial westerly zone to the west of the moisture burst. Time sections of wind sounding are indicative of the variations to be expected with tropical upper tropospheric troughs (TUTT). In many of the analyses, synoptic scale wind changes are difficult to detect below 500 mb.

3. Hadley Cell. In the zonal average, moisture bursts look like local intensifications of the mean meridional Hadley cell. When moisture bursts are absent, the mean tropical meridional circulation may reverse, with near-equatorial subsidence.

4. Momentum Budget. Each term of the zonal momentum equation was calculated and mapped for each time period and level, and for the vertical integral. Only preliminary interpretation of this calculation has been completed.

i) Almost no coherent pattern appears below 500 mb.

ii) The ageostrophic component (the difference between pressure

and Coriolis forces) possesses a coherent pattern, but it is weak; this pattern is limited to regions north of 10°N, as it is with nearly all the terms.

iii) Boundary terms--fluxes and zonal pressure forces--are small, except possibly along the western portion of the northern border of the domain.

iv) As with most momentum studies, the residual term makes a large coherent contribution to the momentum budget.

d. Objective analysis:

Comparison of ECMWF and GFDL streamline analysis with the II(b) data suggests that significant pieces of wind information are not being accepted by the Optimal Interpolation (OI) process. In data sparse regions, where rapid synoptic development is occurring, accurate data are likely to be flagged and deleted by the analysis because they differ too much from the model-generated first guess. We subjectively re-analyzed a number of 300- and 850-mb maps to examine the effect of incorporating the flagged, questionable data into the analysis. Little could be done at 850 mb because very little data existed at all. At upper levels, a significantly-different, coherent picture emerged as an alternative analysis. Development was much more vigorous, with winds in excess of 80 m/sec observed, twice the magnitude of those analyzed through OI. In the reanalysis, the subtropical jet (supposedly) appears to emerge directly from the moisture burst as a direct result of its development. Analysis of the momentum budget, using this alternate wind analysis, has not yet been attempted.

7. PUBLICATIONS AND OTHER DOCUMENTS PREPARED FOR NASA CONTRACT NAS8-35182

The contract results are in the form of scientific articles and other similar documents. These include articles submitted to scientific journals, Texas A&M theses and dissertations, and extended abstracts and preprint papers of presentations at scientific and technical conferences. There have been 22 of these documents prepared as a part of the contract activity. The total pages involved in all the manuscripts approaches 900, far too many to include in this Final Report. Rather, we have chosen to list all the documents, including the abstracts of the longer articles in the remainder of this section. Since this would leave our Final Report without any quantitative or pictorial summarization of the results of our research efforts, we have chosen to include the dozen Conference preprint papers as an Appendix, in the order in which they were prepared and presented. They offer a summary of our studies; however, they do not span the entire range of accomplished tasks, reported in the longer documents.

Published papers:

McGuirk, J., L. Anderson and A. Thompson, 1985: Satellite-derived synoptic climatology in data-sparse regions. Adv. Space Res., Vol. 5, No. 6, pp. 45-48.

McGuirk, J. P., A. H. Thompson and N. R. Smith, 1987: Moisture bursts over the tropical Pacific Ocean. Mon. Wea. Rev., 115, 787-798.

Paper submitted and returned for revision recommended by editors and reviewers; revision is being prepared now:

McGuirk, J. P., A. H. Thompson and L. L. Anderson, Jr., 1987: Views of synoptic scale moisture variation over the tropical Pacific Ocean. Submitted to Mon. Wea. Rev.

Paper submitted for publication.

Thompson, A. H., J. P. McGuirk and J. R. Schaefer, 1987: Synoptic behavior of eastern Pacific moisture bursts. To be Submitted to Mon. Wea. Rev.

Papers still in draft form, being prepared for submission:

Thompson, A. H., and J. P. McGuirk, 1987: Synoptic scale moisture budgets of the tropical eastern Pacific Ocean (tentative title). To be submitted to Weather and Forecasting or Mon. Wea. Rev.

Doctoral Dissertation:

Anderson, Lloyd L., Jr., 1986: "Multispectral Analysis of a Tropical Radiance Set from the TIROS Operational Vertical Sounder." Doctoral Dissertation submitted to Texas A&M University. 228 pp.

Master's Theses:

Snyder, Bruce Alan, 1985: "The Divergent Wind Component in Data Sparse Tropical Wind Fields." A Master of Science Thesis submitted to Texas A&M University. 105 pp.

Schaefer, James Royal, 1985: "Observing the Synoptic Structure of Two Moisture Bursts." A Master of Science Thesis submitted to Texas A&M University. 145 pp.

Stockton, Jay Richard, 1986: "The Structure of a Late-Spring Moisture Burst." A Master of Science Thesis submitted to Texas A&M University. 90 pp.

Smith, Neil Ray, 1986: "A Climatology of Tropical Moisture Bursts in the Eastern North Pacific Ocean." A Master of Science Thesis submitted to Texas A&M University. 77 pp.

Papers presented at scientific conferences and printed in preprint or proceedings volumes:

McGuirk, J. P., A. H. Thompson, L. L. Anderson, Jr., and N. R. Smith, 1984: Reliability of circulation statistics over the tropical Pacific Ocean based on FGGE data. Proceedings of the Eighth Annual Climate Diagnostics Workshop, Oct. 17-21, 1983, Downsview, Ontario. pp. 247-257.

McGuirk, J., and A. Thompson, 1984: Transient tropical disturbances within the Pacific Hadley cell. Postprint

Volume, 15th Technical Conference on Hurricanes and Tropical Meteorology., Amer. Meteor. Soc., Miami FL. pp. 137-142.

McGuirk, J., L. Anderson and A. Thompson, 1984: Satellite-derived synoptic climatology in data-sparse regions. COSPAR Symopsium on Space Observations for Climate Studies, Graz, Austria, 25-29 June, 1984. Paper 4.6.1. This paper was also published in Adv. Space Res. See item under "Published paper."

Thompson, A., J. McGuirk , L. Anderson and N. Smith, 1984: Analysis of tropical synoptic disturbances using satellite-derived soundings and radiance data from selected channels. Preprint Volume, Conference on Satellite/Remote Sensing and Applications. Amer. Meteor. Soc., Clearwater Beach, FL, pp. 137-142.

McGuirk, J., A. Thompson and N. Smith, 1985: Observing the eastern Pacific Hadley circulation. Proceedings of the Ninth Climate Diagnostics Workshop, Oct. 22-26, 1984, Corvallis, OR. 429-436.

Thompson, A., J. McGuirk and L. Anderson, 1985: Comparisons between tropical synoptic moisture fields as determined from analysis and from observations. Proc. 16th Conf. on Hurricanes and Tropical Meteorology., Houston, TX, Amer. Meteor. Soc., pp. 54-55.

McGuirk, J., and A. Thompson, 1985: Two modes in the Pacific Hadley cell. op. cit., pp. 136-137.

Smith, N., J. McGuirk and A. Thompson, 1985: The synoptic structure of tropical Pacific moisture bursts. op. cit.,

pp. 192-193.

McGuirk, J. P., A. H. Thompson and B. A. Snyder, 1986: Comparisons of FGGE IIb and IIIb winds in a tropical synoptic system. Preprints, Nat'l. Conf., Scientific Results of the First GARP Global Experiment. Miami, FL, Amer. Meteor. Soc., pp. 40-43.

McGuirk, J. P., A. H. Thompson and L. L. Anderson, Jr., 1986: Wintertime disturbances in the tropical Pacific: FGGE IIIb and satellite comparisons. op. cit., pp. 44-47.

Thompson, A. H. and J. P. McGuirk, 1986: Moisture transports and budgets of "moisture bursts." op. cit., pp. 212-215.

McGuirk, J. P., L. L. Anderson, Jr., and A. H. Thompson, 1986: Tropical synoptic interpretation of inter-channel correlations from TIROS-N. Preprints, Second Conf. on Satellite Meteorology/Remote Sensing and Applications, Williamsburg, VA, Amer. Meteor. Soc., pp. 118-122.

The reminder of this section contains the abstracts of the published scientific papers, the papers already submitted for publication, the dissertation and the four theses.

Reprints of papers contained Conference Preprint Volumes are continued in the Appendix.

SATELLITE-DERIVED SYNOPTIC CLIMATOLOGY IN DATA-SPARSE REGIONS

by

J. P. McGuirk, L. L. Anderson, Jr., and A. H. Thompson

ABSTRACT

Synoptic-scale "moisture bursts" are defined, based on infrared GOES imagery, and their synoptic climatology is developed. Quantitative analysis of satellite-derived individual channel radiance data and vertical eigenfunctions of complete channel data yield rich structural detail; these details do not appear in FGGE analyses in regions void of conventional meteorological data.

Published in

Advances in Space Research, Vol. 5, No. 6, pp. 45-48, 1985.

MOISTURE BURSTS OVER THE TROPICAL PACIFIC OCEAN

by

James P. McGuirk, Aylmer H. Thompson and Neil R. Smith

ABSTRACT

"Moisture bursts" are bands of high clouds or middle and high clouds extending poleward and eastward from deep tropical locations into subtropical and middle latitudes. These events, synoptic in both temporal and spatial scales, are extremely common, particularly over the North Pacific Ocean.

We define moisture bursts objectively, in primarily geometric terms, to emphasize both their synoptic scale and their tropical-extratropical interaction. We apply this definition to infrared satellite imagery for four 6-month cool seasons (November-April) in the eastern North Pacific (160°E to the west coast of the Americas). The frequency of these events is about 10 bursts per month during normal cool seasons, distributed uniformly across the Pacific to the west of 110°W; east of this longitude, few moisture bursts occur. Half of the bursts last two to four days, and no burst lasted longer than 10 days.

Only 36 moisture bursts occurred during the 6-month El Niño cool season of 1982-83, with the location of occurrence shifted eastward. Few bursts occurred in the region of active tropical convection associated with the El Niño event.

Because moisture burst frequency decreases at times when the ITCZ strengthens, we hypothesize two modes in Hadley cell behavior: a strong zonally-symmetric mode, and a weaker mode comprised of the statistical ensemble of a large number of transient moisture bursts. Through analysis

of wind fields, zonal averages across moisture bursts are shown to resemble transient intensification of the mean meridional circulation in regions where the Hadley cell is typically weak.

Published in

Monthly Weather Review, Vol. 115, pp. 787-798 (April 1987).

VIEWS OF SYNOPTIC SCALE MOISTURE VARIATION OVER THE TROPICAL PACIFIC OCEAN

by

James P. McGuirk, Aylmer H. Thompson, and Lloyd L. Anderson, Jr.

ABSTRACT

Moisture observing capability is surveyed over the tropical northeast Pacific ocean. Data are taken from late January 1979, during the FGGE first special observing period. Diagnosis of synoptic scale systems, in this case moisture bursts, in data sparse areas is emphasized. The characteristics of five observing systems, and what they show about two active moisture bursts during the study period, are described. The five systems are: surface observations, satellite cloud imagery, radio- and dropsondes, satellite individual channel brightness temperatures, and model analysis from the European Center for Medium Range Weather Forecasting. The various systems are examined individually and intercompared as well.

Surface observations carry almost insignificant moisture information over the tropical oceans. Capability of GOES imagery is well known; however, clouds hide a wealth of important moisture structure, and clouds do not always define moisture patterns well, even at cloud level. Soundings are adequate for synoptic diagnosis, if there were enough of them; however, dropsondes carry significantly less detail than radiosondes. Satellite channel data provide thorough coverage, and even show some detail in nearly overcast regions; ambiguity of interpretation remains a problem, although multispectral techniques (like EOF analysis) appear promising. Given the lack of moisture observations for initialization, European Center analysis provides surprisingly realistic moisture patterns. Certain model biases must be treated carefully, however.

Quantitative intercomparison of data, where possible, is generally discouraging. Field comparisons of analysis and satellite observations are poor, with only marginal statistical significance. Both systems, however, clearly define the synoptically active regions in their variability statistics; they both perform better in moist regions, where quantitative estimates of moisture are most important. Comparisons with radiosondes are poor as well. Correspondence of analysis, satellite and radiosondes is good in moist regions, but all three have serious observational problems when radiosonde-observed relative humidity falls below 50%.

The two most significant conclusions are: 1) The observational needs for model initialization and forecasting are different than those for system diagnosis, and initialization procedures may not be optimum for diagnosis; 2) Although the east Pacific is data-sparse, an equally serious problem is that it may be data-interpretation-sparse, as well.

This manuscript was submitted to Monthly Weather Review. It is now being revised in response to Editors' critique.

SYNOPTIC BEHAVIOR OF EASTERN PACIFIC MOISTURE BURSTS

by

Aylmer H. Thompson, James P. McGuirk and James R. Schaefer

ABSTRACT

Synoptic scale cloud/moisture systems, called moisture bursts, from disturbances in the eastern Pacific ITCZ and in conjunction with amplifying troughs to the north; a common spatial pattern and temporal evolution accompany most events. This structure involves upper and lower level wind fields, thermal and moisture fields and vertical motion fields as well. In spite of the data sparse area in which they evolve, a blend of many kinds of data and analyses allowed us to deduce much of this structure through a case study of a typical system; this moisture burst developed during the first Special Observing Period of the First GARP Global Experiment. Conclusions are corroborated with a climatology of 41 systems and a less detailed climatology of over 200 moisture bursts described by McGuirk et al (1987).

Moisture bursts are associated with subtropical troughs to the northwest, intense drying and subsidence within this trough, and a strong subtropical jet accompanying the cloud mass, which is the moisture burst. The subtropical jet may originate near the equator in moisture bursts. Low level disturbances in the tropical easterlies are present when the burst initiates, and these structures organize as the burst evolves. A variety of smaller scale disturbances with both horizontal and vertical structures appear within the burst cloud mass. A moisture burst may develop simultaneously out of several of these systems. Evidence of frontogenesis appears along the northwest flank and downstream of the moisture burst:

intensifying moisture gradient, developing thermal gradient, jet level winds, solenoidal overturning, deepening of the tradewind inversion and its extension towards midlatitudes. Moisture bursts cease normally when their tropical and non-tropical aspects become separated.

This manuscript was submitted to Monthly Weather Review.
It is now (June 1987) undergoing peer review.

Doctoral Dissertation

ABSTRACT

Multispectral Analysis of a Tropical Radiance Set from the TIROS Operational Vertical Sounder. (December 1986)

Lloyd Lynn Anderson, Jr., B.S., U.S. Air Force Academy;

M.Ed., Phillips University

Co-Chairmen of Advisory Committee: Dr. James P. McGuirk
Dr. Aylmer H. Thompson

Analysis of the state of the atmosphere is constrained by the quantity and quality of the observations. In data sparse areas, meteorological analysis relies heavily on remotely sensed data, especially those collected by earth orbiting satellites. This research examines the information content of the TIROS-N Operational Vertical Sounder (TOVS) during 20-29 January 1979 over the tropical Pacific Ocean. Vertical, horizontal, and temporal statistical characteristics are examined. The TOVS channels are highly correlated ($|r|>0.6$) except for the infrared water vapor channels and the microwave window and 300 mb channels. The horizontal structure varies according to spectral channel (absorbing constituent and effective evaluation), geography, and synoptic condition. Horizontal correlation is particularly sensitive to water vapor and cloud amount. In equatorial sectors, moisture channels have higher correlations and larger length scales than thermal sensing channels; in the subtropics, the opposite is true. Temporal variation is largest in the water vapor and microwave window channels, and in synoptically active regions with brightness temperature variances typically ten times larger than in synoptically quiescent regions.

Attempts to augment TOVS data in cloudy regions and for missing passes using a full quadratic response surface regression model were only marginally successful. At some locations, thermal infrared channels had brightness temperature RMS errors of 0.5 to 2.5 standard deviations from the mean, and the water vapor and microwave window channels had RMS errors of 2.5 to 5.5 standard deviations from mean values.

The TOVS channels with peak energy contribution from below 90 mb were synthesized using principal components analysis. Over 94 percent of the areal variance at any particular time is represented by the first 5 eigenfunctions. The first two eigenfunctions, vertical mean thermal and mid-tropospheric moisture representations respectively, typically account for 65% and 15% of the observed spatial variance. Eigenfunctions 3 through 5 (each accounting for 5 to 7% of the variance are dominated by the microwave window and 300 mb channels and the water vapor channels. These eigenfunctions represent moisture structure, surface type, and/or precipitation contamination discriminators. The leading eigenfunctions and their horizontal patterns are consistent with the available sounding data and satellite imagery.

This methodology can be developed to augment synoptic analysis in data sparse regions.

Master's Thesis

ABSTRACT

Observing the Synoptic Structure of Two Moisture Bursts. (December 1985)

James Royal Schaefer, B.S., University of Wisconsin, Eau Clairs;

B.S., University of Utah

Co-Chairmen of Advisory Committee: Dr. James P. McGuirk
Dr. Aylmer H. Thompson

The moisture burst is characterized by large amounts of cloudiness emanating from tropical regions and often affecting middle-latitude regions. Due to data scarcity, the study of moisture burst near their origin is difficult. Supplementary data available during the First GARP Global Experiment make such a study feasible.

Through the use of in situ observations and computer-generated model analyses, this thesis presents results of a synoptic case study of two moisture bursts. Satellite-derived data are shown to be useful in this region, although lack of certain satellite radiance channels during the time period precludes their use. The FGGE IIIb model analyses are first proven to be reliable by comparison with satellite observations and are then used extensively.

A significant upper-level trough, with strong subtropical jet stream winds, existed during the origin periods of both bursts. A large northward meridional component to the subtropical jet stream was found on the downstream side of the troughs. There was a low-level easterly wave trough near the origin of the first burst. Associated with at least the first moisture burst, evidence was found suggesting an upper-level cold front near an area of rapid development of the burst.

Most importantly, it was found that these two moisture bursts were not homogeneous masses of clouds, but were composed of several separate cloud masses which combined to form the moisture burst. These cloud masses include elements associated with the intertropical convergence, with a southward moving frontal disturbance, and with convective development between the first two. Additional evidence suggests that the moisture burst is not merely an extension of ITCZ activity into the subtropics. Therefore, it is proposed that the moisture burst is due not to any one, or even two, major features, but is a combination of a number of interrelated elements.

Master's Thesis

ABSTRACT

The Divergent Wind Component in Data Sparse Tropical Wind Fields.

(December 1985)

Bruce Alan Snyder, B.S. Texas A&M University:

M.B.A., Golden Gate University

Co-Chairmen of Advisory Committee: Dr. James P. McGuirk
Dr. Aylmer H. Thompson

Tropical wind field analyses produced by assimilation schemes, which are extratropical techniques modified to function in the tropics, have been shown to produce questionable results. A major problem has been the underestimation of the divergent wind component by these schemes. The gridded u and v wind data from the FGGE level IIIb analyses for a region in the eastern tropical Pacific Ocean from 20-29 January 1917 were obtained. Various analyses were performed on these data to gain an understanding of the influence of the divergent component on the appearance of the tropical wind field.

After testing a number of previously proposed boundary conditions for the streamfunction and velocity potential, Sangster's (1960) method was used to separate the wind into its divergent and nondivergent components. The Liebman relaxation technique was used to solve Poisson equations for streamfunction and velocity potential. Streamline analyses of original and reconstructed wind fields were performed using the algorithm proposed by Whittaker (1977). Insight into the relationship of the divergent wind component to the tropical wind field was obtained by computing various estimates of divergence, studying the time continuity of the streamfunction

and velocity potential fields, and by performing various wind vector error analyses.

These studies were conducted on both the 850 mb and 200 mb wind fields. The analyses generally indicate that the divergent wind component has little effect on the appearance of the upper level wind field and the lower level wind field is affected only in regions where the strongest convergence/divergence occurs. The main problem in obtaining accurate tropical wind field analyses seems to be the inability to resolve the scale of the diabatically induced divergence field on either convective or smaller synoptic scales.

Master's Thesis

ABSTRACT

The Structure of a Late-Spring Moisture Burst. (May 1986)

Jay Richard Stockton, B.S. Texas A&M University

Co-Chairmen of Advisory Committee: Dr. James P. McGuirk
Dr. Aylmer H. Thompson

A case study of a May 1979 occurrence of a phenomenon known as a moisture burst is performed utilizing the enhanced data coverage available during FGGE SOP II.

Both tν σττξ and satellite data are developed and prepared for the case study. A moisture burst climatology is developed and shows that burst occurrence in the spring remains near winter levels in the 'normal year' climatology. After the El Niño episode of 1982-83, burst activity increased greatly in the spring after a lull in winter burst activity.

A useful framework for picturing the evolution of a moisture burst is described in terms of the movement of moisture into and through the system. The framework, or model, consists of the following four elements:

1) A low level moisture source;
2) A vertical transport mechanism;
3) An upper level horizontal transport mechanism; and,
4) Upper level conditions favoring the development of clouds downstream of the moisture source.

The representation of the burst in GOES-W IR imagery is discussed and the presence of points 2, 3 and 4 of the model is tentatively verified. Upper level moisture patterns associated with the burst are examined. A detailed study of the model shows that: 1) The low level moisture source is the low level tropical air located over the central tropical Pacific

near the southwest extremity of the burst; 2) The vertical transport mechanism appears as areas of enhanced convection in the ITCZ, but a single cause of this enhanced convection could not be ascertained; 3) The upper level transport mechanism is the subtropical jet, displaced well south of its climatological position in association with a strengthening upper-level trough and a possible large-scale wave instability located near the ITCZ; 4) The upper level conditions favoring cloud development downstream of the source occur on the southern flank of the subtropical jet where upper level divergence in the right rear quadrant of the jet maximum favors cloud formation.

Master's Thesis

ABSTRACT

A Climatology of Tropical Moisture Bursts

in the Eastern North Pacific Ocean. (December 1986)

Neil Ray Smith, B.S., Texas A&M University

Co-Chairmen of Advisory Committee: Dr. James P. McGuirk
Dr. Aylmer H. Thompson

A tropical moisture burst in this study refers to a continuous band of high clouds that originates from a tropical disturbance and extends poleward to extratropical latitudes. It is objectively defined in terms of appearance in unenhanced IR satellite imagery as a continuous band of upper, or middle and upper, level clouds which is 2000 km in length and crosses 15°N. The definition is primarily geometric and does not presuppose physical mechanisms.

Statistics of occurrence during three 6-month periods (November-April) show that the moisture burst is a common event of the eastern North Pacific (160°E to 90°W). An average of 60 events occur per cool season. Monthly frequency is about 10 bursts per month. Spatial distribution is essentially uniform west of 110°W with very few occurring east of this longitude. Mean moisture burst duration is 2.6 days, while the maximum observed was almost 10 days. The burst cloud band is confined to subtropical latitudes in the mean, but during mid to late winter, a majority of cloud bands extend to middle latitudes.

Only 36 moisture bursts occurred during the 6-month ENSO cool season of 1982-83. Spatial and temporal frequency of occurrence was drastically reduced west of 140°W. This region during ENSO was also an area of

anomalously active ITCZ convection.

Upper- and lower-level wind fields are examined for a 41-event subset of the moisture bursts identified in the first three cool seasons. A 200 mb trough is a consistent feature of the upper-level moisture burst wind field. The trough is present, on average, about 600 km upstream of the burst origin cloud mass, and appears to play a significant role in cloud band propagation and event termination. A majority of bursts originate in anticyclonic flow with a southerly component at the 850 mb level. Though there is no consistent low-level wind field configuration, the most commonly observed pattern is a frontal-like col deformation of the wind flow in the region of the moisture burst cloud band.

8. DISCUSSION AND CONCLUSIONS

This Report, by design, is a summarization and discussion of the many scientific papers, theses, dissertation and conference proceedings prepared during the studies we have undertaken. These documents have been listed in Section 7, which also includes abstracts of the longer scientific documents, the dissertation and the theses. There seems no point in a "summary of the summary." Instead, we conclude our report with some pertinent comments on continuing and future work.

Although we have learned a great deal about moisture bursts and about the synoptic scale properties of satellite channel data, we have barely begun to tap the full capability of quantitative satellite channel data. We make the following recommendations, and propose to tackle most of these items under a new contract.

1. Moisture behavior.

i) Use the moisture channel brightness temperatures as a measure of the top of the moisture layer; then use the temporal variation to estimate middle and upper tropospheric vertical motion.

ii) Obtain moisture tracked winds for the February 1984 period from the University of Wisconsin and incorporate into our diagnostic description of moisture bursts.

iii) Improve moisture advection estimates (in part from new analyses to be available from ECMWF and GLA) and relate to precipitation estimates (to be available from MSFC). Also, perform more complete budgets based on ECMWF analysis.

2. Synoptic and general circulation behavior.

iv) Define tropical synoptic variability over the eastern Pacific using data over a much longer time period.

v) Prepare more case studies (including events during February 1984) to better document typical moisture burst behavior and to investigate the full range of moisture burst structural variability.

vi) Describe downwind synoptic effects, particularly baroclinicity and jetstream intensification. Special emphasis should be placed on the appearance of moisture bursts in moisture channel imagery. This view is somewhat different than that seen in infrared window channel imagery.

vii) Investigate the dynamical causes of moisture bursts and the associated jet acceleration.

3. Synoptic-scale satellite techniques.

viii) Define individual channel information content through study of horizontal structure functions over a broader range of conditions.

ix) Refine interpretation of EOF patterns and develop other multi-spectral techniques (split-window and overlaying, for example).

x) Implement a radiative transfer model to assist in the interpretation of satellite channel brightness temperatures. Two models will be available, one developed at GLA and the other developed at the University of Wisconsin and available through MSFC. We currently envision two possibilities: Extrapolation of features like inversions and moist layers away from sounding locations and the definition of the signatures of specific features of the tropical atmosphere.

xi) Investigate additional information on synoptic structure and behavior contained in analyses of the synthetic brightness temperature fields mapped from the various individual channels of the satellite-borne sounding systems, such as HIRS, MSU, VAS and their successors. We have developed already a significant ability to understand what the data from the individual channels is telling us about the synoptic structure, but we

must enhance further this understanding.

xii) Continue investigation of the water vapor (6.7 micrometers) imagery and Outgoing Longwave Radiation data (OLR) available routinely for synoptic use from the GOES system and polar orbiters. We mention this separately from the channel data mentioned in the preceding item in part because availability of the 6.7 micrometer imagery and OLR Fields are so different from availability of individual channels from the sounding systems.

APPENDIX

This Appendix contains reprints of all Conference Proceedings and similar papers. See the discussion at the beginning of Section 7, page 31. The order of the papers here is the same as the listing of "Papers presented at scientific conferences...," beginning on page 33.

Reliability of Circulation Statistics over the Tropical Pacific Ocean Based on FGGE Data*

J. P. McGuirk, A. H. Thompson, L. L. Anderson, Jr., and N. R. Smith
Texas A&M University, College Station, TX 77843

Satellite and FGGE Special Observing Period (SOP) data are used to examine the structure and behavior of the tropical Eastern Pacific atmosphere, a data-sparse area nearly the size of North America.

We focus on a tropical synoptic feature, designated a "moisture burst." It appears as a stream of middle and high clouds, emanating from the ITCZ and moving northeastwards out of the tropics and often into northern Mexico and the U.S. A schematic of the temporal development of a burst during the FGGE winter SOP appears as Fig. 1. Table I summarizes the definition of a moisture burst in terms of objective geometric properties. Figs. 2 - 4 and Table II document its "climatology," based on only two 6-month sequences of GOES West infrared imagery during the 1977-78 and 1981-82 cold seasons.

The salient features of this brief climatology are:

a) Approximately 10 bursts occur per month between 160°E and 100°W, lasting an average of 2.5 days each, but with 20% of them lasting four days or longer.

b) The distribution of bursts along the ITCZ is nearly uniform between 160°E and 120°W, with decreasing activity approaching the coast of North America.

c) Bursts occur less frequently in mid-winter (February).

d) At least one burst was active somewhere in the Pacific domain 75% of the time; thus, periods exist when the Hadley circulation is not apparent in the eastern Pacific.

e) Approximately one third of the events appeared to be related to a front, which acted either as a trigger or as a phase of the burst development.

TIROS N soundings (TOVS) and other FGGE data for SOP 1 were obtained from the NCAR archive. The NCAR's TIROS N data are an abridged FGGE set, containing less than 10% of the available satellite retrievals. Figs. 5 and 6 depict typical coverage of sounding data. Fig. 7 compares satellite/raob differences for approximately co-located soundings. The clear sky satellite soundings were systematically colder than co-located raobs by nearly 2°C; although this bias is different than other published results, it is known to be sensitive to geographical regions and meteorological condition. Satellite moisture measurements were systematically drier than and had a large rms difference as compared to raobs; on the other hand, nearly every raob moisture sensor failed to yield reliable information at some dry layer below 700 mb.

Fig. 8 - 14 summarize the time changes of the atmosphere's vertical structure at 6 locations over the Pacific as determined from TIROS N retrievals. Except at location 2 and 6, under a pair of moisture bursts, approximate raobs were present for comparison. Figs. 15 - 18 show related raob time profiles.

---

* This work is funded under Contract No. NAS8-35182 through NASA's George C. Marshall Space Flight Center.

From Proceedings of the Eighth Annual Climate Diagnostics Workshop, Oct. 17-21, 1983, U. S. Dep't. of Commerce, NOAA. Pp. 247-257.

The following conclusions can be drawn from these figures:

a) Large temperature variations occur above 500 mb unaccompanied by significant variations in the lower troposphere. The satellite detects this variation, although it tends to underestimate the amplitude; small lower tropospheric variations are also often detected (compare TOVS 1 with raob 91285 and 91165 over Hawaii).

b) TOVS 1 follows the low level moisture trend well at Hilo, even though the trends at Hilo and Lihue are quite different.

c) Some raob temporal changes are well-matched by the satellite reconstructions, whereas others are missed or are displaced in time. Problems exist with distant co-location and the large time gaps between satellite data.

Fig. 18 in conjunction with fig. 10 and fig. 14 can be used for preliminary examination of satellite representation of two moisture bursts.

d) The appearance of the burst in the upper troposphere occurs as an initial cool event (around Jan. 21 and 22 over the ocean, Jan. 20-25 at San Diego), followed by a strong warm departure, at least through the 27th at all three locations.

e) Large stability changes accompany these temperature changes, at least at group 6 and San Diego.

f) The group 2 satellite retrievals, which were taken both within the high cloud region (at the edge) and under fairly clear conditions, exhibit changes throughout the depth of the atmosphere between the 20th and 29th from one anomaly sign to the other. All retrievals were, at least in part, cloud contaminated. The observed temperature changes may be simply an artifact of the retrieval procedure.

g) Many of the details at group 2 and San Diego are similar, particularly the mid-tropospheric warm and cold anomalies. However, the strong cooling in the upper troposphere (raob) is undetected by the satellite.

Fig. 19 - 23 depict classical cross-sectional analyses of the raob data along the coast as the moisture burst crosses the section (see fig. 8). In these sections, we see:

h) Frontal character and frontogenesis south of San Diego (MYF), between the 22nd and the 24th, although the triggering of the event did not appear frontal on satellite images;

i) Strong lower tropospheric stability decreases south of the apparent frontal region;

j) Large temperature increases at tropopause level north of the moisture burst;

k) A weakening, but spreading of the wind maximum, with the appearance of at least four westerly wind maxima where, before the moisture burst, only a single westerly maximum was present;

l) An intensification of the lower tropospheric wind shear which is consistent with the increased horizontal temperature gradient.

Table I. Objective geometric definition of a moisture burst, as observed on infrared imagery from geostationary satellites.

DEFINITION:
1) a continuous band of upper and middle clouds;
2) at least 2000 km in length;
3) a cloud source equatorward of 15°N;
4) a cloudband extending poleward of 15°N.

BEGINNING:
IR photo time and date of the first evidence of poleward progression of cloud cover.

ENDING:
IR photo time and date of any one of the following:
1) cessation of source convective activity equatorward of 15°N;
2) a break in continuous cloud band equatorward of 15°N;
3) recession of the cloud band equatorward of 15°N.

Table II. Distribution of moisture bursts as a function of duration for two cold seasons. Numbers give bursts out of 124 events which lasted the specified number of days.

DURATION (DAYS)	77-78	(NUMBER OF BURSTS)	81-82
1	32		19
2	14		19
3	6		11
4	4		5
5	4		3
6+	4		3

Mean Duration = 2.5 Days

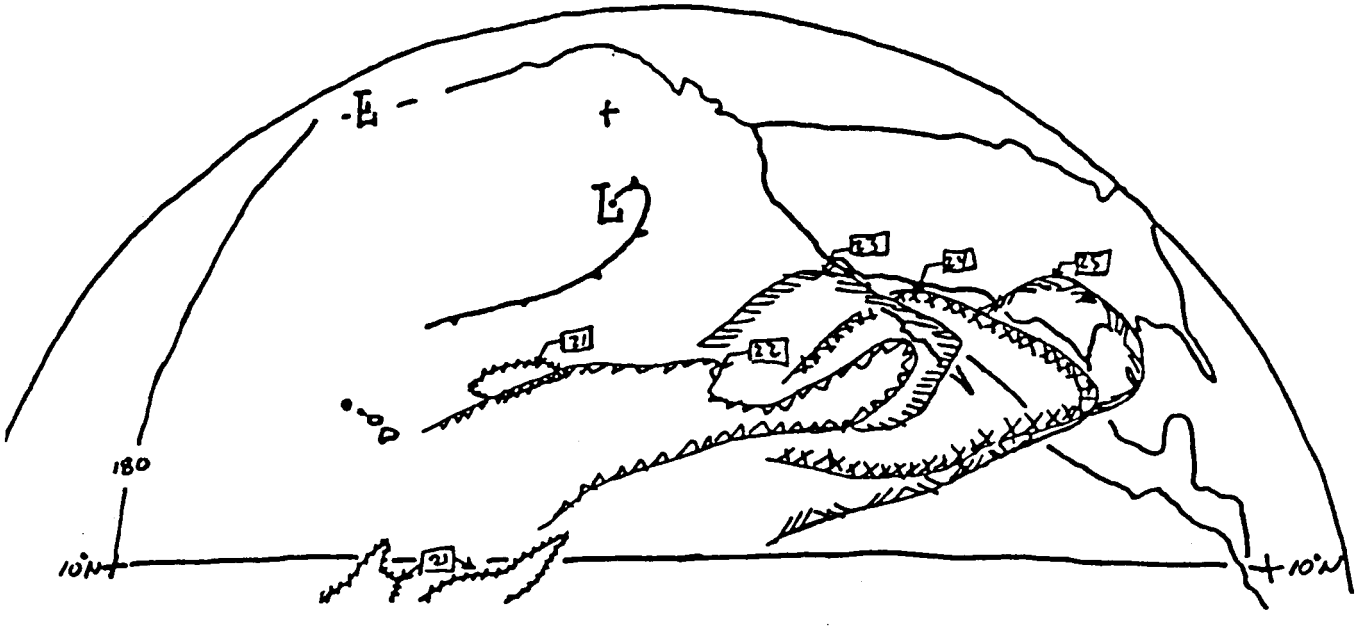

Fig. 1. Schematic depiction of the time evolution of the high cloud boundary of a moisture burst occurring between Jan. 21 and Jan. 25, 1979. Squared numbers give the date of the associated cloud boundary.

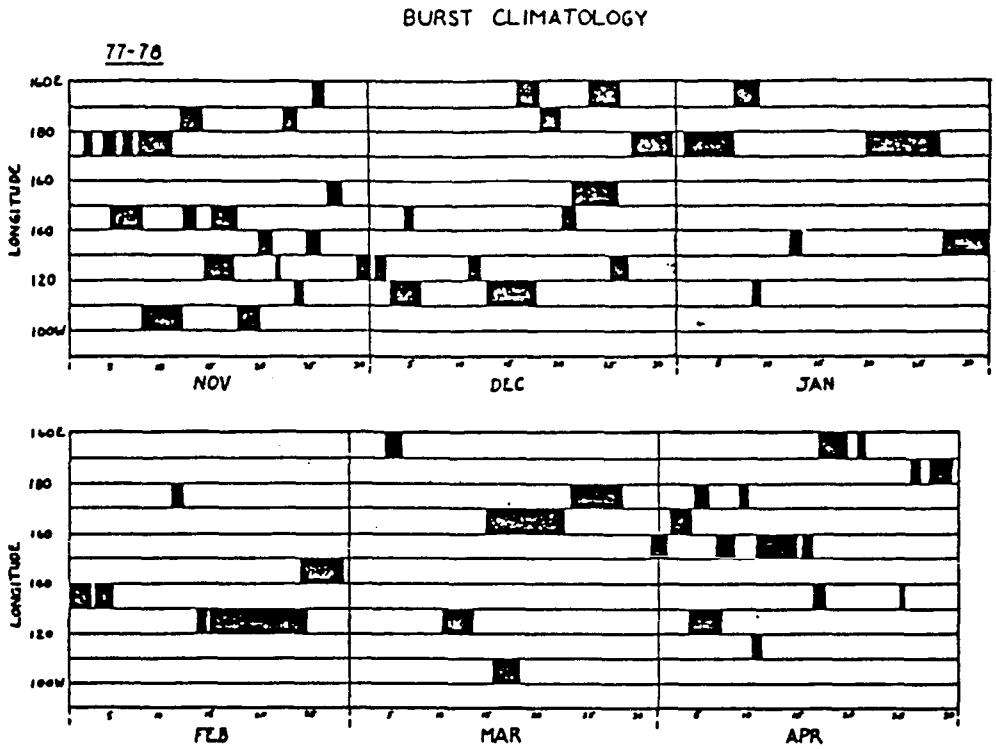

Fig. 2. Catalog of 1977-78 cold season moisture bursts as a function of time and longitude. Black segments depict bursts as defined in Table I.

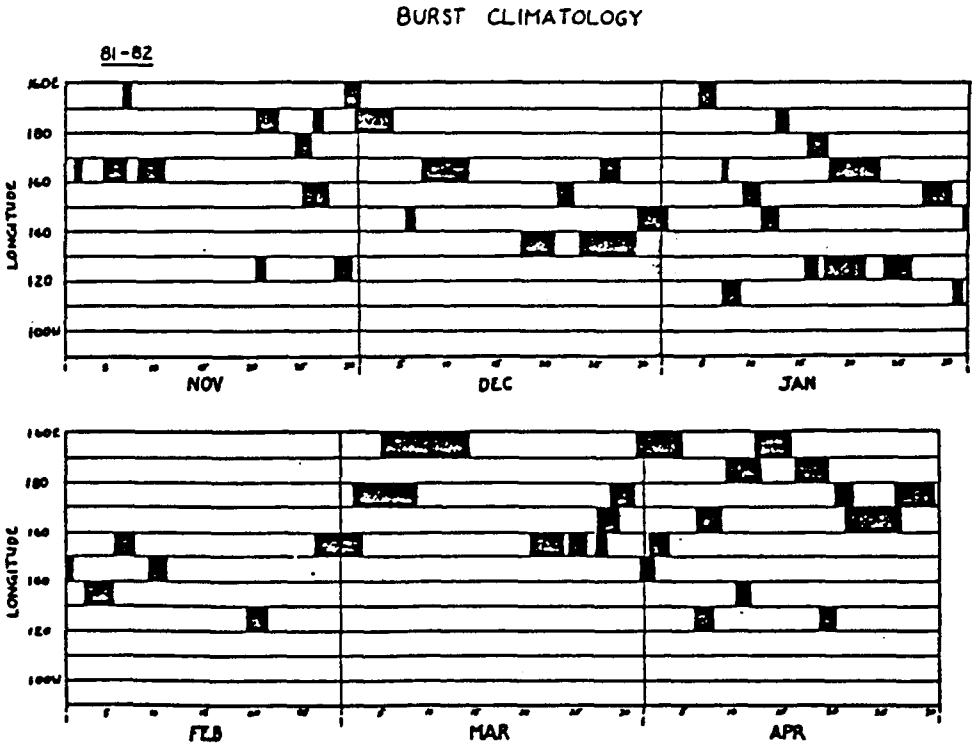

Fig. 3. As in Fig. 2, except for 1981-82 cold season.

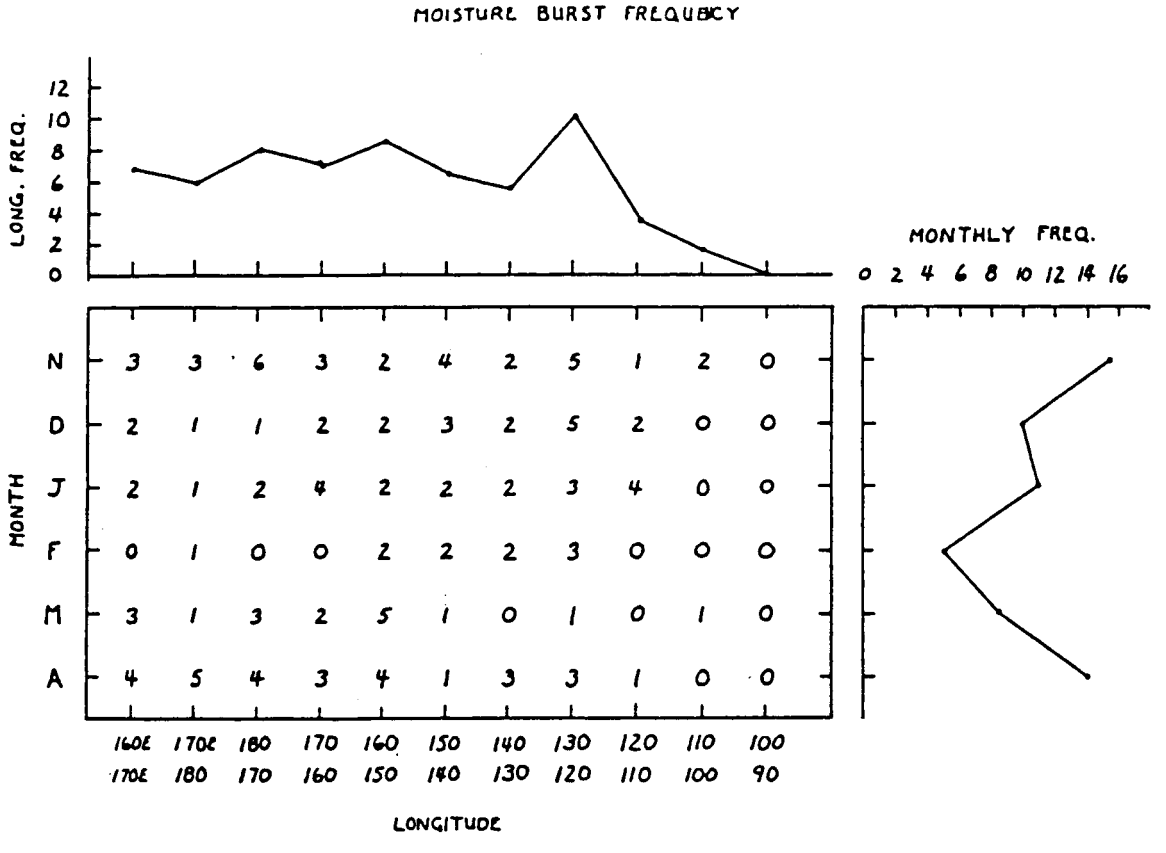

Fig. 4. Distribution of moisture bursts as a function of longitude of origin and month, averaged over the two cold seasons.

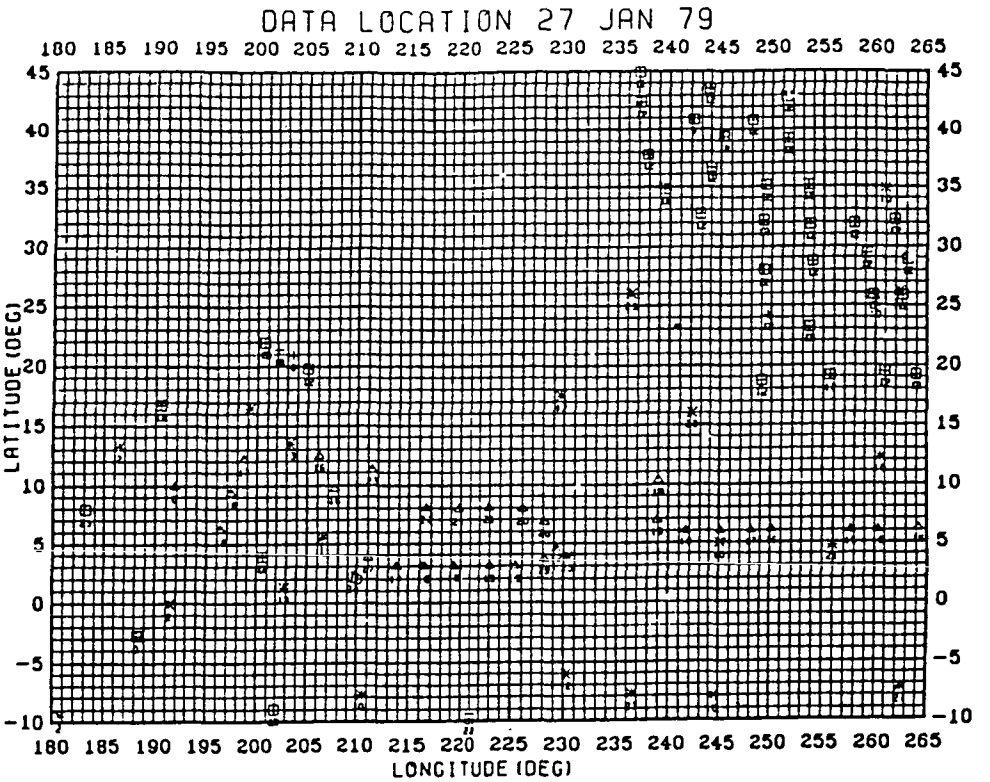

Fig. 5. Sample of sounding-data coverage from NCAR data set on the day of best coverage (most data) during Jan. 1979 moisture burst. Squares represent rawinsondes, crosses are windsondes, asterisks are satellite retrievals (TOVS), triangles are dropsondes. Numbers under the symbols indicate hour of observation. Not shown are the many single-level observations (cloud tracked winds, aircraft, balloons, and surface ships).

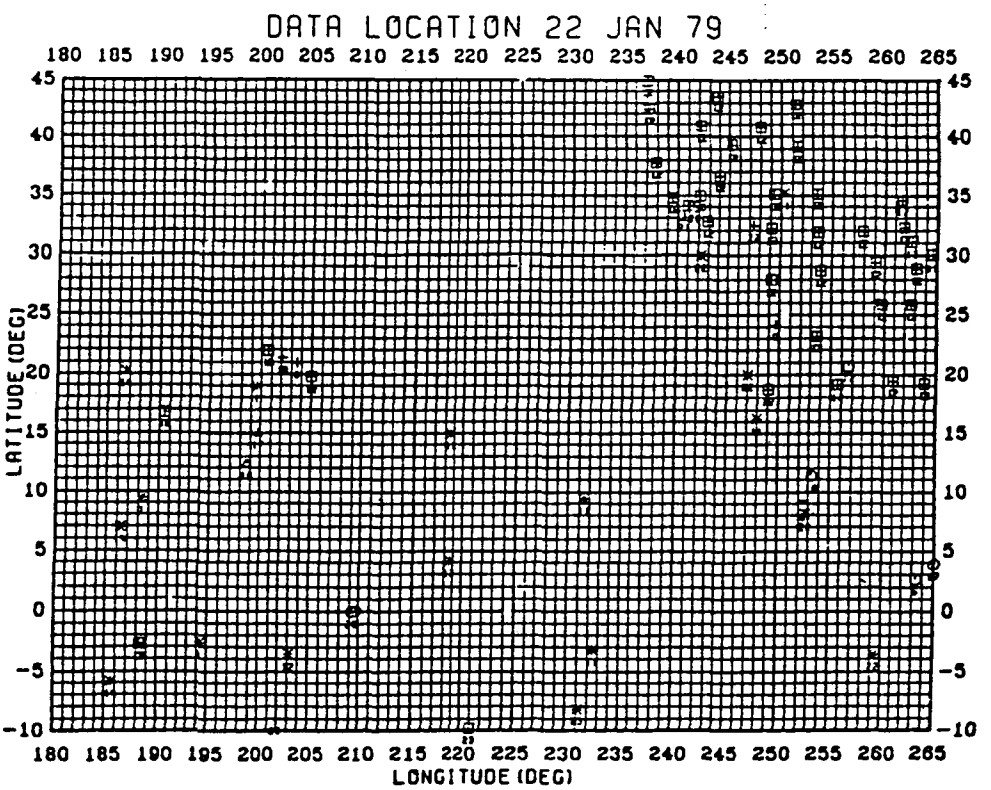

Fig. 6. As in Fig. 5, except for day of minimum coverage.

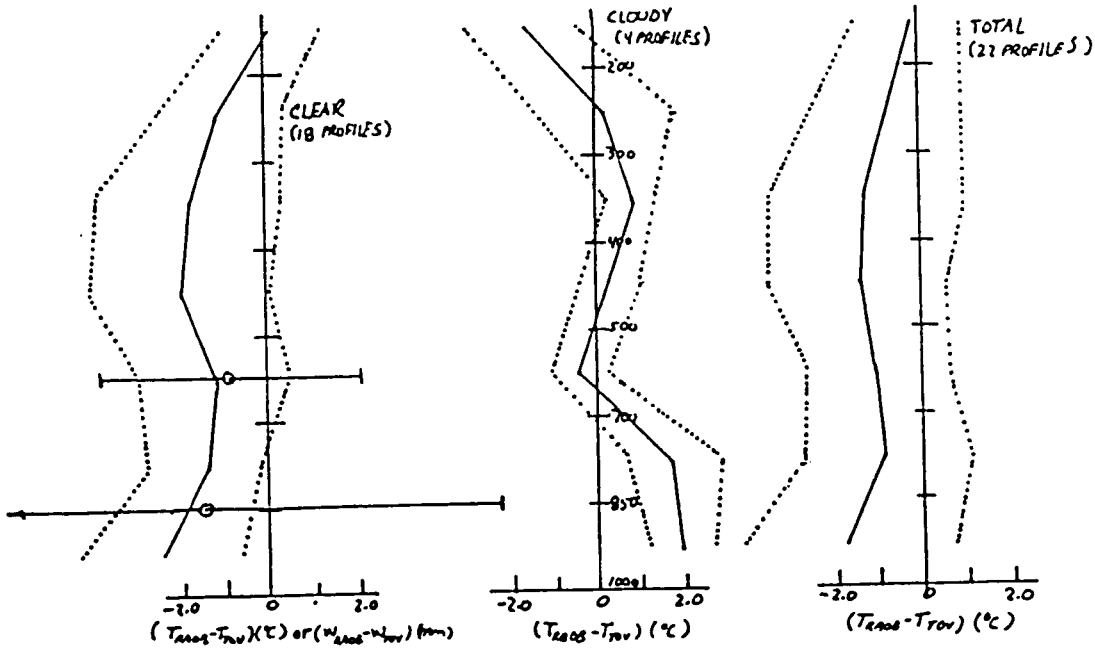

Fig. 7. Mean difference between raob and satellite-derived layer average temperatures for approximately co-located observations (solid lines) for the time period 20-28 Jan. 1979, and over the tropical eastern Pacific. Also shown is the standard deviation of the difference at each layer (dotted line). Clear sky retrievals appear on left; cloudy, microwave-only retrievals in the center, and all retrievals on the right. Precipitable water differences are shown by circles and standard deviations by bars on the leftmost profile.

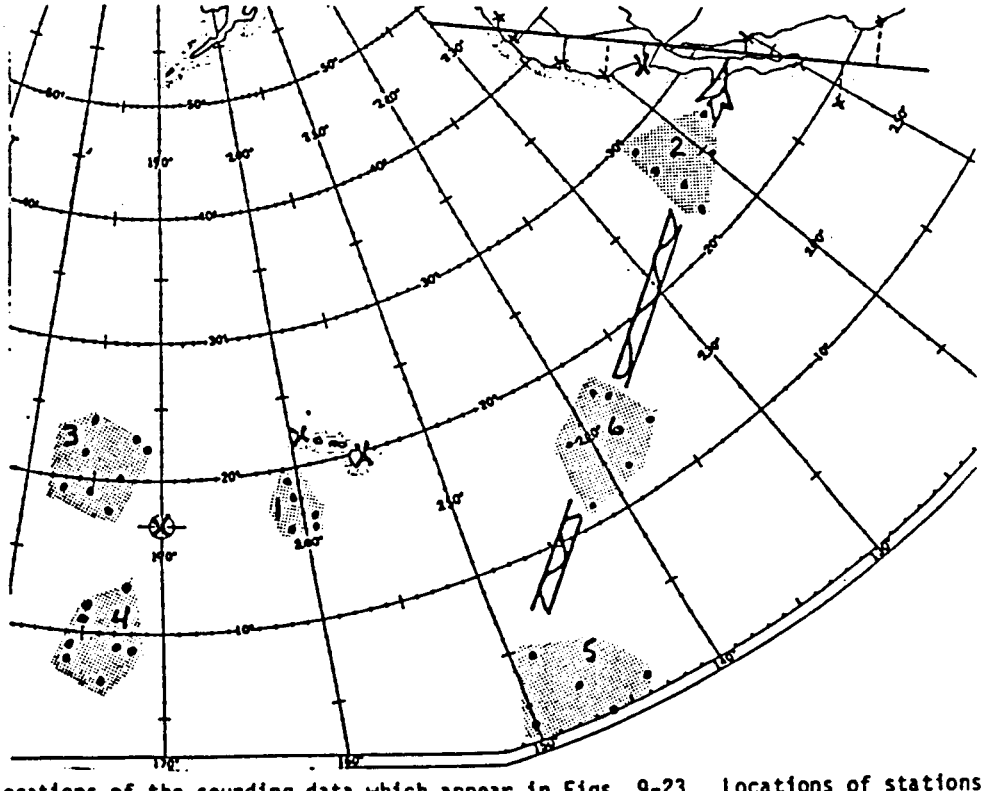

Fig. 8. Locations of the sounding data which appear in Figs. 9-23. Locations of stations for time-section soundings are marked by large X's; marked with small x's are soundings for the sections in Figs. 19-23. Groups of co-located satellite soundings are marked by dots within the shaded regions. The arrow signifies the axis of the two moisture bursts.

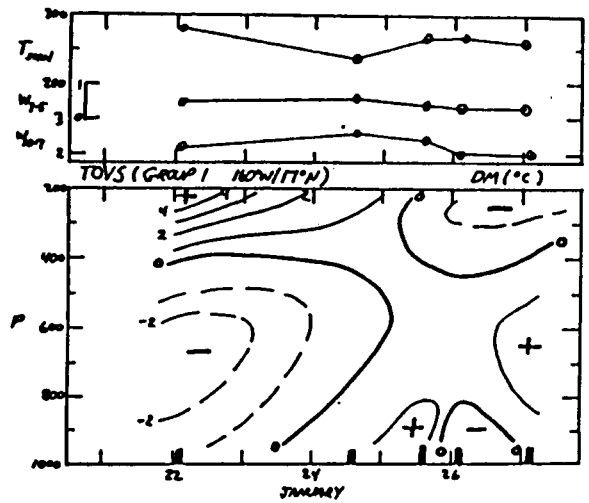

Fig. 9. Time section of TOVS group 1 soundings (see Fig. 8 for location). Data represent temperature deviations (in °C) from the group mean (DM). Upper portion of the figure depicts precipitable water between 1000 and 700 mb and between 700 and 500 mb (in cm) and satellite estimated surface temperature (in K). Solid bars on abscissa indicate actual times of soundings.

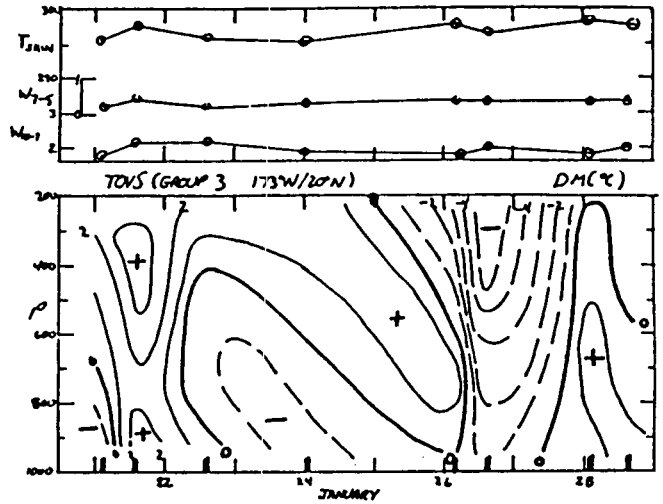

Fig. 11. As in Fig. 9, except for group 3 (see Fig. 8 for location).

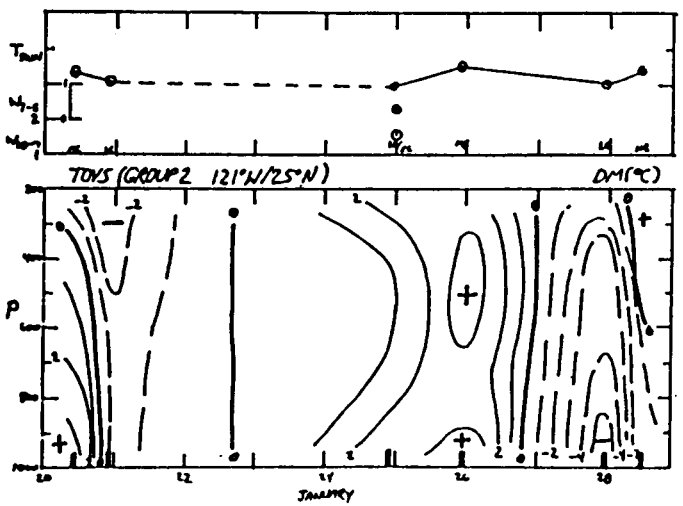

Fig. 10. As in Fig. 9, except for group 2 (see Fig. 8 for location). Letters along abscissa in upper figure denote cloud conditions over location: MC = middle clouds; LC = low clouds; MB = moisture burst; SC = scattered low clouds.

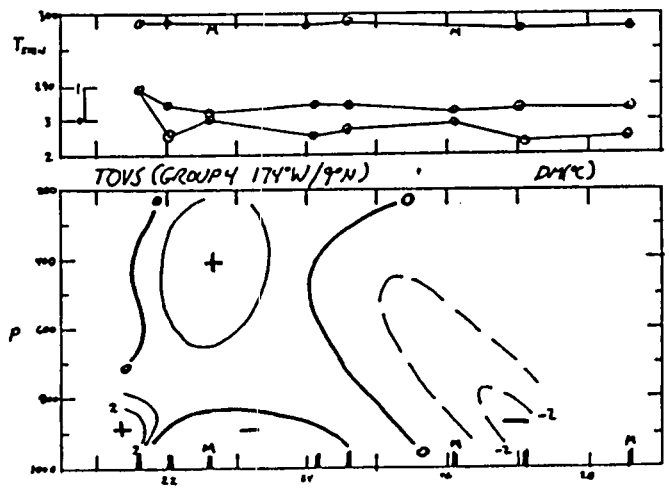

Fig. 12. As in Fig. 9, except for group 4 (see Fig. 8 for location).

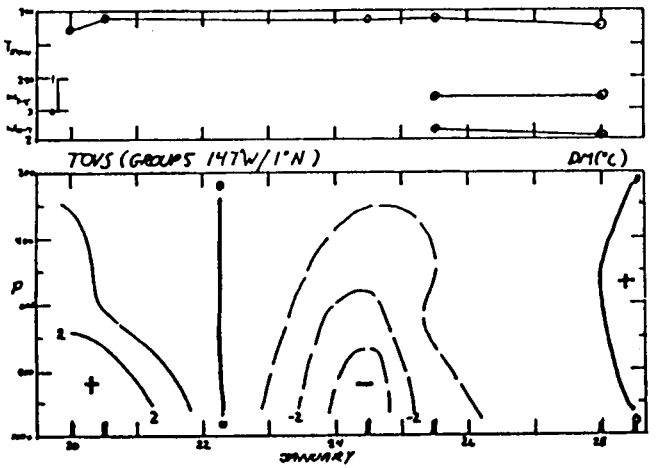

Fig. 13. As in Fig. 9, except for group 5 (see Fig. 8 for location).

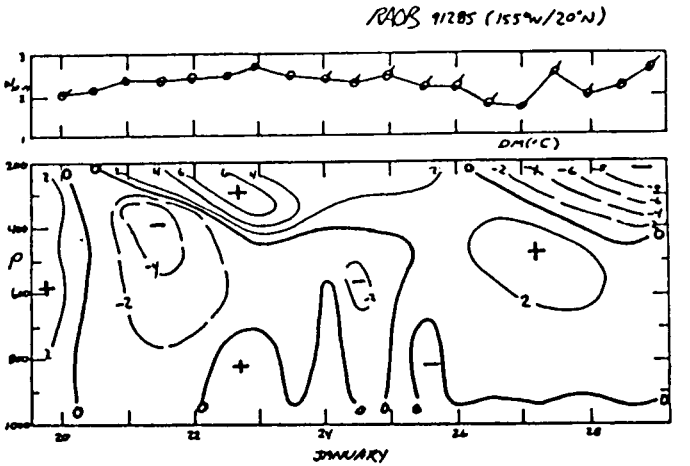

Fig. 15. Layer-averaged temperature sounding for Hilo, given in terms o departure from the time series mean (°C). Upper figure gives time series of precipitable water in the 1000-700 mb layer (cm). Flagged values occur where some layer below 700 mb measured a dew point depression equal to 30°C, i.e., too dry to measure. This station is approximately co-located with group 1 (Fig. 9).

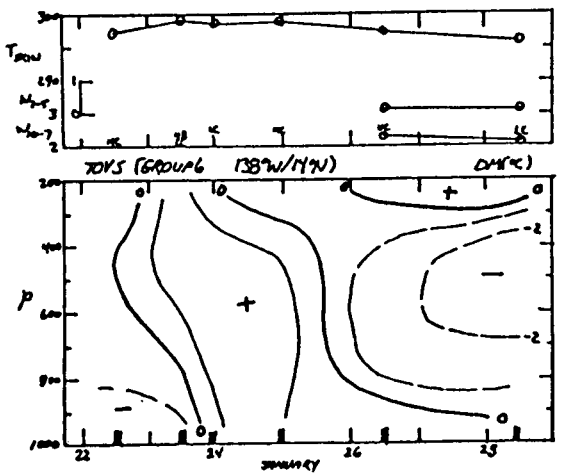

Fig. 14. As in Fig. 9, except for group 6 (see Fig. 8 for location, and Fig. 10 for cloud cover notation).

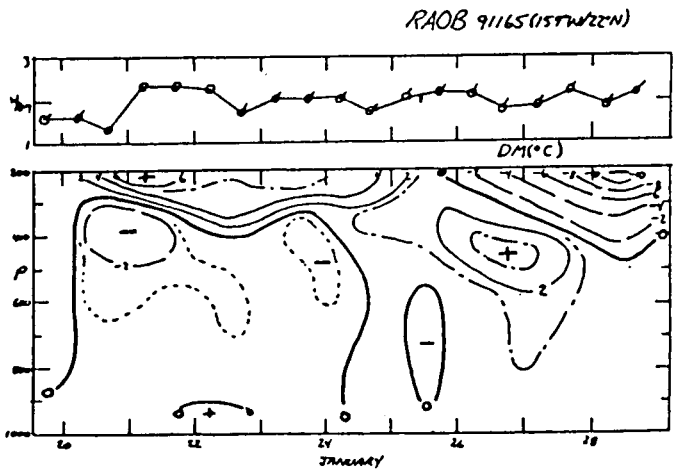

Fig. 16. As in Fig. 15, except that station is Lihue. This station i approximately co-located with Hilo (Fig. 15) and group 1 (Fig. 9).

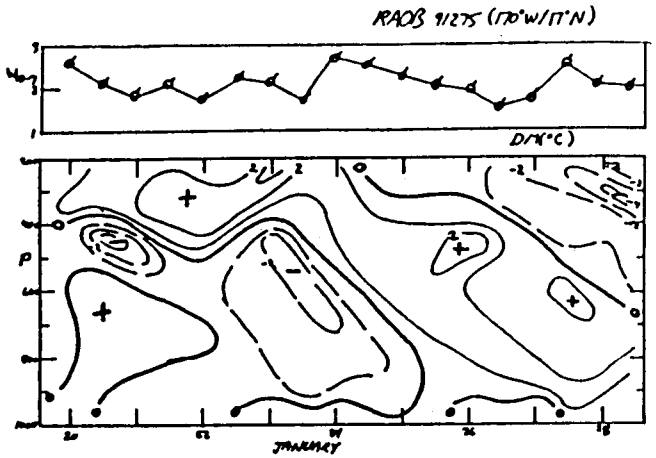

Fig. 17. As in Fig. 15, except that station is Johnston Island. This station is approximately co-located with groups 3 (Fig. 11) and 4 (Fig. 12).

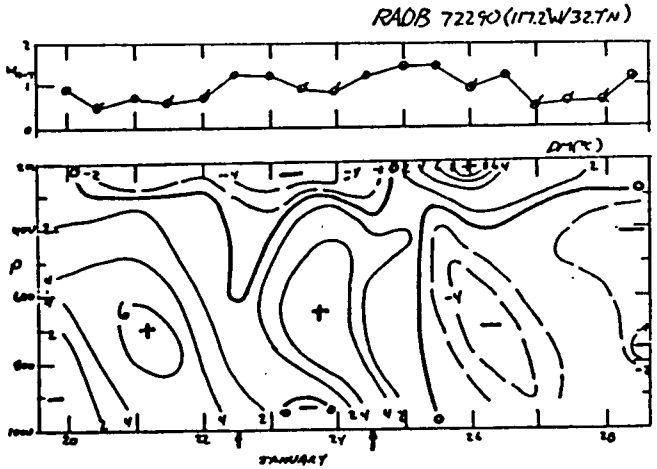

Fig. 18. As in Fig. 15, except that station is San Diego, about 1000 km northeast of group 2.

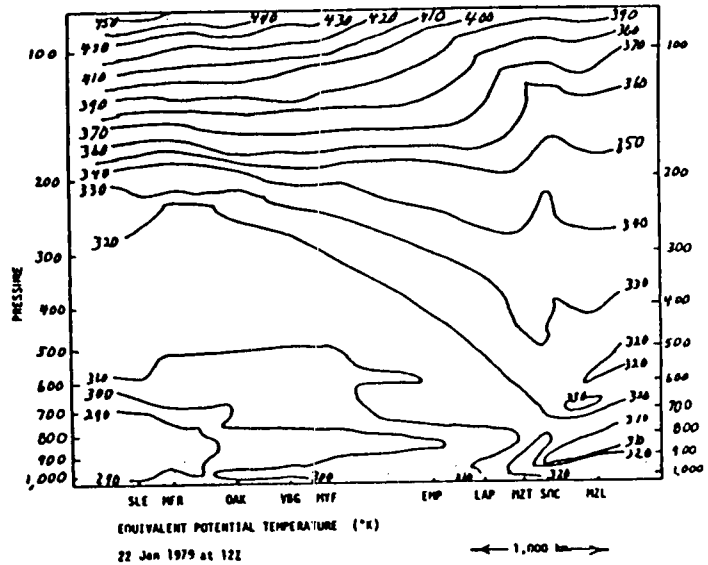

Fig. 19. Cross-section of equivalent potential temperature approximately along the west coast from 20 to 45°N, valid at 12 Z, 22 Jan. 1979.

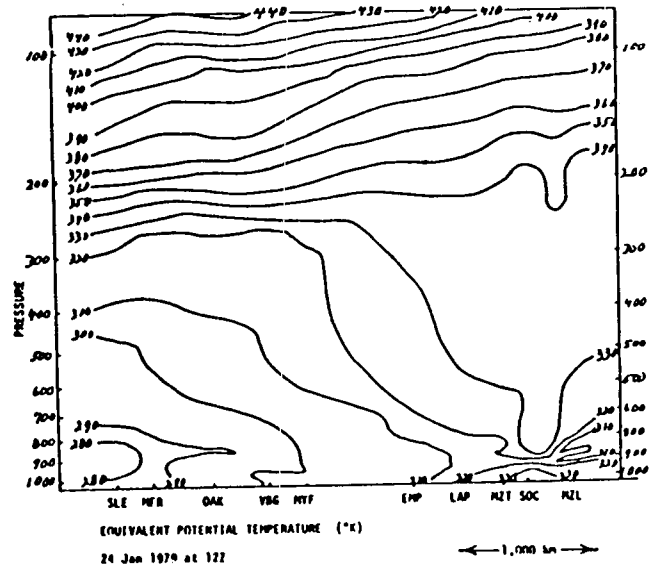

Fig. 20. As in Fig. 19, except valid at 12 Z, 24 Jan. 1979.

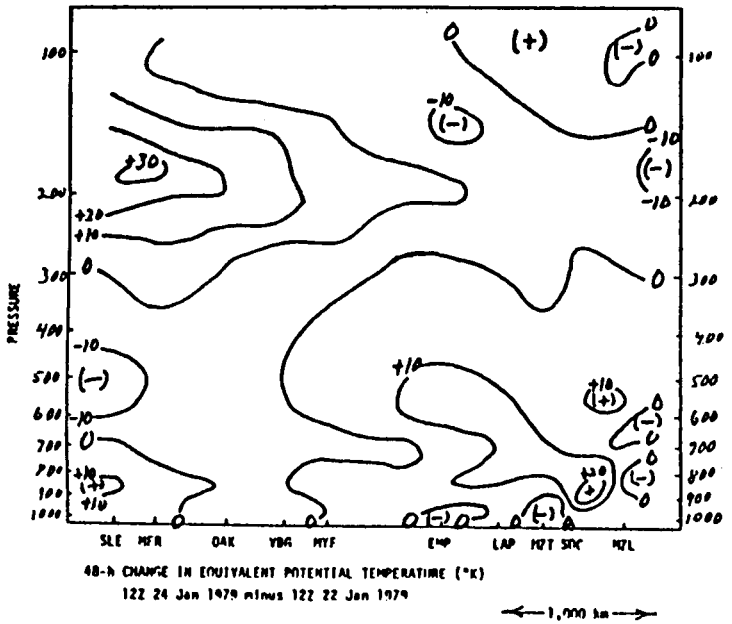

Fig. 21. 48-hour change in equivalent potential temperature, obtained by subtracting the data in Fig. 20 from that in Fig. 21.

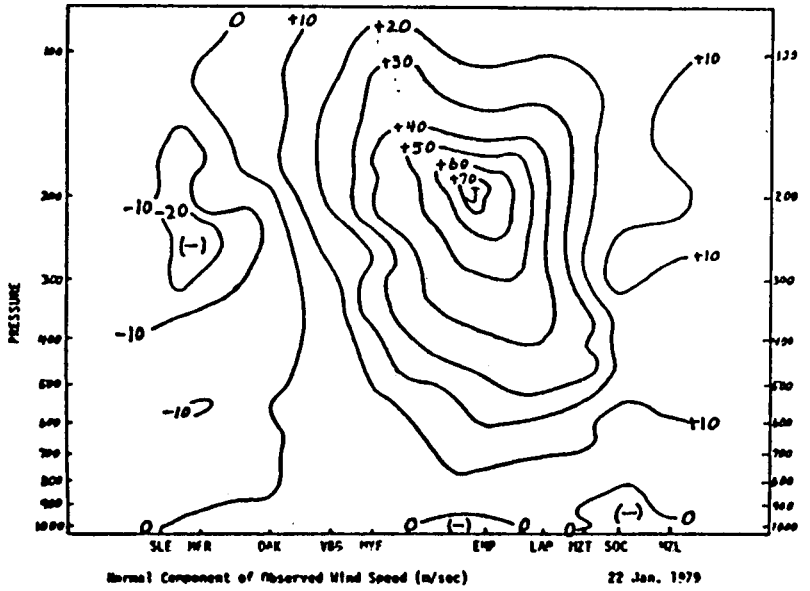

Fig. 22. Isotachs of the wind component normal to the cross-section (positive into the page) for 12 Z, 22 Jan. 1979 (m/sec.). Note the surface easterlies south of San Diego and the easterly wind maximum in the upper troposphere over the northern portion of the section.

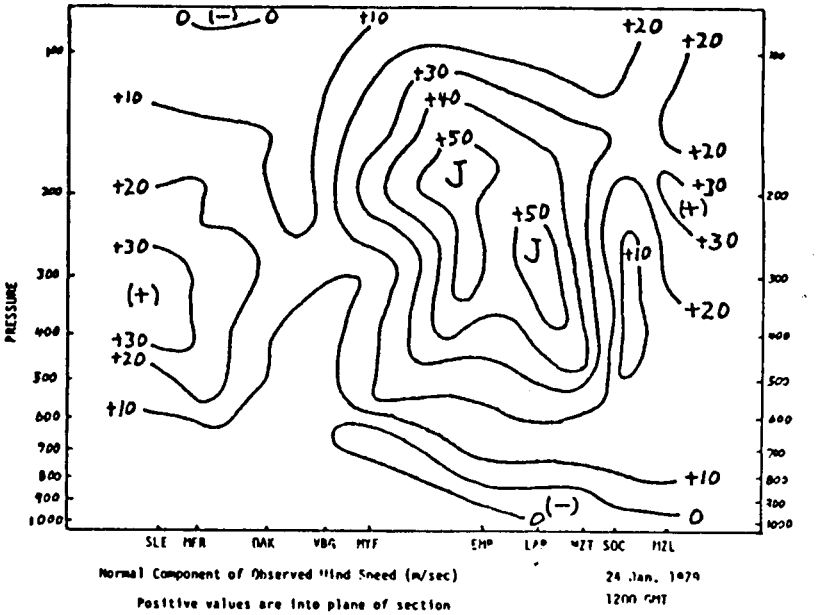

Fig. 23. As in Fig. 22, except for 12 Z, 24 Jan. 1979. Note the broadening of the westerly maximum and the appearance of four discrete maxima.

Paper presented at
15th Technical Conference on Hurricanes
and Tropical Meteorology, American Meteorological Society, Miami, FL, 9-13 Jan. 1984
See pp. 249-255 of Postprint Volume

TRANSIENT TROPICAL DISTURBANCES WITHIN THE PACIFIC HADLEY CELL

James P. McGuirk and Aylmer H. Thompson
Texas A&M University
College Station, Texas 77843-3146

1. INTRODUCTION

The Hadley cell is a statistical composite, averaged over time and longitude. It is the net result of many systems, covering a range of scales from individual convective towers to continental-size monsoonal circulations. Often, over the tropical oceans, an organized band of middle and high level clouds develops in the region of the ITCZ and extends eastwards and polewards for several thousand kilometers into the subtropics. Over the Pacific Ocean the cloud band often sweeps northeastwards across northern Mexico and the southern tier of states. In its fully-developed stage, it is usually associated with the subtropical jetstream and seems to be related to cyclogenesis, particularly east of the Rocky Mountains. We have termed the cloud band a moisture burst, documented its occurrence over three cold seasons, and made use of the detailed data available during the January 1979 FGGE Special Observing Period to investigate the development of two individual moisture bursts.

An example of the progression of the leading edge of the cloud band of a typical burst appears as Fig. 1. This burst originated along the ITCZ at about 4°N and about 155°W between 00 and 15 Z 21 January 1979. The burst occurred during the first FGGE Special Observing Period and constitutes our first case study. The explosive development of this burst is clear in the comparison of the cloud borders on 00 Z 21 and 22 January.

The cloud bands we refer to as moisture bursts have been observed by others—Morel et al. (1978), Davis (1981), and Thepenier and Cruette (1981)—but a description of their origin, structure, and relation to other circulation features has not been developed. Thepenier and Cruette have documented bursts' mid-latitude connections, showing that they are often associated with deep mid-latitude troughs which extend well into the subtropics, and that the cloud band is eventually collocated with the subtropical jet axis. Although they show that the cloud bands often become associated with mid-latitude cyclones, they do not examine the bursts in the origin region over the tropical oceans.

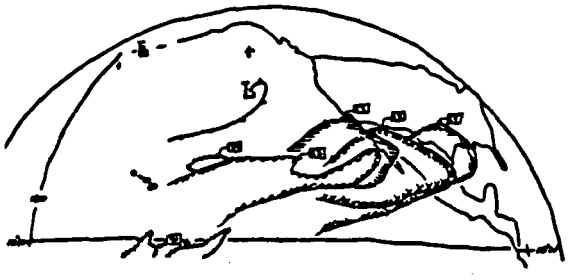

Fig. 1. *Schematic depiction of the time evolution of the high cloud boundary of a moisture burst occurring between 21 and 25 January 1979. Flagged numbers give the date of the associated cloud leading edge.*

Riehl (1981) and Cressman (1981) describe some of the problems with explaining the source of kinetic energy in the origin regions of the subtropical jet. If bursts are associated with jet formation, then it seems essential to understand the triggering mechanisms and development of bursts. Clouds in the region of burst origins sometimes move into the cloud band from the southern hemisphere; often the clouds exhibit jet wind speeds in a nearly meridional direction in the vicinity of the ITCZ. Neither of these observations is consistent with our understanding of the subtropical circulation. The Hadley cell may be, in part, the composite of a large number of bursts. We may be forced to re-evaluate our thinking of this cell as the mean result of a number of synoptic systems, occurring nearly randomly, at least on seasonal time scales, along the ITCZ; the current view of the mid-latitude indirect cell has already undergone this re-evaluation.

2. DATA

The FGGE Special Observing Period provides us with a unique tropical data set with which to analyze eastern Pacific moisture bursts. Using these data, we examine two bursts, commencing on 21 and 25 January 1979. The data include satellite-derived winds, temperatures and radiances; supplementary rawinsondes, dropsondes, and pibals; and an expansion of the operationally-available aircraft, surface and ship reports. In addition to the FGGE set, we examined two six-month sets of GOES infrared imagery and one six-month set of infrared mosaics from NOAA-7. The GOES imagery was used to produce a "climatology" of burst occurrence and the NOAA-7 imagery was used to examine bursts in the context of El Nino. Some properties of these data sets in the context of moisture bursts are described by McGuirk et al. (1984).

3. MEAN BURST BEHAVIOR

An objective definition of a moisture

burst was developed so that quantitative information could be extracted from the GOES imagery. It is based solely on geometric properties to maintain objectivity and to avoid anticipating physical mechanisms or synoptic associations. The definition is summarized in Table I.

Table I

Moisture burst definition.

DEFINITION:

1) A continuous band of upper and middle level clouds;
2) At least 2000 km in length;
3) A cloud source equatorward of 15°N;
4) A cloudband extending poleward of 15°N.

BEGINNING:

Time and date of the first evidence of poleward progression of cloud cover.

ENDING:

Time and date of any of the following:

1) Cessation of convection equatorward of 15°N;
2) A break in cloud cover equatorward of 15°N;
3) A recession of the cloud band equatorward of 15°N.

Based on this definition, 128 moisture bursts were documented during the two six-month cold seasons of 1977-78 and 1981-82 between 160°E and 90°W. The mean distribution of the origin of these bursts as a function of month and longitude is summarized in Fig. 2. The frequency of occurrence is approximately constant west of 120°W and decreases abruptly east of this longitude. Nearly eleven bursts occur in an average month with a minimum in midwinter. Additional important characteristics of the burst are as follows: The average duration is 2.5 days with 20% of the bursts lasting 4 days or longer. Somewhere in the Pacific domain, at least one burst is active about 75% of the time. Approximately one third of the bursts are related to mid-latitude frontal activity, as perceived from GOES imagery; this relation occurs as either a causative mechanism, as a front moves southward into the deep tropics, or can occur as a wave development on a cloud band sometime after its inception. It is likely that most of the cloud bands, not initially related to fronts and the associated jet streams, become associated with mid-latitude synoptic activity after their source region becomes inactive. This occurrance is in accordance with the observations of Thepenier and Cruette (1981). A check of 15 consecutive bursts in January 1979 showed that eleven were accompanied by a mid-latitude trough extending into tropical latitudes (as observed from European Center 200 mb analysis). In four of the five remaining, a weak trough could be inferred from cloud patterns in GOES imagery. Thepenier and Cruette's observation that troughs are associated with fully-developed moisture bursts can be extended backward in time to include the period of burst initiation.

4. BURSTS AND EL NIÑO

The 1982-83 El Niño event was a period in which the tropical circulation was disturbed to an extent unequaled during the modern data-gathering era (Quiroz, [1983]). Examination of the moisture bursts during this cold season allows additional comment on the tropical circulation typical of El Niño, and also raises intriguing questions regarding moisture-burst association with the Hadley circulation.

A distribution of moisture bursts over the time span November 1982 to April 1983 was prepared similarly to the procedure above. Due to the premature failure of GOES, it was necessary to use mosaics prepared from the polar-orbiting NOAA-7. The photo reproductions were of slightly lower quality than our GOES archive and were available at only 12-hour intervals instead of 6. Nevertheless, reliable information was obtained. A summary of burst activity during the El Niño cold season appears in Fig. 3, which has the same format as Fig. 2. The difference in behavior from "climatology" is immediately apparent. Fewer bursts occurred in 1982-83, particularly in March

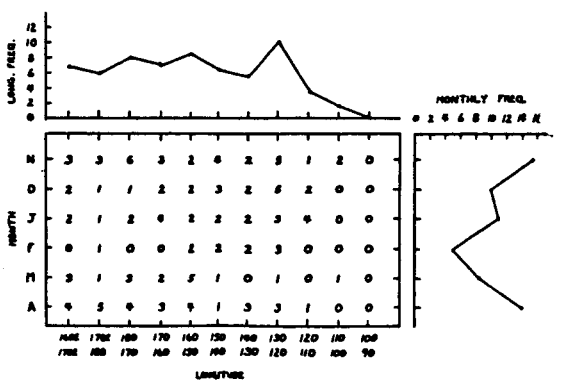

Fig. 2. *Distribution of the occurrence of moisture bursts as a function of longitude of origin and month. Numbers in the tabulation give twelve-month totals; curves give cold season or monthly average.*

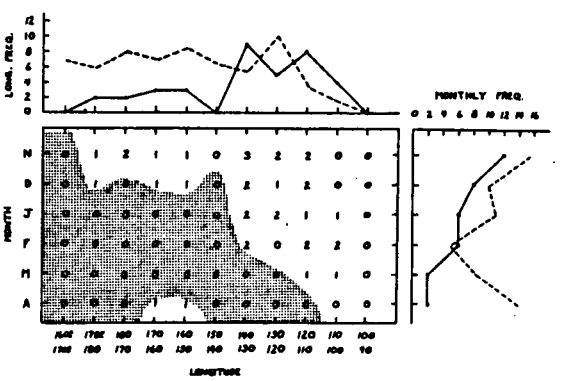

Fig. 3. *As in Fig. 2, except for the 1982-83 El Niño year. Dashed lines from Fig. 2 are for reference. Shaded area emphasizes the mid-Pacific quiescent region.*

and April; only six bursts occurred per month, on average, compared with a "normal" eleven. Few bursts occurred west of 140°W, with a large number of bursts occurring in the normally quiescent region east of 110°W. Most of the winter bursts occurred almost continuously in the narrow longiture band between 135°and 105°W. After the break of El Niño in late December, burst activity disappeared from the central Pacific for several months; see the shaded region of Fig. 3. Because 1982-83 bursts last about as long as climatologically expected, their infrequency results in extended periods of time during which no burst is active anywhere in the Pacific domain: 59% of the time quiescent compared to only 25% in the "climatology."

We thus observe a curious feature of the 1982-83 winter Hadley circulation. Associated with the El Niño, anomalously warm surface waters spread eastward from the dateline, with temperatures exceeding 29°C. With this warm water, the ITCZ convective activity became tremendously strengthened, between 150°E and 100°W. Outgoing Longwave Radiation (OLR) anomalies, a good measure of ITCZ convection, exceeded -80°W/m^2, with mean values more typifying the Indian summer monsoon. The OLR fields also show a broad maximum centered at about 20°N, indicative of enhanced cloud-free subsidence all the way across the Pacific. The high and low OLR anomalies are both consistent with enhanced Hadley circulation. See the data collection by Arkin et al. (1983) for further details. In spite of the anomalously active ITCZ, burst activity decreased considerably and adjusted its spacial distribution to fit the warm SST anomalies. In general, the burst activity was centered more closely at the region of maximum SST anomaly and not at the region of maximum SST.

Apparently, increasing the strength of the ITCZ is not sufficient to guarantee the enhancement of moisture burst activity. Secondly, it is possible to increase the apparent strength of the Hadley cell without increasing that component of it which is controlled by burst activity. Finally, the increase in strength of North American West Coast storm activity and its accociation with moisture burst activity during the El Niño year was not related to the frequency of bursts although it was related to their origin region and intensity of individual systems.* It seems clear that something more than merely a warm ocean and a weakened Walker circulation is required in the vicinity of the ITCZ to generate a moisture burst.

5. A MOISTURE BURST CASE STUDY

In an effort to understand the triggering of moisture bursts and the coupling of the tropics and mid-latitudes by means of moisture bursts, we have begun a case study of a pair of bursts occurring in January 1979. See Fig. 1 for the leading edge cloud boundary of the first event. This burst developed explosively along the ITCZ, spreading a band of clouds northeastwards for over 4500 km in less than 12 hours. Some of this development must have occurred simultaneously along the burst axis. The clouds then were advected northeastwards from the 22nd to the 25th by which time the leading edge had passed Louisiana. Eastwards of 120°W it was associated with the sub-tropical jet.

What follows is an enumeration of the findings based on analysis of the FGGE data. An attempt to integrate these observations into a complete explanation is premature at this time.

5.1. West Coast Structure

Sufficient rawinsonde stations exist along the west coast of North America to allow examination of the cross-sectional structure of the developed moisture burst as the leading edge of the cloud band crossed land (see Fig. 1). Figs. 4(a) and 4(b) depict cross sections of equivalent potential temperature (θ_e) 48 hours apart, bracketing the motion of clouds through the section.

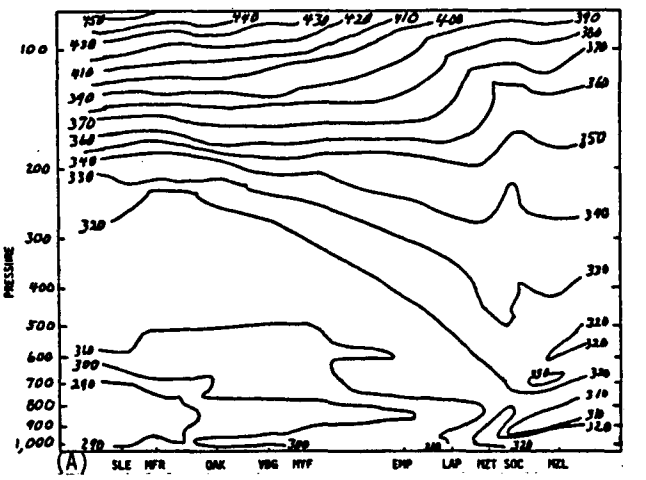

Fig. 4(a). *Cross-section of equivalent potential temperature, approximately along the west coast of North America from 20°N (to the right) to 45°N, valid at 12 Z, 22 January 1979. Isotherms in °K.*

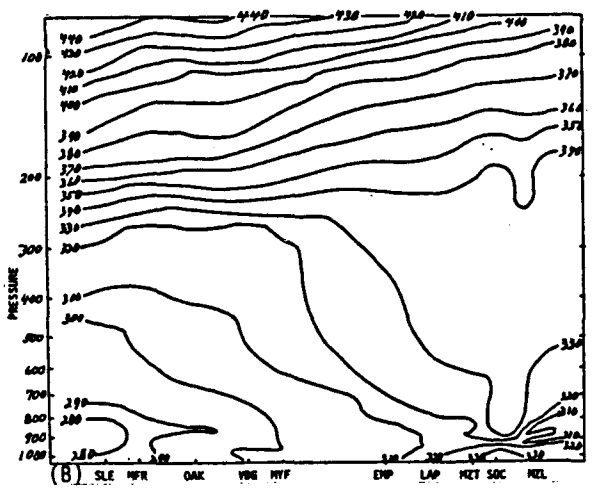

Fig. 4(b). *As in (a), except at 12 Z, 24 January 1979.*

* A. V. Douglas and P. Englehart, 1983: Factors leading to the heavy precipitation regimes of 1982-83 in the United States and Mexico, presented at the 8th Climate Diagnostics Workshop, Toronto, October 17-21.

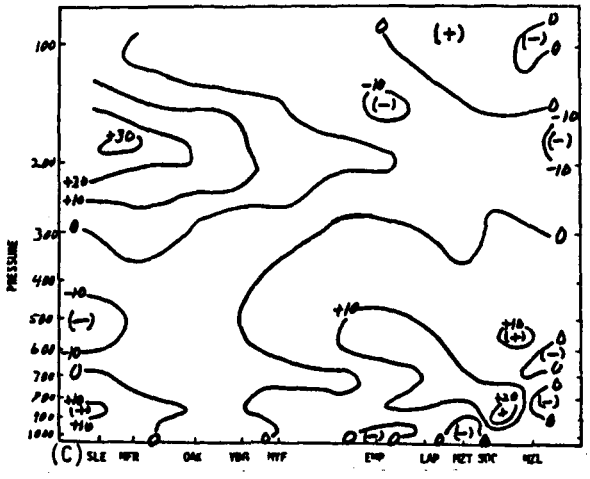

Fig. 4(c). *The arithmetic difference between* (a) *and* (b), *in* °C. *Positive values denote warming.*

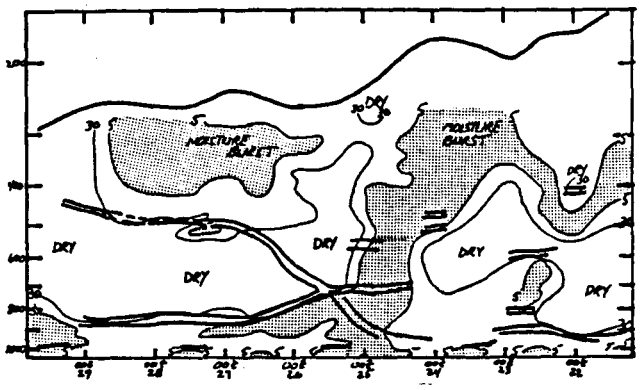

Fig. 5. *Time section of dewpoint depression at Empalme, over which both bursts passed. Light lines give 5 and 30°C depressions. Shading denotes depressions less than 5°C. Heavy lines denote stable layers, inversions, and tropopause, as depicted by the temperature field (not shown).*

Fig. 4(c) shows Fig. 4(b) minus Fig. 4(a). The following points bear emphasis:

a) The increasing horizontal gradient of θ_e due to both temperature and humidity changes, but due primarily to moistening south of LaPaz;

b) Destabilization of the lower- and mid-troposphere south of Mazatlan;

c) The upper tropospheric warming north of Empalme due to the continuous lowering of the tropopause;

d) The strong mid-tropospheric cooling north of San Diego (MYF in Fig. 4) of over 10°C, centered at 500 mb;

e) The associated weakening and southward spreading of the jet maximum from 70 m/sec on the 22nd to 50 m/sec on the 24th at 200 mb (figure not shown).

A further examination of the changes in vertical structure is shown in Fig. 5, a time section at Empalme. The heavy lines delineate stable layers and inversions derived from temperature data (isotherms are not shown), and the light lines are isopleths of dew point depression. In this figure appears:

a) Moist convection with a top at 600 mb on the 22nd, at the same time the leading edge of the moisture burst between 400 and 300 mb passed Empalme;

b) A moistening of the entire troposphere on the 24th, just before the burst passed out of the Empalme region;

c) Strong evidence of moist convection at least as high as 400 mb at Empalme on the 24th;

d) Sporadic stable layers above the trade wind inversion throughout the duration of the first moisture burst;

e) No evidence of large-scale frontogenesis at Empalme although the lapse rate becomes somewhat more stable below 500 mb;

f) The likely passage of a surface front at about 00 Z on the 25th, just ahead of the second moisture burst aloft (although the front is supported by the thermal field at midlevels, no evidence is found in the continuously dry air between 700 and 500 mb);

g) An unusual moist region below the 500 mb inversion on the 27th.

The time section in Fig. 5 suggests that the two fully-developed moisture bursts appear to be very different entities as they enter North America. The first burst shows little frontal character, in spite of the increase in horizontal gradients shown in Fig. 4. The second burst seems to be strongly associated with a moving cold front and seems to have no signal below 550 mb except a slight cooling of the atmosphere expected with the frontal passage.

5.2 Subtropical Pacific Structure

These bursts can be examined over the subtropical Pacific with the aid of satellite-derived soundings (TOVS) from the FGGE data archive. A time series of soundings (with time increasing to the right) centered at 25°N and 121°W appears in Fig. 6; this location is on the northwestern edge of the first burst and directly under the second. Also shown in Fig. 6 is a similar time series of rawinsonde data at San Diego, 900 km to the northeast. Both of these time sections are plotted in terms of departures from the section mean. Available moisture data are not discussed.

Though more numerous than radiosondes, the satellite soundings are not as detailed; in addition, in the presence of clouds, different retrieval procedures are employed and these soundings are biased differently than clear sky retrievals. A collocation study of radiosonde and satellite soundings over the Pacific during this period show that the clear-sky TOVS are sytematically cold

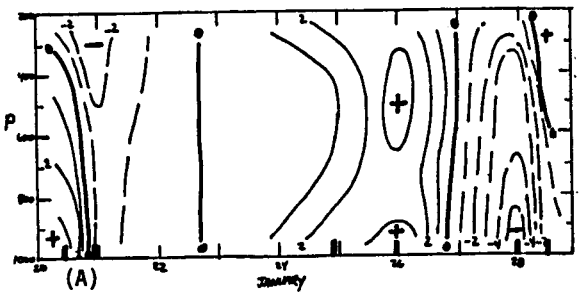

Fig. 6(a). *Time section of satellite-derived temperature (with time increasing to the right) located approximately at 25 N and 121 W. The isotherms are departures from the section mean at each pressure level in C.*

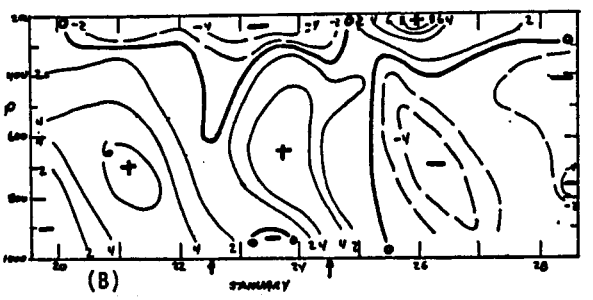

Fig. 6(b). *As in* (a), *except the data are from rawinsondes at San Diego.*

and dry and the cloud contaminated TOVS are systematically warm. See McGuirk et al. (1984). These biases are different than indicated in previous reports; see Schlatter (1981), for example.

Satellite time section reveals the following points:

a) The satellite shows large temperature changes as the bursts pass, but the changes are of uniform sign throughout the troposphere;

b) Cooling is observed before the burst erupts and then warming occurs as the cloud band passes on the 21st and again on the 26th;

c) For both bursts, the cooling occurs with a maximum at the surface.

The rawinsonde section for San Diego shows the following:

d) Temperature changes are similar in the upper troposphere, except they are much larger than the satellite-observed values;

d) In the lower troposphere, temperature changes occur with signs opposite to those of the upper troposphere.

It is uncertain whether the burst behavior is different over the ocean and over San Diego. The burst is not completely an advective effect; the first burst erupted as a band of clouds extending from nearly 160°W along the ITCZ at 3°N between 00 and 15 Z on the 21st. For clouds to have moved from the origin to the coast of Baja California, they would have had to average 80 m/sec, even in the vicinity of the equator; there is no evidence of these speeds. The clouds more-likely appeared nearly simultaneously along a long stretch of the moisture axis. Thus, continuity of structure between the TOVS location and San Diego is not essential. Secondly, only one of the TOVS retrievals was not cloud contaminated, and a four-day gap appeared in the TOVS time section during the period of the first burst.* Finally, careful analysis is being initiated to determine the ability of satellite to properly represent atmospheric structure in this normally data-sparse area of the tropical Pacific.

5.3 Equatorial Structure

Moisture bursts' variation with the El Niño event calls to question what kind of feature can trigger the bursts. Although a definitive answer is not yet available, certain observations are apparent. As previously mentioned, bursts are normally associated with troughs extending southward out of the northern mid-latitudes; however, bursts are not often triggered by obvious frontal interactions.

200 mb wind fields prepared by the European Center indicate a weak trough, centered at about 165°W extending as far southward as 12°N on the 20th. The trough intensified and extended southward, so that by 00 Z on the 22nd, when the burst had already appeared, the trough could be seen at 8°S. The burst occurred in the region of the southwesterly jet associated with this trough. At the same time this trough amplified, a southern hemispheric disturbance at 145°W intensified, so that by 00 Z on the 22nd, strong southerlies existed from 30°S, streaming across the equator between 130 and 150°W. On the equator itself, a southerly jet of 25 m/sec was observed. If this wind maximum is associated with the subtropical jetstream, it does not fit the customary model. Huang and Vincent (1983) show that these cross-equatorial southerlies were a persistent feature for at least ten days before the burst.

Anomalous flows also occurred in the lower atmosphere. Figs. 7(a) and 7(b) show the satellite-derived cloud-tracked winds before and during the first burst. Cloud boundaries encircle clouds above 770 mb and thick arrows indicate additional rawinsonde and pibal data. The northeasterly tradewinds north of the equator are close to climatology. The easterlies on the equator between 210 and 235°E are also climatologically expected; however, the enhanced cloudiness in this region is associated with a westward moving wave centered on the equator and moving only a few meters per second. The unusual feature of both wind fields is the equatorial westerlies between the dateline and 210°E. These westerlies cannot be observed in the satellite data of the 20th because of the presence of shielding middle and high cloudiness. On the 24th, westerlies extended at least as far as 5°N and 207°E. These westerlies can be explained by two features. First, if the South

* The FGGE satellite archive available through NCAR is an abridged set, and this type of gap will be eliminated using the full FGGE set available through the World Data Center.

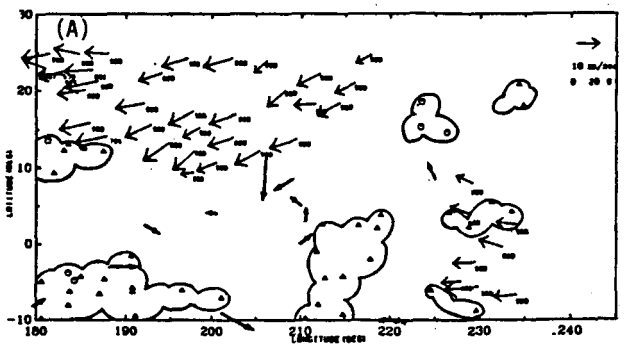

Fig. 7(a). *Satellite-derived winds based on cloud motions below 770 mb observed at 0C Z 20 January 1979. Speed scale is in upper right hand corner. Thick arrows denote auxilliary 850 mb pibal winds. Scalloped lines depict cloud boundaries for middle and high clouds.*

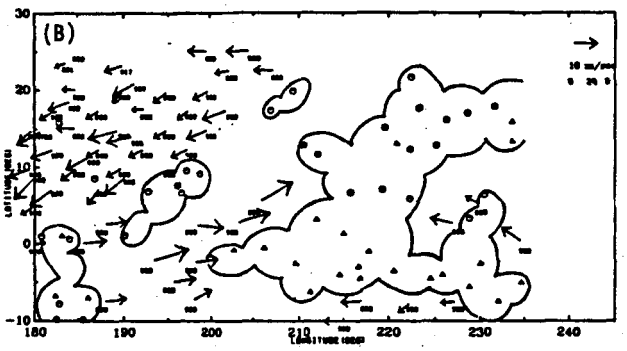

Fig. 7(b). *As in* (a), *except for 24 January 1979.*

Pacific Convergence Zone (SPCZ) extended some 40° farther east than its climatologically-expected eastern margin, westerlies would result (Atkinson and Sadler, [1970]). Unfortunately, Huang and Vincent's (1983) analysis shows no evidence of these westerlies, even though they show that the SPCZ was displaced far east of its normal position. Second, a wave centered at about 10°S was observed to move eastward at about 15 m/sec; the middle and high clouds are associated with this wave. Both of these low-level waves are easily identified on NMC low-level satellite-wind analyses.

As these two low level waves approached each other, an interesting feature occurred. While they were well-separated, the clouds associated with them remained in the vicinity of the ITCZ. The moisture burst erupted explosively when the two waves approached and became indistinguishable from each other.

It is not clear what role these two disturbances played in the triggering of the moisture burst. On the other hand, the disturbances and the change of burst frequency during El Niño indicate that certain kinds of disturbances along the ITCZ are necessary for moisture bursts. Without them, the Hadley cell can be very active, but bursts and the concomitant coupling between the tropics and the midlatitudes will not be observed.

6. CONCLUSIONS

Moisture bursts exist and constitute a typical behavior along the ITCZ. The bursts are synoptic in both length scale and duration. They occur anywhere along the Pacific ITCZ but general circulation anomalies--El Niño--can modify their occurrence immensely.

Satellite and FGGE special data can be used to investigate individual bursts, but the data quality and frequency is still far short of optimum. The two bursts studied are both related to, and different from, frontogenesis. The largest changes downstream of the origin region on the ITCZ include upper tropospheric warming, southward expansion of the subtropical jet, and moistening and destabilization of the troposphere south of the jet core.

In the origin region, the triggering of the observed bursts are related to upper level troughs from the northern mid-latitudes, strong cross-equatorial flow at 200 mb from the southern subtropics, and both eastward and westward moving disturbances in the lower troposphere. Anomalous lower tropospheric equatorial westerlies occurred directly east of the point of origin and extended underneath the cloud band as it extended northeastwards from the ITCZ.

7. ACKNOWLEDGEMENTS

The authors acknowledge the financial and technical support of NASA's George C. Marshall Space Flight Center under contract No. NAS8-35182. We also acknowledge the data analysis of our colleagues L. L. Anderson Jr., N. R. Smith, and P. E. Riba.

8. REFERENCES

Arkin, P. A., J. D. Kopman, and R. W. Reynolds, 1983: 1982-83 El Niño/Southern oscillation event quick look atlas, NOAA/NWS/NMC/CAC, Washington, D.C. 20233.

Atkinson, G. D., and J. C. Sadler, 1970: Mean-cloudiness and gradient-level-wind charts over the tropics, Air Weather Service, Tech. Rept. 215, 48 pp.

Cressman, G. P., 1981: Circulations of the west Packfic jet stream, Mon. Wea. Rev., 109, 2450-2462.

Davis, N. E., 1981: NETEOSAT looks at the general circulation: III. Tropical-expratropical interaction, Weather, 36, 168-173.

Huang, H., and D. G. Vincent, 1983: Major changes in circulation features over the South Pacific during FGGE, 10-27 January 1979, Mon. Wea. Rev., 111, 1611-1618.

McGuirk, J. P., A. H. Thompson, L. L. Anderson, and N. R. Smith, 1984: Reliability of circulation statistics over the tropical Pacific Ocean based on FGGE data, Proc., 8th Climate Diagnostics Workshop, Toronto, October 12-16, 1983.

Morel, P., M. Desbois, and G. Szejwach, 1978: A new insight into the troposphere with the water vapor channel of Meteosat, Bul. Am. Met. Soc., 59, 711-714.

Quiroz, R. S., 1983: The climate of the "El Niño" winter of 1982-83--A season of extraordinary climate anomalies, Mon. Wea. Rev., 111, 1685-1706.

Riehl, H., 1981: The limits of the subtropical jet stream, Contrib. Atmos. Phys., 54, 335-351.

Schlatter, T. W., 1981: An assessment of operational TIROS-N temperature retrievals over the United States, Mon. Wea. Rev., 109, 110-119.

Thepenier, R., and D. Cruette, 1981: Formation of cloud bands associated with the American subtropical jet stream and their interaction with midlatitude synoptic disturbances reaching Europe, Mon. Wea. Rev., 109, 2209-2220.

COSPAR-JUNE 84
PAPER 4.6.1
BASIC VARIABLES

Presented at COSPAR Symposium on Space Observations for Climate Studies, Graz, Austria, 25-29 June, 1984. Also published in Adv. Space Res., Vol. 5, No. 6, pp. 45-48.

SATELLITE-DERIVED SYNOPTIC CLIMATOLOGY IN DATA-SPARSE REGIONS

J. P. McGuirk, L. L. Anderson, Jr. and A. H. Thompson

Department of Meteorology, Texas A&M University,
College Station, TX 77843, U.S.A.

ABSTRACT

Synoptic-scale "moisture bursts" are defined, based on infrared GOES imagery, and their synoptic climatology is developed. Quantitative analysis of satellite-derived individual channel radiance data and vertical eigenfunctions of complete channel data yield rich structural detail; these details do not appear in FGGE analyses in regions void of conventional meteorological data.

INTRODUCTION

Tropical circulation has been characterized as steady, sluggish, and dominated by convective-scale events. Modern evolution of satellite observing systems has demonstrated the richness and frequency of larger-scale circulation systems. Sophisticated analysis procedures have contributed to the interpretation of diverse data sets, and have even made extrapolation into data-sparse regions possible. These satellite-observed weather systems can be classified in a synoptic climatology sense, and their mean structures deduced.

One stumbling block in the analysis and classification is the proper interpretation of the various forms of satellite data. Satellite imagery generally is used only to delimit cloudy and moist areas. Both temperature reconstruction /1/ and wind computations /2/ possess serious biases dependent on the synoptic behavior they try to quantify. Temperature and moisture reconstructions in the vertical are smoothed both by the satellite measurement capability and by the statistical retrieval techniques invoked. In data-sparse regions in the tropics, four-dimensional analysis schemes introduce large, and uncertain, errors /2,3/. We present an example of a type of tropical synoptic system, outline how its climatology is established from satellite imagery and introduce two quantitative satellite-analysis procedures to summarize the system's thermodynamic structure.

QUALITATIVE METHODS

Often bands of middle and high cloud move out of the ITCZ, extending thousands of kilometers northeastward into the midlatitudes /4,5/. These synoptic-scale systems, when fully developed, are typically linked with the subtropic jetstream. An example of the event, called a "moisture burst", appears in Fig. 1. Its behavior can be rigorously documented through satellite infrared imagery by a judicious definition of its typical appearance. The key

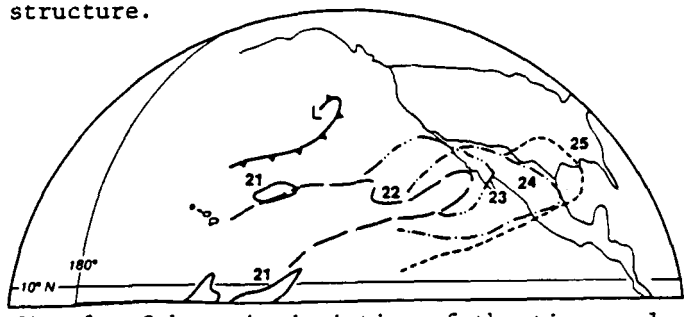

Fig. 1. Schematic depiction of the time evolution of the high-cloud leading-edge of a moisture burst occurring between 21 and 25 January 1979. Numbers give the date.

elements of the burst definition, applied to infrared GOES West imagery, are: (1) continuous high- or mid-level cloud band (detected from images of false-color brightness temperatures), (2) at least 2000 km in length, (3) source equatorward of 15°N, and, finally (4) extends poleward of 15°N. It begins when a cloud mass is first detected in the burst's source region and terminated when one of the four criteria above is violated. This definition can be extended by including other qualitative satellite products, though these procedures are not discussed herein.

Based on this definition, 124 moisture bursts over the central and eastern tropical Pacific Ocean were documented during the 1977-78 and 1981-82 cold seasons. The synoptic climatology of these events, Fig. 2, summarizes their frequency and distribution with longitude and time of year. About ten bursts per month occur with a relative minimum frequency in mid-winter. They appear uniformly across the Pacific from 150°E (the western limit of the GOES field of view) to 120°W; their frequency decreases sharply eastward of 120°W. Their mean duration is 2.5 days with about 25% of them lasting 4 days or longer. With more years of data, the variation of this synoptic event can be linked to variations in planetary-scale forcing; for example, preliminary work indicates a marked decrease in moisture burst frequency during El Niño.

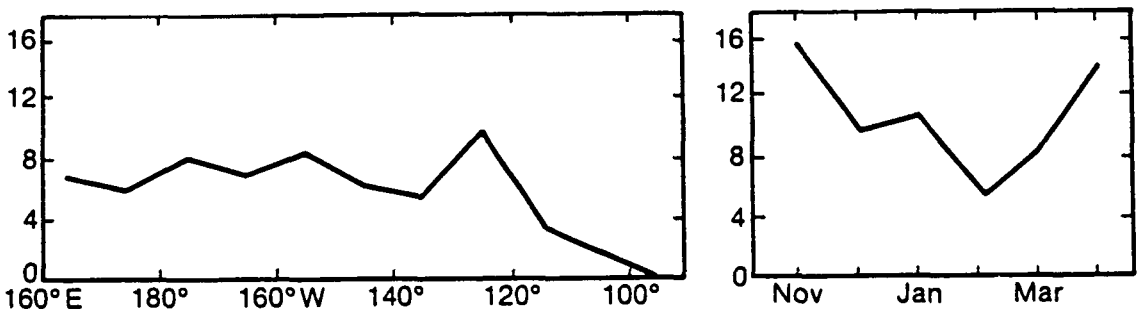

Fig. 2. Frequency of moisture bursts. The average number of bursts per six-month cold season occurring per 10° longitudinal sector (left); the average number of bursts occurring between 160°E and 100°W per month (right).

Fig. 3 summarizes the vertical moisture and stability distribution, as depicted by radiosonde data, of a pair of bursts as they cross the west coast of North America. Of particular interest is the high variability in the vertical distributions. The burst is apparently much more than a passive tracer marking the subtropical jet axis. In fact, as indicated in the time section, the two bursts have very different structures: the first, moist throughout the troposphere and accompanying frontogenesis; the second, essentially dry below 400 mb and above the boundary layer.

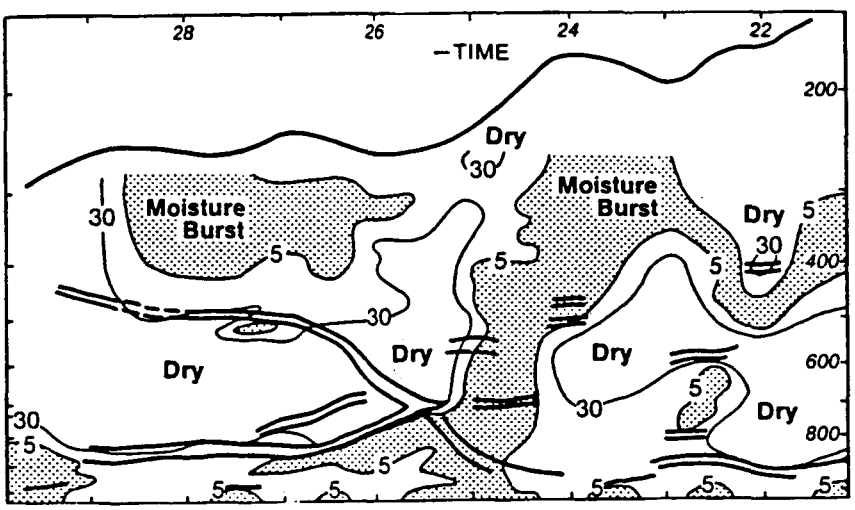

Fig. 3. Time section of moisture and stability at Empalme, Mexico during January 1979, as two bursts passed over the radiosonde station. Thin lines represent the 5 and 30°C dew point depressions, with the shading giving nearly saturated regions. Heavy lines give temperature inversions.

QUANTITATIVE METHODS

To minimize the aforementioned vertical smoothing of satellite radiance data, we propose to examine the horizontal structure of satellite radiances (reduced to equivalent brightness temperatures) before these data are processed into vertically-reconstructed soundings /6/. Two products have been prepared.

The first, Fig. 4 is the horizontal distribution of brightness temperatures of an individual spectral channel from TIROS-N. The channel is a microwave one with peak energy contribution from near the surface, decreasing to 50% at about 700 mb. The heavy arrow represents the moisture burst axis. The strong gradient in signal in the northeast corner is spurious and due to the emissivity differences between ocean and land surfaces. The three warm cores along the axis infer warm regions close to the surface and an absence of deep cloud layers. A second channel, not shown, suggests that the warm cores appear under a cold trough extending southward across the equator at 700 mb. The reason for, and meaning of, these warm cores is unclear, but they do not appear in the FGGE gridded analyses. Thus, Fig. 3 exhibits a richness of structure which does not appear in current analysis products.

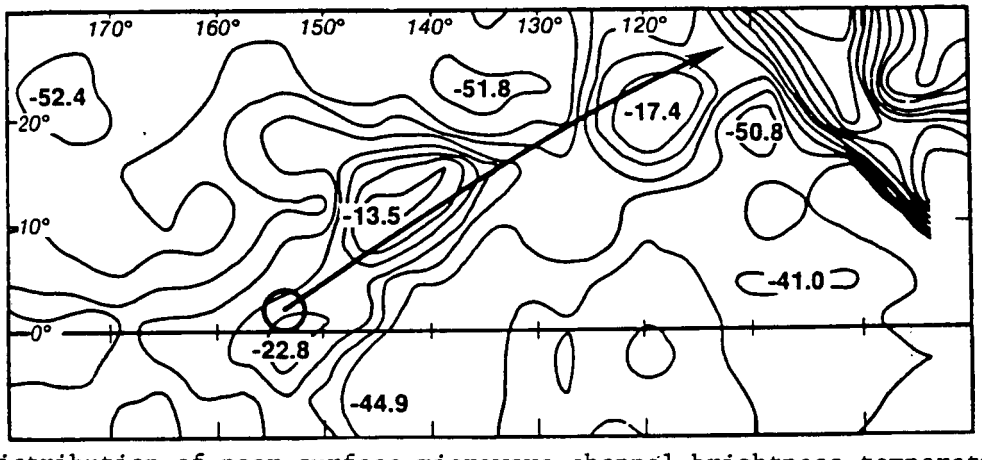

Fig. 4. Distribution of near-surface microwave channel brightness temperatures for 23 January 1979. Isopleth interval is 5°C. Heavy arrow and circle gives moisture burst axis and origin. See text for interpretation.

The second satellite product is a statistical assimilation of a large collection of satellite channel data, again emphasizing horizontal variability. The TIROS-N sounding data are decomposed into vertical eigenfunctions (in a process similar to that used in sounding reconstruction). The horizontal distributions of the amplitudes of these vertical eigenfunctions are then analyzed. Fig. 5 depicts a typical eigenfunction which, although it explains only 1.8% of the total field variance for this time period, clearly represents a portion of the moisture burst signal. This eigenfunction is essentially a tropopause and surface-layer thermal and boundary-layer moisture signal. Fig. 5 indicates a strong gradient across the burst axis, warm tropopause, and warm, dry boundary layer to the south of the burst axis. A strong positive center southwest of the burst origin is related to an easterly wave which appears in low-level streamlines analyses (not shown).

Two important additions to the eigenfunction and the channel-radiance analyses are being developed. The satellite data base is plagued by occasional missing passes; further, no tropospheric infrared information is available in overcast regions. We have used various regression procedures to estimate TIROS channel data from NOAA 5 data, and from available TIROS microwave data in cloudy regions. Tests with this procedure reproduce 40 to 90% of the variance of most TIROS-N channels. The only deficiency of the procedure is that the moisture channels above 900 mb seem to be poorly reproduced.

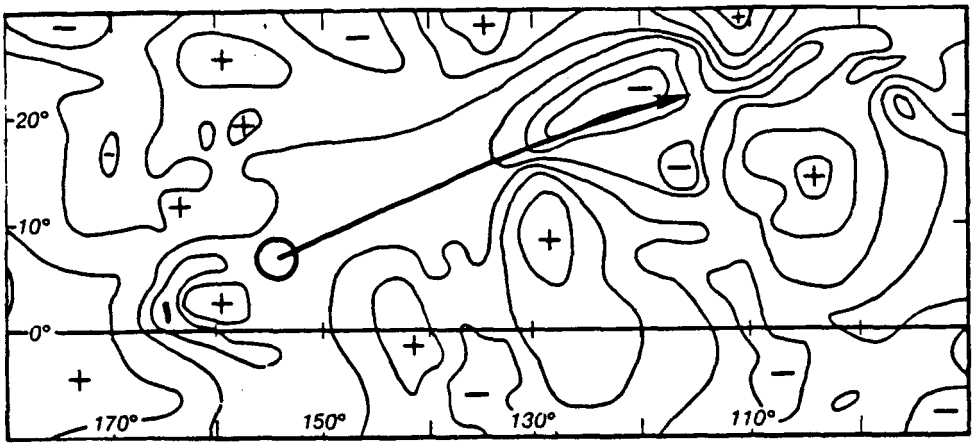

Fig. 5. Horizontal distribution of amplitudes of an eigenfunction of TIROS-N channel radiance data for 23 January 1979. Positive values represent warm, dry boundary layer and warm tropopause, approximately. Heavy arrow represents burst axis and the circle the burst origin region.

SUMMARY

We have described one qualitative and two quantitative techniques for applying satellite data to the development of synoptic climatologies in data-sparse regions. For the example of synoptic-scale bursts, it is seen that simply-applied geometric definitions can effectively characterize certain synoptic systems. The quantitative procedures utilize the excellent horizontal and temporal resolution of satellites, while minimizing their relatively poor vertical resolution.

ACKNOWLEDGEMENT

The authors acknowledge the financial and technical support of George C. Marshall Space Flight Center, NASA, Huntsville, AL, U.S.A. under contract No. NAS8-35182.

REFERENCES

1. N.A. Phillips, L.M. McMillin, A. Gruber and D.Q. Wark, An evaluation of early operational temperature soundings from TIROS-N, Bull. Amer. Meteor. Soc., 60, 118 (1981).

2. P. Kallberg, S. Uppala, N. Gustaffson and J. Pailleux, The impact of cloud track wind data on global analyses and medium range forecasts, Centre for Forecasts, ECMWF Tech. Rep. No. 34 (December 1982).

3. R.D. McPherson, K.H. Bergman, R.E. Kistler, G.E. Rasch and D.S. Gordon, The NMC Operational Global Data Assimilation System, Mon. Wea. Rev., 107, 1445 (1979).

4. J.P. McGuirk, A.H. Thompson, L.L. Anderson, Jr. and N.R. Smith, Reliability of circulation statistics over the tropical Pacific Ocean based on FGGE data, in: Proceedings of the Eight Annual Climate Diagnostic Workshop, Toronto 1983, p. 247.

5. R. Thepenier and D. Cruette, Formation of cloud bands associated with the American subtropical jet stream and their interaction with midlatitude synoptic disturbances reaching Europe, Mon. Wea. Rev., 109, 2209 (1981).

6. A.H. Thompson, J.P. McGuirk, L.L. Anderson, Jr. and N.R. Smith, Analysis of tropical synoptic disturbances using satellite-derived soundings and radiance data from selected channels, Proceedings of the Amer. Met. Soc. Conference on Satellite Meteorology/ Remote Sensing and Applications, Clearwater Beach, FL, U.S.A. (June 1984).

Paper presented at
Conference on Satellite Meteorology/
Remote Sensing and Applications, American Meteorological Society, Clearwater
Beach, FL, June 25-29, 1984. Preprint
Volume, pp. 137-142.

ANALYSIS OF TROPICAL SYNOPTIC DISTURBANCES USING SATELLITE-DERIVED SOUNDINGS AND RADIANCE DATA FROM SELECTED CHANNELS

A.H. Thompson, J.P. McGuirk, L.L. Anderson, Jr., and N.R. Smith

Texas A&M University
College Station, Texas 77843-3146

1. INTRODUCTION

Recent interest in the Southern Oscillation, the Walker circulation, and El Niño has led to increased demand for reliable analyses of the structure of the atmosphere of the eastern portion of the tropical and subtropical Pacific Ocean. Our own interest in these analyses is related to the phenomena listed above, but also is because of concern with plumes, or bursts, of middle and high clouds which originate in or near the intertropical convergence zone (ITCZ) of the eastern Pacific Ocean. These bursts move northeastward into middle latitudes, as either a jet-stream or merging there with the jet stream; they are often associated with cyclogenesis and precipitation events over the southern tier of states. We require analyses of the area mentioned above to examine the origin and subsequent behavior of the moisture plumes or "moisture bursts" as we have chosen to call them. The most satisfactory procedure in attaining analyses for such data-poor regions as the eastern Pacific is to combine conventional meteorological data with data retrieved from satellite radiance measurements. This paper presents some of the results of comparing and combining information from the two sources (satellite and conventional) in determining the atmospheric structure associated with a portion of the life cycle of an eastern Pacific moisture burst.

The cloud bands we refer to as moisture bursts have been observed by others, for example, Morel et al. (1978), Davis (1981), and Thepenier and Cruette (1981). McGuirk and Thompson (1984) describe the bursts in some detail and suggest that they may be related to the behavior of the Hadley circulation. Figure 1 shows a schematic depiction of the moisture burst of the period described in the paper. Thepenier and Cruette suggest that if the bursts are associated with (subtropical) jet formation and/or with subsequent cyclogenesis and precipitation events, then it seems essential to understand more of the triggering and development processes. McGuirk and Thompson also note that clouds in the vicinity of the burst genesis region sometimes move into the region from the southern hemisphere. Further, the clouds sometimes exhibit winds with the meridional component exhibiting "jet stream" speeds near, or south of, the ITCZ. Neither observation is consistent with conventional understanding of the subtropical circulation or of the Hadley cell. Such concepts require further evaluation.

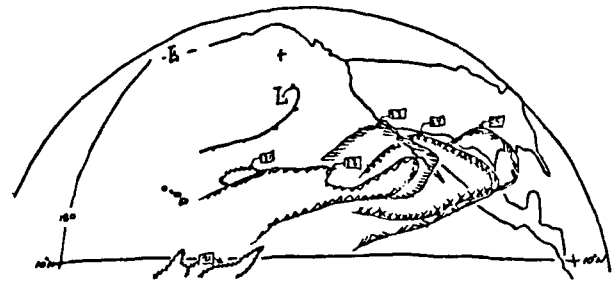

Fig. 1. *Schematic depiction of the time evolution of the high cloud boundary of a moisture burst occurring between 21 and 25 January 1979. Flagged numbers give the date of the associated cloud leading edge. (From McGuirk and Thompson, 1984.)*

2. DATA AND ANALYSES

The current investigation uses data from the First GARP Global Experiment (FGGE) Special Observing Period (SOP). The tropical eastern Pacific Ocean is characteristically a data-sparse region. The supplementary radiosondes, dropsondes and pibals, together with an expansion of the operationally available aircraft, surface and ship reports aid in making the FGGE SOP more amenable to study. Even these special data, however, leave the coverage far from ideal.

The satellite coverage also was increased during the SOP. Enhanced coverage of satellite-derived winds and temperatures and radiance data for several wavelength channels were available for melding with the conventional data.

Data from two satellite systems were used. These systems were the Geostationary Operational Environmental Satellite (GOES) system (especially GOES-West) and the sun-synchronous TIROS-N satellite. Data from the NOAA-5 system, in polar orbit, have been prepared but are not included in this paper. Infrared radiances mapped out as pictures of the cloud cover were obtained from the GOES system. Information from the TIROS-N Operational Vertical Sounder (TOVS) was also used. The TOVS was described by Smith et al., (1979). We are using mapped data from several of the individual channels of TOVS radiance measurements, and also retrieved atmospheric temperature soundings. In this paper we have used information

from only four of the channels. The channels used include Channels 10 and 12 of the High resolution Infrared Radiation Sounder (HIRS-2) and Channels 1 and 2 of the Microwave Sounding Unit (MSU). For convenience, we have chosen in our diagrams to refer to the two MSU channels as Ch. 21 and Ch. 22, respectively.

Another form of information retrieved from the satellite data is the wind obtained by tracking identifiable portions of the cloud patterns, or the "cloud-tracked winds". The upper cloud-tracked winds are based on cloud elements estimated to be at or above the 30 kPa pressure level. The lower cloud-tracked winds are presumed to represent flow below the 70 kPa pressure level. These data are available from the FGGE Level II archive. We have superimposed the upper-level cloud-tracked winds on the brightness temperature analysis of the Ch. 12 data, while the lower-level winds are on the corresponding chart of the Ch. 10 information.

Extensive use was made of the Level IIb and Level IIIb data as prepared by the European Center for Medium Range Weather Forecasts (ECMWF). Gridded data from the ECMWF set were extracted for an area bounded by latitudes 20°S and 30°N and by longitudes 180° and 90°W on a 3.75° x 3.75° lat/lon grid. Analyses of the satellite-derived data cover the same area when possible, and are our own objective analysis based on the Level IIb data.

The period examined in detail extended from 21 January 1979 to 28 January 1979. The examples presented in this paper were selected from mappings for the 24th and 25th.

3. SYNOPTIC PATTERNS DETECTED BY TOVS MICROWAVE AND WATER VAPOR CHANNELS

The four TOVS channels are selected to depict synoptic scale systems over the Pacific Ocean. The two microwave channels discussed herein represent, approximately, brightness temperatures in the vicinity of 70 kPa (Ch. 22) and the surface (Ch. 21). The infrared channels measure, approximately, moisture (expressed as brightness temperature) at the 50 kPa (Ch. 12) and 90 kPa (Ch. 10) levels. Additionally, 20 kPa temperature and 85 kPa geopotential height and relative humidity fields from the ECMWF Level IIIb analyses are used. Comparisons are made between the synoptic patterns for 00 GMT on 24 January and those for 00 GMT on 25 January.

The microwave channels are used because of their ability to probe through clouds where IR channel data are not available. The water vapor channels are used to delineate moisture-rich areas and also to track wind maxima (Martin and Salomonson, 1970). The cloud-tracked winds are unreliable in the presence of an overcast cloud cover.

3.1 Case 1: 00 GMT on 24 January 1979

3.1a Upper Troposphere (70 kPa and above)

There are two upper tropospheric microwave channels available from the TOVS MSU. The uppermost channel has a peak energy contribution from near the 30 kPa level. The features in this channel are not shown because they are very broad and lack detail. The MSU Channel 2, [here referred to as TOVS Channel 22] is discussed instead. North of 20°N (see Fig. 2) the temperature field is predominantly zonal with small-amplitude short waves embedded. The striking feature is the deep cold axis near 145°W extending from 20°N to a position south of the equator. In addition, there is a southern hemisphere cold axis near 140°W which also extends across the equator into the northern hemisphere. These two cold axes could be interpreted readily as a single cold axis extending across the equator between 140°W and 150°W. The eastern and western equatorial regions are dominated by broad zonally-oriented warmer regions.

The HIRS Water Vapor Channel 12 (50 kPa) and the cloud-tracked winds above 30 kPa are illustrated in Fig. 3. As can be seen, there is good synoptic-scale detail in the satellite-derived pattern, with extensive troughs and ridges. There also appear to be large embedded mesoscale (500-1,000 km) features.

A warm (or dry) axis extends from 10°N, 170°W to 25°N, 140°W to 25°N, 120°W, where the data become sparse; it appears again at 30°N, 95°W. According to Martin and Salomonson (1970), certain water vapor channel radiances have a strong relationship to the southwesterly subtropical jet stream (STJ) maxima over the United States. The suggestion is that the STJ parallels the high (dry) temperature axis which extends deep into the tropics. Other high temperature axes exist in the eastern Pacific Ocean, and also one is centered at 10°S, 135°W to 2°N, 142 °W. The cloud-tracked winds, denoted in the figures by arrows, appear to lie in the areas of tight gradient except at 15°N between 125°W and 105°W, where they are transverse to the low temperature (wet) axis.

Low temperature axes in this channel should delineate moisture-rich areas. Since this is an IR channel peaking at approximately 50 kPa, it is not a mapping of cloud tops, but primarily of water vapor. An extensive cold (wet) axis (Fig. 3) extends from 5°S, 165°W to the equator at 150°W where it splits into northern and southern branches. The northern branch runs from 2°N, 147°W to 20°N, 115°W while the southern branch curves from 2°N, 147°W to 2°N, 131°W then southeastward. The two branches suggest a moisture "canal" extending from the southern hemisphere tropics into the mid-latitudes and also a branch circulating near the equator in the southern hemisphere. These two features are well depicted in the Level IIIb relative humidity analysis for 70 kPa (not shown).

The Level IIIb 200-mb temperature analysis for 20 kPa (Fig. 4) shows an extensive cold axis from 10°N, 145°W northeastward and a cold core near 15°S, 140°W. By comparing Figs. 2, 3 and 4, we can see that the cloud-tracked winds are closely associated with both microwave and 20 kPa temperature patterns. Also, the moisture "canal" present in the water vapor channel lies just east of the microwave cold axis and generally parallels the cold axis at 20 kPa. The southern hemisphere moisture "canal" is easily associated

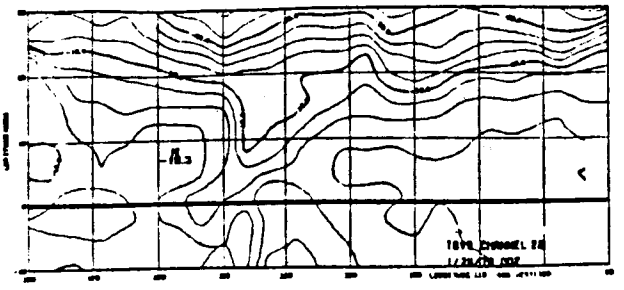

Fig. 2. *Mapping of grid-point values of brightness temperature (Celsius) of Ch. 22 (Ch. 2, 0.358 cm, of the MSU, with peak energy contribution from near 70 kPa) radiances. Approximately 00 GMT 24 January 1979.*

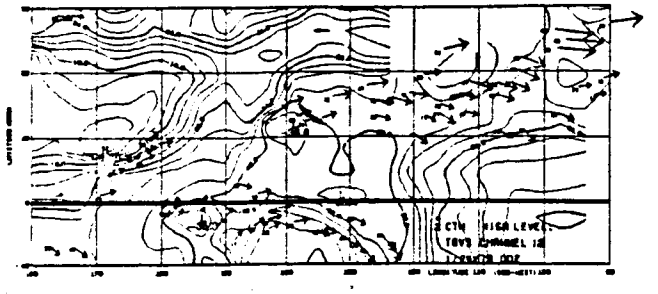

Fig. 3. *Mapping of grid-point values of brightness temperature (Celsius) of HIRS Ch. 12 (6.70 μm, a water vapor channel with peak energy contribution from near 50 kPa) radiances. The upper cloud-track winds are superimposed (speeds in m/sec). Approximately 00 GMT 24 January 1979.*

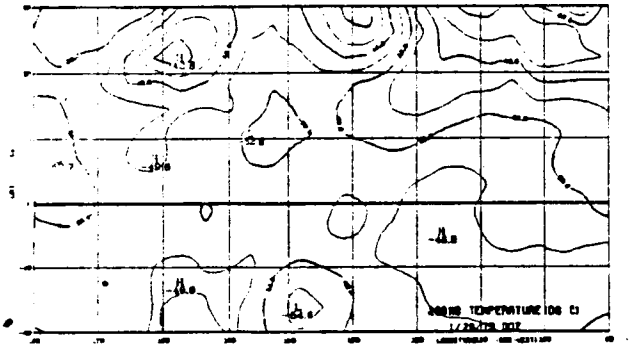

Fig. 4. *Temperature (Celsius) at the 20 kPa surface from the ECMWF Level IIIb analysis. For 0000 GMT 24 January 1979.*

with the microwave channel and the 20 kPa analysis patterns.

Appropriate TOVS channels and Level IIIb analyses in the lower troposphere are now discussed.

3.1b Lower Troposphere (below 70 kPa)

The lower tropospheric microwave channel (MSU Channel 1, here referred to as TOVS Channel 21) is a "window" channel with peak energy contribution from the surface. Figure 5 shows that considerable detail is available in this channel, with a major warm axis along the equator from 180° to 155°W then northeastward to 30°N, 105°W.

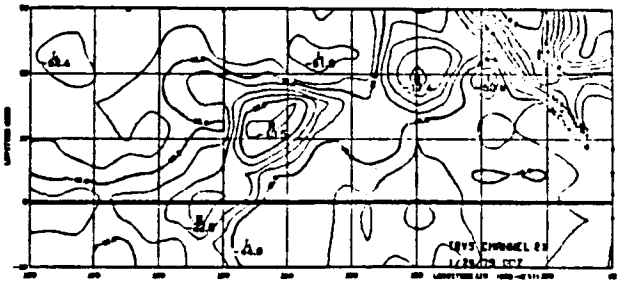

Fig. 5. *Mapping of grid-point values of brightness temperature (Celsius) of Ch. 21 (Ch. 1, 0.596 cm, of the MSU, with peak energy contribution from the surface) radiances. Approximately 00 GMT 24 January 1979.*

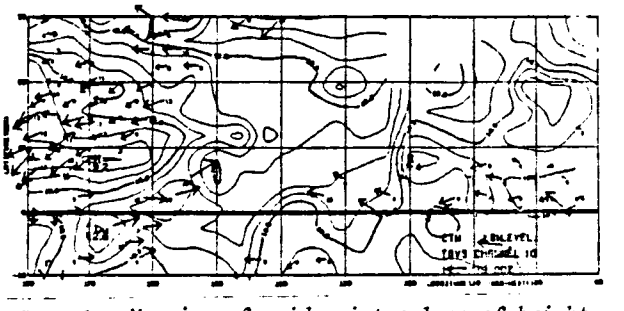

Fig. 6. *Mapping of grid-point values of brightness temperature (Celsius) of HIRS Ch. 10 (8.30 μm, a water vapor channel with peak energy contribution from near 90 kPa) radiances. The lower cloud-track winds are superimposed (speeds in m/sec). Approximately 00 GMT 24 January 1979.*

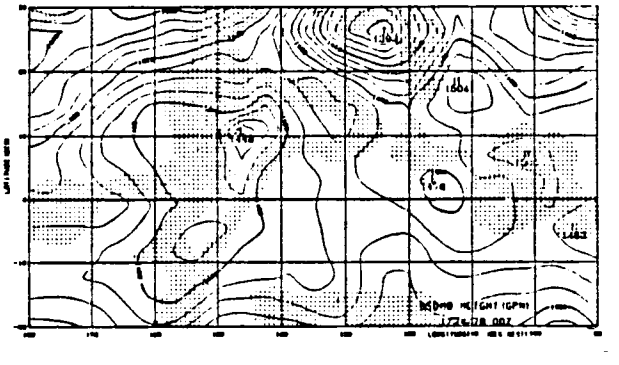

Fig. 7. *Height (gpm) of the 85 kPa (850 mb) surface from the ECMWF Level IIIb analysis. The stippled areas have relative humidities at 85 kPa between 70 % and 90 %. For 00 GMT 24 January 1979.*

This warm axis coincides very closely with the upper tropospheric moisture "canal" (see Fig. 3) and the upper microwave cold axis (Fig. 2). The Channel 21 cold axis from 10°S, 115°W to 25°N, 135°W does not relate as well to the upper tropospheric warm axis. Thus, the moisture burst shows its signal throughout the depth of the troposphere.

TOVS Channel 10 is a water vapor channel, peaking at 90 kPa. As with the upper tropospheric water vapor channel, cold axes should delineate moisture-rich areas ("canals"). The lower tropospheric cold (wet) axes (Fig. 6) reflect the upper tropospheric patterns (Fig. 3) but with

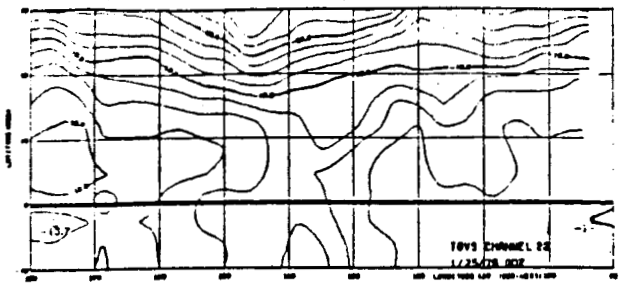

Fig. 8. *Same as Fig. 2 except for 00 GMT 25 January 1979.*

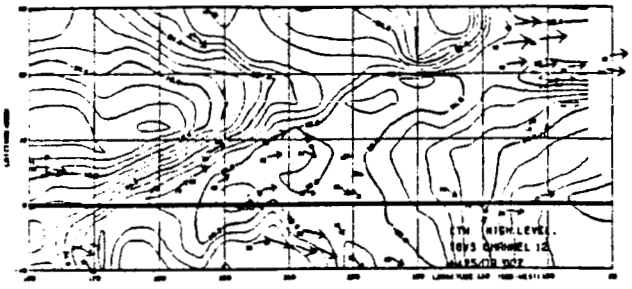

Fig. 9. *Same as Fig. 3 except for 00 GMT 25 January 1979.*

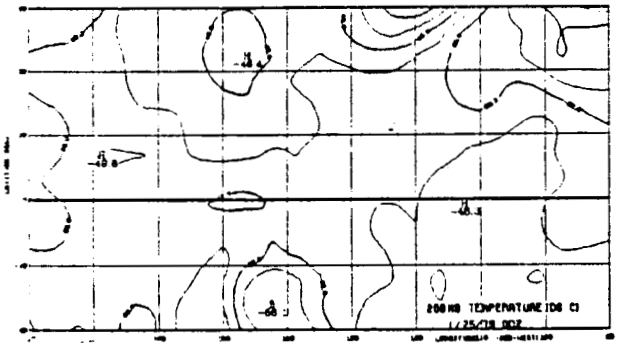

Fig. 10. *Same as Fig. 4 except for 00 GMT 25 January 1979.*

much less detail. There are broad warm (dry) areas in the eastern and western parts of the region which are similar to upper tropospheric patterns, but the upper warm (dry) axis paralleling the STJ is not reflected near the surface. The cloud-tracked winds (Fig. 6) indicate the expected easterly (trade) winds in the east and relatively strong easterlies a short distance east of the dateline. The interesting feature is the belt of strong westerlies, up to 16 m/s, along the equator near 175°W and along the moisture "canal" to 10°N. Although the South Pacific Convergence Zone was located 30° to 40° east of its normal position, these westerlies do not seem to be a northward extension of that complex. The lower water vapor channel does not appear to be as useful a signal of the wind pattern as the upper water vapor channel, with the possible exception of the unusually strong westerlies feeding the moisture "canal". Notice also the cross-equatorial flow in the moisture "canal" denoting the southern hemisphere's contribution to northern mid-latitude moisture.

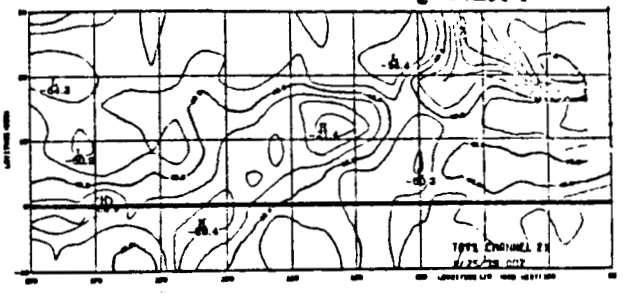

Fig. 11. *Same as Fig. 5 except for 00 GMT 25 January 1979.*

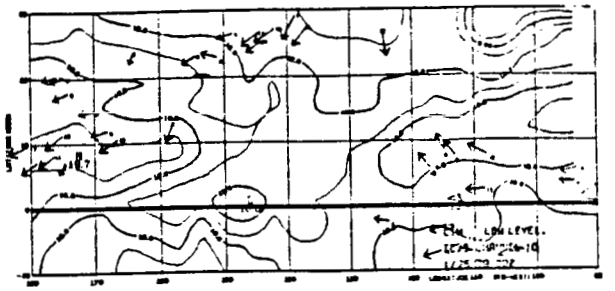

Fig. 12. *Same as Fig. 6 except for 00 GMT 25 January 1979.*

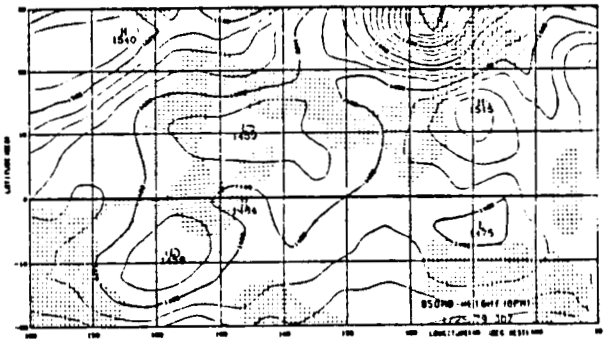

Fig. 13. *Same as Fig. 7 except for 00 GMT 25 January 1979.*

The Level IIIb height and relative humidity fields for 85 kPa are shown in Fig. 7. The height field shows an extensive trough throughout the tropics from 20°S, 160°W to 25°N, 125°W. This trough coincides with the microwave warm axis and the water vapor channel cold (wet) axis (moisture "canal"). The cloud-tracked winds correspond quite well to the height field: parallel to the contours at locations away from the equator and blowing from high to low along the equator. The 85 kPa relative humidity field is captured well by the moisture "canals" with the exception of the eastern equatorial region in which the Level IIIb analysis denotes high relative humidity and the satellite data indicate dryness; which is representative in this case is uncertain.

3.2 Case 2: 00 GMT on 25 January 1979

We discuss the same TOVS Channels and Level IIIb analyses as are presented for Case 1.

3.2a Upper troposphere (70 kPa and above)

The synoptic-scale patterns detected in the microwave temperature (Channel 22) data (Fig. 8) are similar to those 24 h earlier, but moved 10° to 15° of longitude to the east. Zonal patterns still are predominant north of 20°N with broad warm regions over most of the equatorial region. The cross-equatorial cold axis is now located near 140°W and is less distinct than before. The cloud-tracked winds (Fig. 9) indicate that the southern hemispheric circulation has extended northward across the equator to nearly 10°N.

The cloud-tracked winds (Fig. 9) also indicate some upper-level troughing near the equator in the eastern part of the region. This is supported by a cold axis in the microwave channel and a warm dry axis in the water vapor Channel 12. The cloud-tracked winds, as earlier, appear parallel to the warm dry axes in the Channel 12 high gradient areas. Also, the Channel 12 cold wet axes, or moisture "canals", coincide with the circulation inferred from the cloud-tracked winds with the exception of the troughing near the equator in the east. The moisture "canal" once again extends from the southern hemisphere near 155°W northeastward into the mid-latitudes. The southern hemisphere branch is still evident, now near 130°W. The moisture "canal" branches for the most part parallel the microwave cold axes.

The Level IIIb 20 kPa temperature analysis (Fig. 10) shows a strengthened cold cell in the southern hemisphere which is stationary. The northern hemisphere cold axis has greatly diminished while moving northeastward. The cloud-tracked wind trough near the equator at 105°W is not discernable in the 20 kPa temperature analysis.

The features are consistent during the 24 hour period up to 00 GMT on the 25th except for the appearance of a cold axis in the microwave pattern from 15°N, 115°W to the equator at 105°W. The new cold axis is reflected in the troughing in the cloud-tracked winds. It also appears that the southern hemisphere circulation pattern is nearly stationary near 140°W while the northern hemisphere cold axis moves eastward.

3.2b Lower Troposphere (below 70 kPa)

The microwave channel (21) shows that the warm axis has moved east approximately 5° of longitude to 10°S, 155°W northeastward to 25°N, 100°W (Fig. 11). This warm axis is the only clear synoptic scale feature as there are no continuous cold axes present.

As before, the microwave warm axis is approximately colocated with the lower water vapor channel (10) cold (wet) axis. This cold axis (Fig. 12) extends from the equator near 160°W to 30°N, 105°W approximately 5° longitude east of its previous position. Extension of the cold axis, or moisture "canal", into the southern hemisphere is not apparent at this time. Zonal warm regions flank the moisture "canal" near 10°N. The cloud-tracked winds (Fig. 12) indicate easterly (trade) winds persisting in the east and northwest while the previous strong westerlies feeding the moisture "canal" in the west are not detected. However, higher level cloud-tracked winds are now indicated (Fig. 9) over the low-level moisture "canal", suggesting changes in cloud height and/or depth. Thus, the low-level cloud motions which would reveal the westerlies (if present) have been masked by higher clouds. Comparison of the two 85 kPa analyses (Figs. 7 and 13; see also the next paragraph) suggests that the low-level westerlies may still be present, though perhaps shifted eastward a few degrees.

The 85 kPa Level IIIb height analysis bears little resemblance to the microwave temperature field. The 85 kPa trough (Fig. 13) extending from 10°S, 160°W to 30°N,115°W, broadly bounds the water vapor cold axis, or moisture "canal". The trough in the height field has moved little in the equatorial region and weakened somewhat. Figure 13 also shows that the 85 kPa humidity field has become less distinct and the cross-equatorial continuity, observed 24 hours earlier, is no longer present.

3.3 Atmospheric cross sections

Vertical sections along the west coast of North America and along zonal transects at 8°N and 3°N were constructed using radiosondes and dropsondes. Temperature retrievals from the TOVS were utilized to prepare satellite-derived cross sections for approximately the same times and locations. Although these data are not described herein, we expect to show and discuss results in the verbal Conference presentation.

4. SUMMARY AND REMARKS

The satellite-derived data, consisting of microwave and water vapor channel brightness temperature fields and cloud-tracked winds, detect synoptic scale patterns of temperature, moisture and winds. The water vapor channel data are not available in overcast cloud areas; the cloud-tracked winds are limited to cloudy areas and are normally mutually exclusive high cloud winds or low cloud winds. The microwave channel temperatures provide "all weather" coverage but require special interpretation in rain areas. The satellite data do capture time variation in synoptic scale features, as illustrated by the changes over the 24-h period between 00 GMT 24 January and 00 GMT 25 January 1979, even in the equatorial tropics where horizontal contrasts are thought to be weak.

Promising results include the ability of the upper tropospheric microwave channel to detect temperature variations in the tropical region and the presence of a moisture "canal" in the water vapor channels. The moisture "canal" extends from the southern hemisphere or near the equator northward toward mid-latitudes in both time periods.

Microwave temperatures, the water vapor channel moisture "canals" and the cloud-tracked winds all suggest a quasi-stationary southern hemisphere circulation "coupled" with a transient

northern hemisphere system.

Strong equatorial westerlies are initially present at low levels, apparently feeding the moisture "canal," but are not detected 24 h later. Also, the lower tropospheric microwave warm axis lying in the moisture "canal" is a persistent feature. These two observations are among features requiring further investigation. Parallelism between satellite-derived analyses and more conventional analyses is not perfect, even though the satellite data are incorporated into the FGGE Level IIIb analyses. Continued evaluation and experience should allow us to improve our abilities to infer structure from the satellite-derived information. Further investigation will include analysis of satellite channel brightness temperature fields using an empirical orthogonal function (EOF) synoptic mapping technique. Emphasis will be placed on using the microwave channels because of their "all weather" capability.

5. ACKNOWLEDGEMENTS

Our efforts are receiving financial and technical support from the George C. Marshall Space Flight Center, National Aeronautical and Space Administration, Huntsville, AL, through Contract No. NAS8-35182. We also acknowledge the assistance of our colleagues P. E. Riba and Shellie L. Craig.

6. REFERENCES

Davis, N. E., 1981: METEOSAT looks at the general circulation: III. Tropical-extratropical interaction, Weather, 36, 168-173.

Martin, R., and V. Salomonson, 1970: Statistical characteristics of subtropical jet-stream features in terms of MRIR observations from Nimbus 2, J. Appl. Meteor., 9, 508-520.

McGuirk, J.P., and A.H. Thompson, 1984: Transient tropical disturbances within the Pacific Hadley cell. Proceedings, 15th Tech. Conf. on Hurricanes and Tropical Meteorology. Amer. Meteor. Soc., Miami, FL, pages unk.

McGuirk, J.P., A.H. Thompson, L.L. Anderson, and N.R. Smith, 1984: Reliability of circulation statistics over the tropical Pacific Ocean based on FGGE data, Proceedings, 8th Climate Diagnostics Workshop, Toronto, October 12-16, 1983.

Morel, P., M. Desbois, and G. Szejwach, 1978: A new insight into the troposphere with the water vapor channel of Meteosat, Bull. Amer. Meteor. Soc., 59, 711-714.

Smith, W., H. Woolf, C. Hayden, D. Wark and L. McMillin, 1979: The TIROS-N operational vertical sounder, Bull. Amer. Meteor. Soc., 60, 1177-1186.

Thepenier, R., and D. Cruette, 1981: Formation of cloud bands associated with the American subtropical jet stream and their interaction with midlatitude synoptic disturbances reaching Europe, Mon. Wea. Rev.,109, 2209-2220.

From: Proceedings of the Ninth Climate Diagnostics Workshop, Oct. 22-26, Corvallis, OR. Pp. 429-436.

Observing the Eastern Pacific Hadley Circulation

James P. McGuirk, Aylmer H. Thompson, and Neil R. Smith
Department of Meteorology
Texas A&M University
College Station, Texas 77843

Some aspects of the tropical Eastern Pacific mean meridional circulation (MMC) can be interpreted in terms of the mean behavior of a synoptic event called a "moisture burst". This event is documented by McGuirk et al., 1984 (8th Climate Diagnostics Workshop). Three different aspects of the interaction of moisture bursts and the Hadley cell are described herein.

1. El Niño Behavior.

A distribution of moisture bursts during the 1982-83 El Niño cool season was prepared from NOAA 7 photo-mosaics (fig. 1). It shows:

(A) During El Niño moisture bursts do not occur in the region of strong ITCZ convection; that is, east of Australia and to the west of the eastern edge of the outgoing longwave radiation (OLR) minimum.

(B) The central Pacific deficit of bursts is more than 5 standard deviations below climatological expectations.

2. Mean Meridional Wind Behavior.

Calculations were performed on a nine-day gridded wind set (FGGE III (b) analysis during the January Special Observing Period). "Zonal averaging" was performed across the sector from the dateline to 112.5°W (7500 km) and from 20°S to 30°N. Meridional sections of the mean meridional wind component are shown for the 9-day average (fig. 2) and for selected days (fig. 3). The time average differs significantly from previous climatologies of the region.

(C) A thermally-direct MMC may be inferred. Climatology has this indirect in the eastern Pacific.

(D) A two-celled MMC appears in the vertical, with stronger southerlies centered at 600 mb and a weaker southerly maximum at the climatologically expected position at 200 mb.

The time sequence (fig. 3) shows large variations in the zonally-averaged meridional winds on a day-to-day basis.

(E) At the peak of the moisture burst on the 23rd and 25th (fig. 3b and 3c), meridional confluence into the ITCZ below 800 mb is intense.

(F) Except on the 27th (fig. 3d), the strongest southerlies are at, or even below, 500 mb, and the flow at tropopause level is two times stronger into the southern hemisphere.

(G) The only "classical" Hadley cell flow appears at the end of the moisture burst period on the 27th (fig. 3d).

(H) The weakest Hadley cell, as measured by low-level meridional confluence, occurs on the 21st, when no moisture bursts were present.

Based on (A), (C), (E), (H), and existing climatology, we tentatively introduce the following speculation. In the absence of synoptic or convective tropical forcing, the Pacific Hadley cell is weak, and may even switch directions, with tropical subsidence. With synoptic forcing, a Hadley cell develops, and its characteristics result as a statistical composite of a number of synoptic events (moisture bursts). This MMC appears primarily in the lower half of the troposphere. With strong convective forcing, moisture bursts do not form, and a strong, deep Hadley cell results--the classical picture.

3. Data Quality (FGGE SOP)

In spite of the intense observational coverage during FGGE, the study area remained data-sparse. The following results are restricted to the boundary layer (below 800 mb) and pertain to analyzed wind (FGGE), satellite winds (SAT), and surface ship and island observations (SFC). Fig. 4 shows the distribution of SAT and total nine-day observation frequency.

(I) Many regions in the equatorial band have no observations.

(J) SAT is synoptically biased, with a sparsity of data, particularly, in the moisture burst region.

(K) Low-level ITCZ convergence calculations are based on SAT at 10°N and west of 150°W, and at 3°N and east of 135°W.

(L) In most regions, simultaneous SFC and SAT observations are not available, making vertical extrapolation tenuous.

Hovmöller-type diagrams of low-level zonally-averaged meridional winds in a time-latitude section appear in fig. 5; the three representations show analysis of SFC only, SAT only, and FGGE data. Analysis assumptions require that these fields present the same signal (in particular, FGGE is derived from SAT and SFC). Clearly, they do not.

(M) FGGE presents considerably fewer southerlies, and weaker southerly amplitudes than either SAT or SFC; it also shows more northerlies at 15°N then either SAT or SFC.

(N) Even where SAT and SFC are consistent, FGGE may "disagree" (at 10°S from the 22nd to the 24th, or 25°N on the 27th and 28th).

(O) There are significant regions of disagreement between the two sets of observations (SFC detects more southerlies; SAT predicts stronger meridional confluence at the ITCZ; SAT is less coherent, both temporally and meridionally).

(P) Similar sections of zonal winds (not shown) yield similar inconsistencies; FGGE shows fewer equatorial westerlies than SAT, but also less variability than SFC.

In an effort to resolve the inconsistencies between FGGE, SAT, and SFC, additional analyses and intercomparisons were performed.

(Q) Examination of the 1000-850 mb wind shear of 50 ship soundings between 9°N and 9°S showed a mean shear of only 1 m/sec but a standard deviation of 7 m/sec with shear direction varying over 360°; in other words there should be little ability to extrapolate synoptic signals upward or downward in the tropical boundary layer.

(R) Fig. 6 shows FGGE 1000-850 mb shear in the equatorial belt. Four regions are identified: I and II with surface winds increasing strength with height; IV with easterlies shifting to westerlies with height; and III, with the trades turning cyclonically with height in the moisture burst region. It is unclear how accurately optimal interpolation represents these regimes in data-sparse regions.

(S) Shear magnitude is not well-related to surface speed.

Finally, an effective analysis error was computed between SAT and FGGE at 850 mb. "Effective" is included because no attempt was made to account for SAT observational errors or differences between observation and analysis times and positions. Two histograms of analysis error are presented in fig. 7 for a single time, comparing FGGE with two SAT sets: GOES (West) and GOES (Indian Ocean). The GOES (Indian Ocean) represents an erroneous calculation; the positions of observations are erroneously located in °W longitude on the World Data Center archive tape, so they were accidentally placed in the eastern Pacific for the analysis-error calculation.

(T) Although there is larger analysis error for the erroneous data, figs. 7a and 7b are quantitatively similar. Correct data show rms analysis errors of 3.6 m/sec whereas the "random data", correct in latitude, but moved from the Indian Ocean to the Pacific, show rms errors of only 4.2 m/sec. Could it be that SAT possesses only about 0.6 m/sec signal in the lower atmosphere?

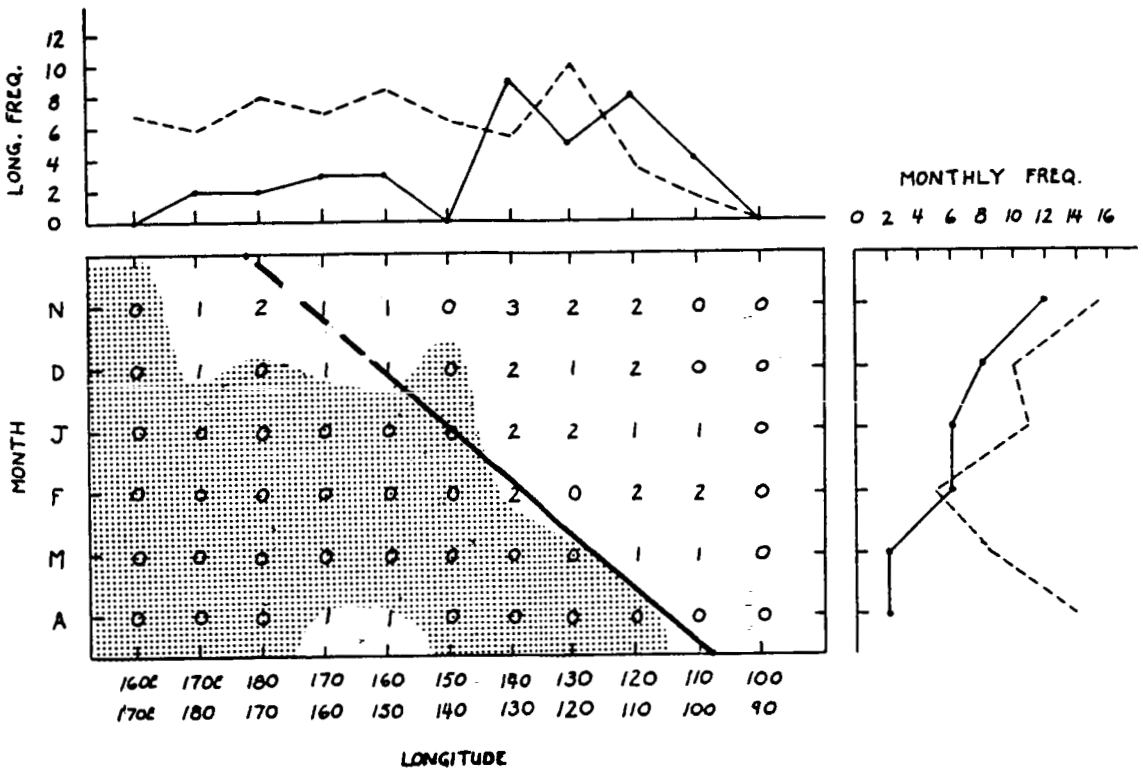

Fig. 1. Distribution of the occurrence of moisture bursts during the 82-83 El Niño as a function of month and longitude of origin. Dashed lines give non-El Niño climatology; heavy line gives approximate position of the eastern edge of the OLR minimum associated with El Niño. Shading emphasizes burst-void region.

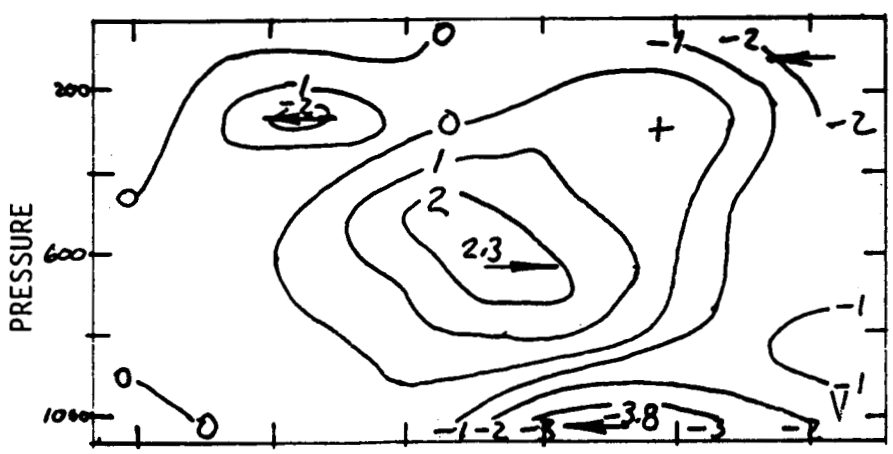

Fig. 2. Meridional section of the temporally (9 days) and zonally (180-112°W) averaged meridional winds. Units of m/sec.

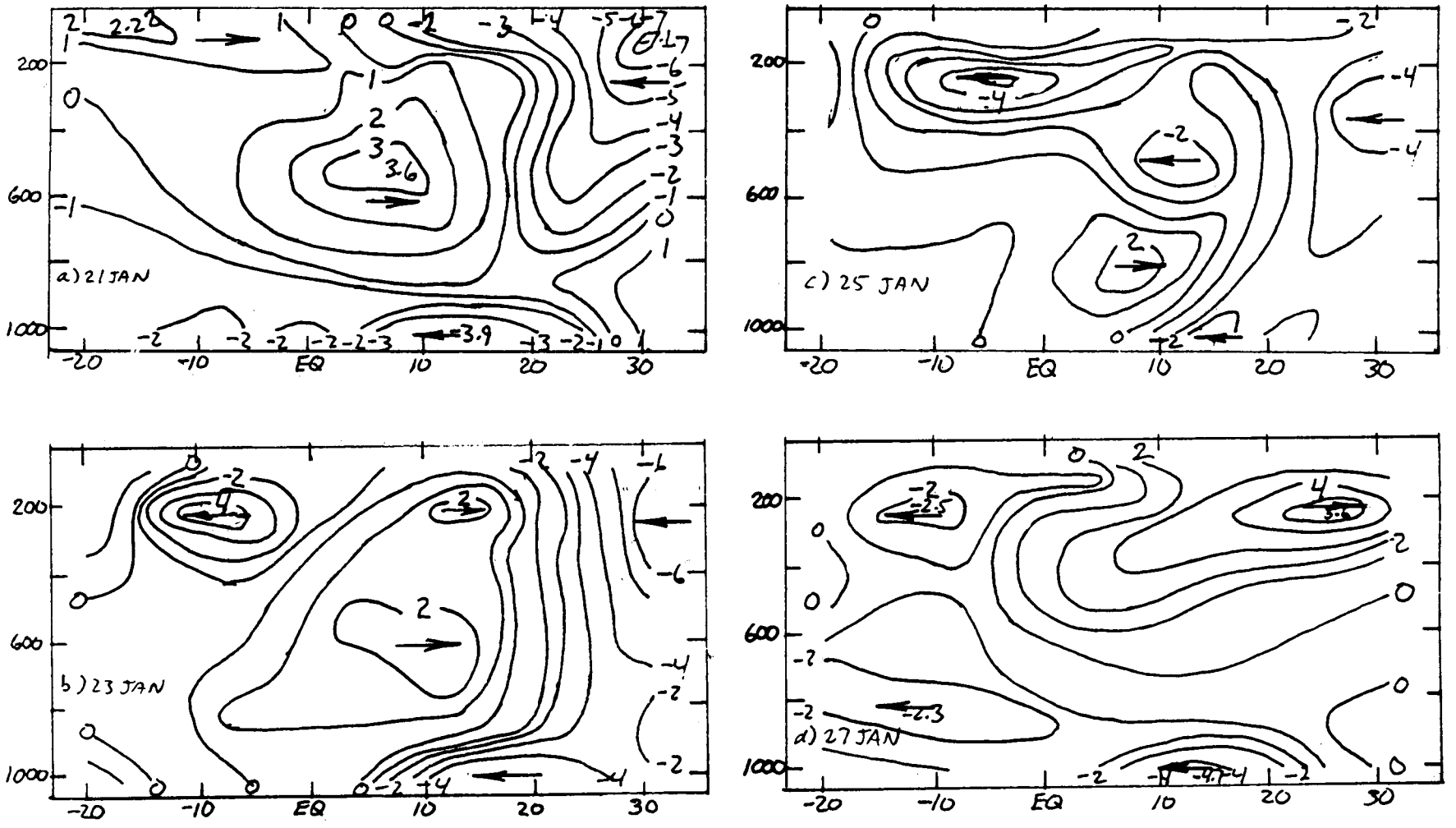

Fig. 3. As in fig. 2 except for individual days.

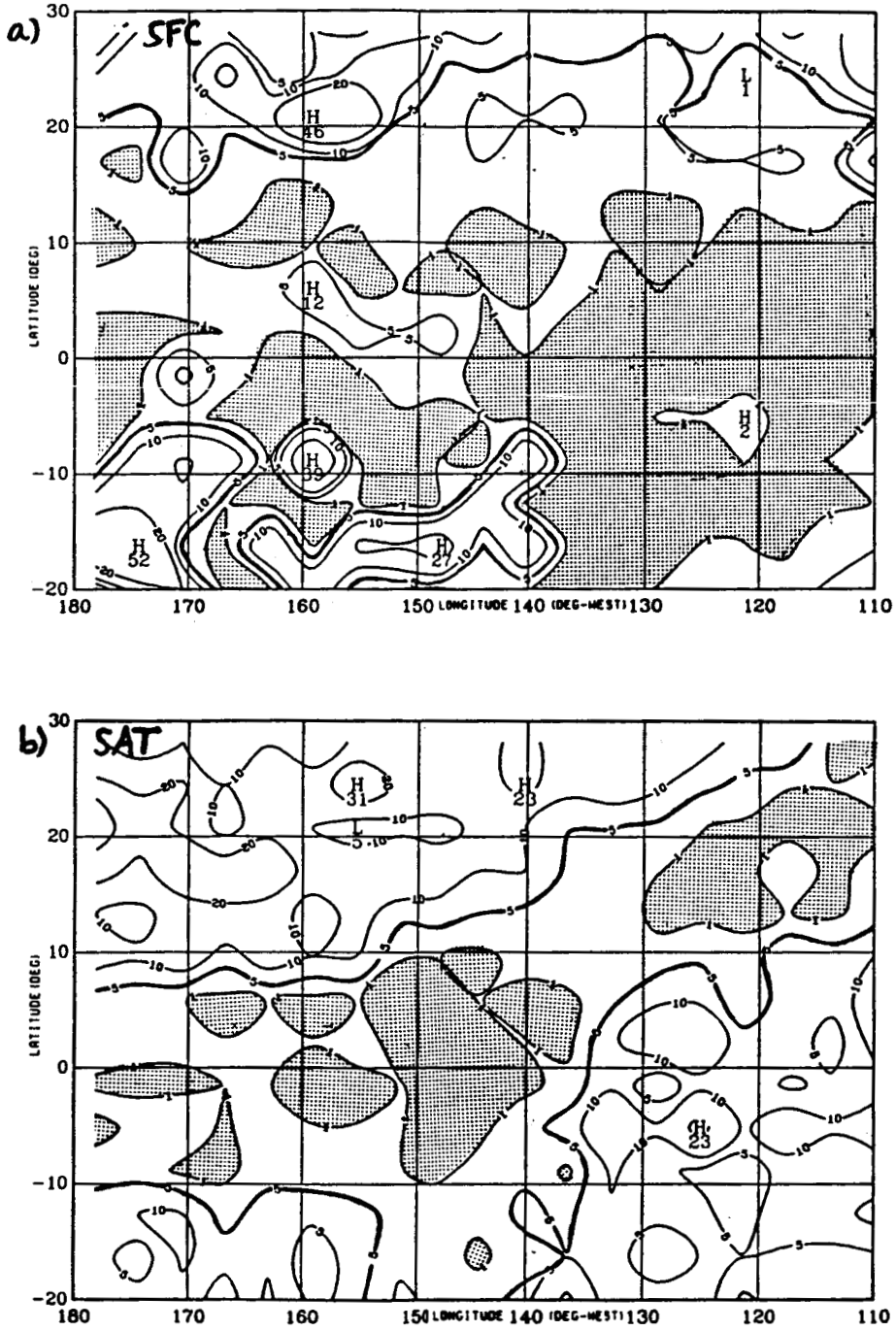

Fig. 4. Number of wind observations per 3.75 X 3.75° lat/lon box for the entire 9-day period. Isopleths are 1 (shaded), 5 (highlighted), 10 and 20 observations. a) Surface (SFC) observations; b) low-level satellite (SAT) observations.

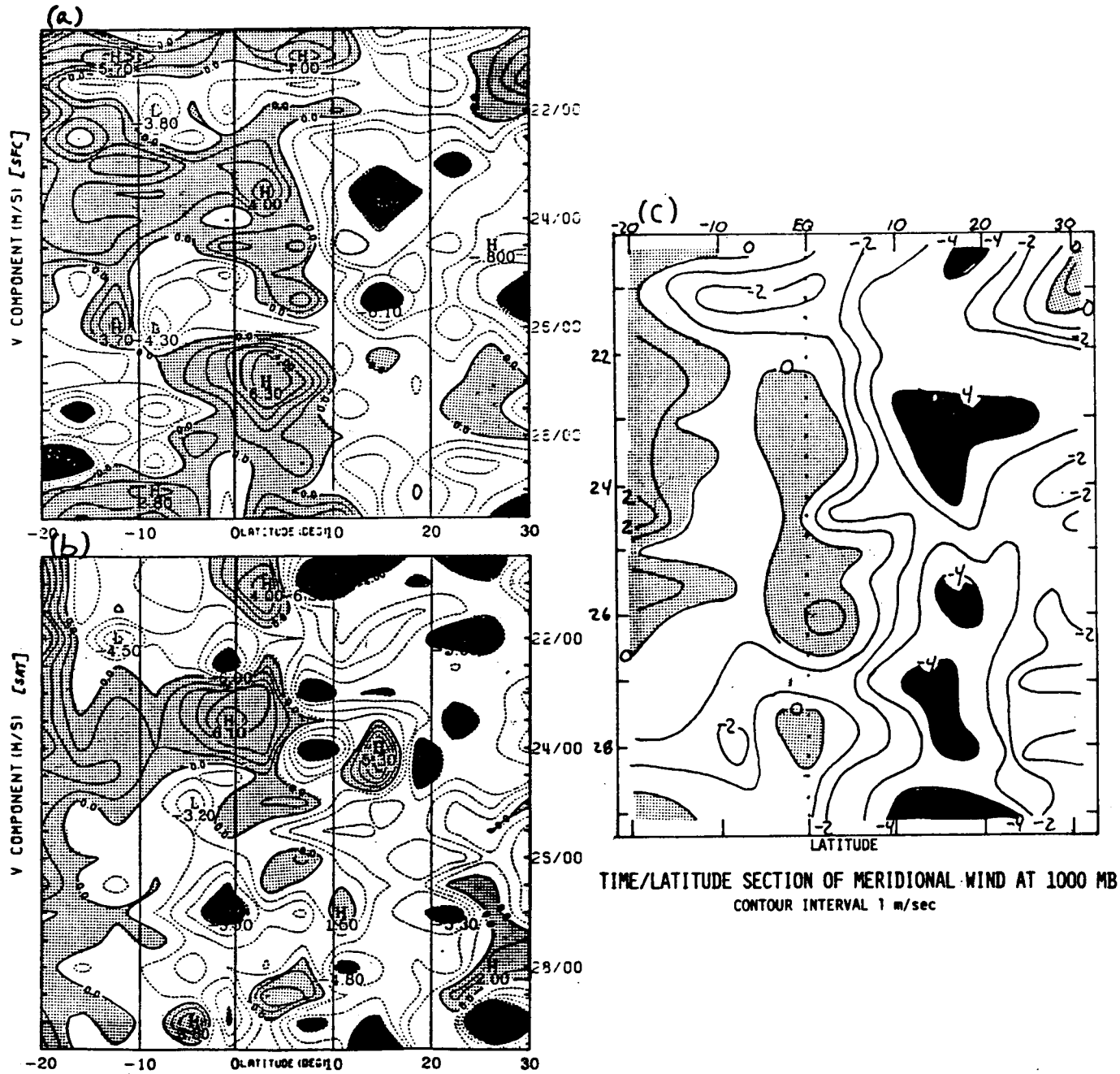

Fig. 5. Time-latitude sections of the zonally-averaged meridional wind between 180 and 112°W. Light shading gives southerlies; heavy shading gives northerlies greater than 4 m/sec. a) SFC observations; b) SAT observations; c) 1000 mb FGGE analysis. Contour interval is 1 m/sec.

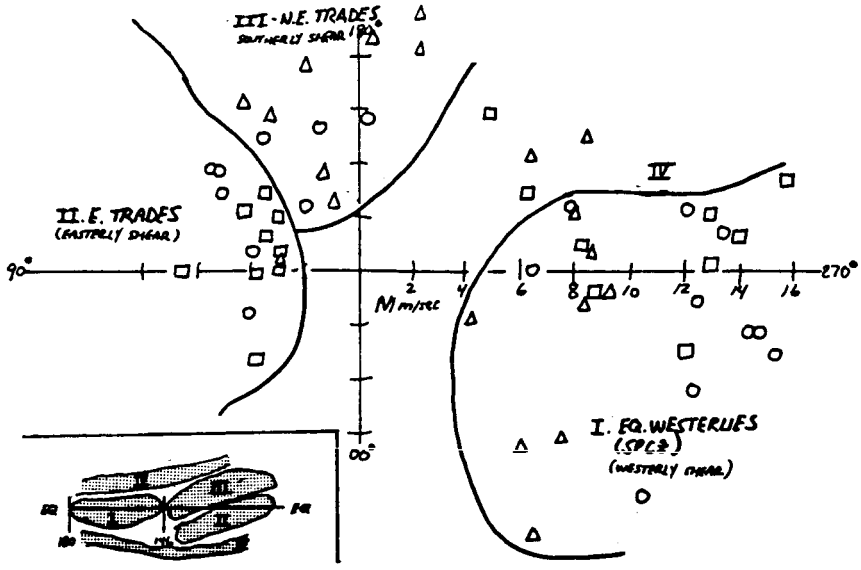

Fig. 6. 850-1000 mb wind shear in the equatorial belt from FGGE analysis. Wind vector from origin to data point gives speed and direction of shear. Data are clustered by surface wind direction, with associated geographical region shown in the inset at the lower left.

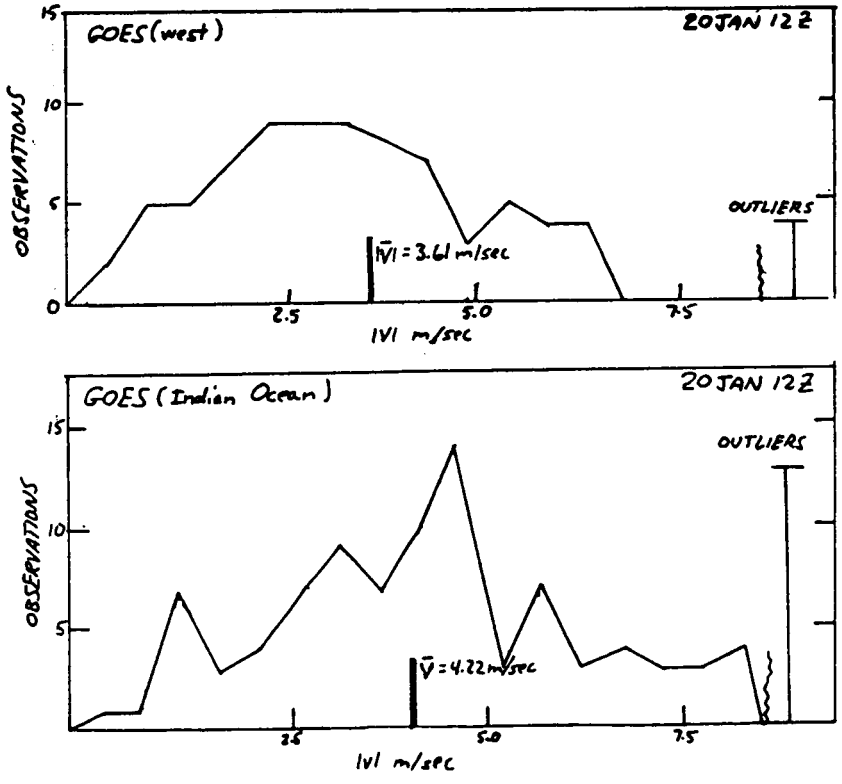

Fig. 7. Histograms of the distribution of effective analysis error between the 850 mb FGGE analysis and colocated SAT observations. a) GOES (west); b) GOES (Indian Ocean), which is erroneous because the data were improperly located in the eastern Pacific. Heavy vertical bars give sample means; vertical lines to right give flagged outliers.

Extended Abstracts Volume: 16th Conf. on Hurricanes & Tropical Meteorology, May 14-17, 1985, Houston, Texas. Published by American Meteorological Society, Boston, Mass. USA

COMPARISONS BETWEEN TROPICAL SYNOPTIC MOISTURE FIELDS AS DETERMINED FROM ANALYSIS AND FROM OBSERVATIONS

A. H. THOMPSON, J. P. McGUIRK, and L. L. ANDERSON, JR.

Department of Meteorology, Texas A&M University
College Station, TX 77843-3146

1. INTRODUCTION

Synoptic scale variations in tropical moisture fields are difficult to diagnose because of a relative absence of in situ measurements and low correlation of vertical structure, making upward extrapolation difficult. During the FGGE observing periods several observation systems were operative, making easier the comparisons between independent methods of estimating tropical moisture. Attention is focused on two wintertime synoptic scale disturbances, or "moisture bursts", which occurred between 20 and 29 January 1979. These bursts are tongues of moisture and clouds which originated near 7°N, 155°W in the ITCZ and moved northeastward over Empalme, Mexico (G in Fig. 1) (McGuirk and Thompson, 1984).

2. DATA AND ANALYSIS

Two different perspectives of the temporal and spatial variation of moisture are given, making use of four nearly independent observing systems, and emphasizing satellite data.

The first perspective is based on brightness temperature from two TIROS N TOVS channels analyzed onto gridpoints for the nine days of the burst events. The temporal standard deviations for each gridpoint are shown in Fig. 1a for the 700 mb infrared moisture channel (HIRS Ch. 11), and in Fig. 1b for the 700 mb microwave temperature channel (MSU Ch. 2). The moisture signal shows large variability from the equator near 180° ENE to Baja California, thus along the burst axis. Minimum variability occurs roughly parallel to the burst axis and some 1200 km to the south.

Although the pattern of thermal variability is weaker than that of moisture (due in part to the decreased sensitivity of the microwave sensor), a pattern is still apparent. A weak maximum extends across the equator due south of the burst origin. From this point, an axis of maximum variability extends NNE to a second maximum near 25°N, to the NW of, and not along, the burst axis.

The letters in Fig. 1 correspond to locations where sounding data are available. Temperature and moisture variability at 700 mb are compared in Table 1 between data from these soundings, the satellite-derived data, and colocated ECMWF analyzed data. These point comparisons show that good correspondence exists between satellite and raob moisture and temperature variability. Less satisfactory agreement is found between ECMWF and satellite values. Little correspondence is observed between thermal and moisture signals from satellite.

The second perspective of variability is displayed in Hovmöller diagrams (Fig. 2), prepared for a 1200-km wide band centered along 7.5°N. Fig. 2a shows ECMWF analysis of relative humidity at 700 mb; Fig. 2b is the TIROS N moisture channel;

Table 1

Temporal standard deviations at points

Location	Satellite Ch. 2(°C)	Satellite Ch.11(°C)	Raob T(°C)	Raob RH(%)	ECMWF RH(%)
A	0.46	1.84	1.33	15	12
B	0.64	3.09	0.90	28	15
C	1.00	2.40	-	14	14
D	1.27	1.90	-	22	8
E	0.58	1.21	1.26	1	14
F	1.00	3.04	1.21	19	23
G	1.70	2.87	2.16	30	12
H	1.09	4.66	1.50	31	19
I	-	-	5.14	28	-
J	0.76	4.01	2.47	36	16

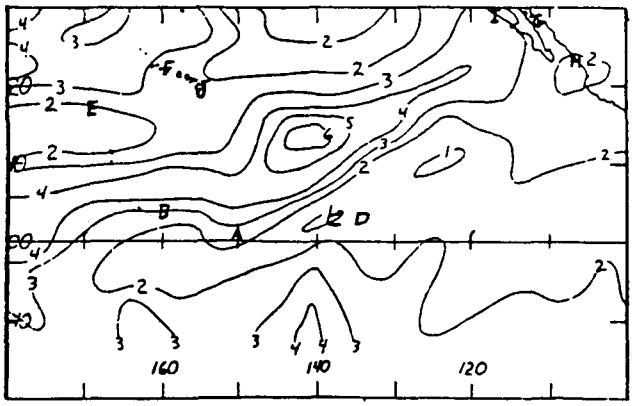

Fig. 1a. Standard deviations of gridpoint values of brightness temperature for the 700 mb infrared moisture channel (7.3 μm) for 20-29 January 1979.

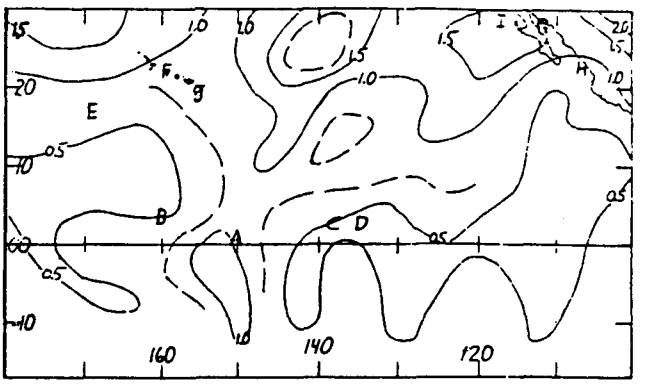

Fig. 1b. Same as Fig. 1a but for 700 mb microwave temperature channel (53.73 GHz). Capital letters here and in Fig. 1a are radiosonde stations.

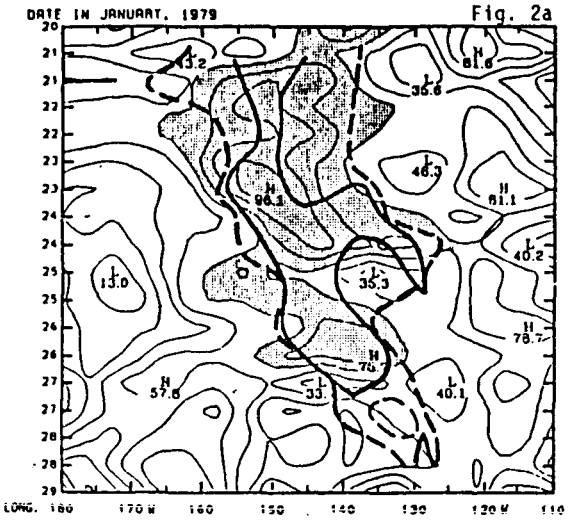

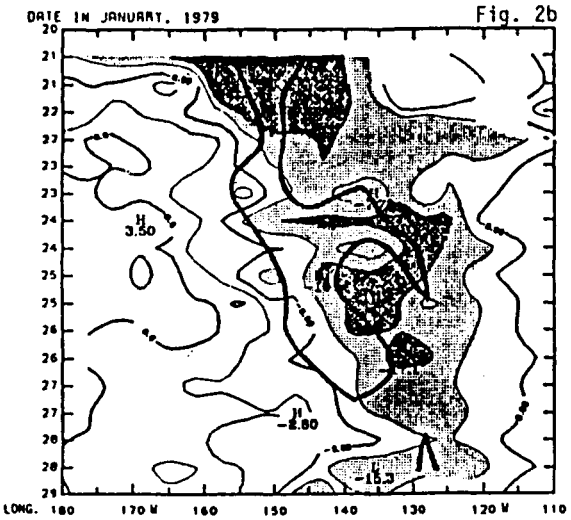

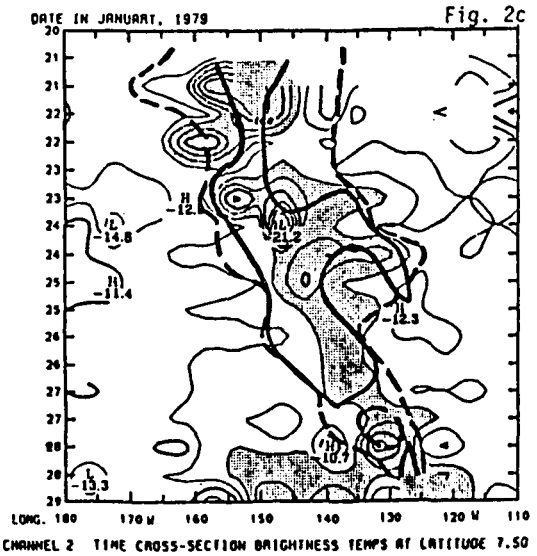

Fig. 2. Hovmöller diagrams of moisture distribution at 7.5°N between 180° and 110°W for 20-29 January 1979. See text for explanation of lines.

Fig. 2c is a TIROS N microwave channel. The latter two are brightness temperatures and represent energy sources which peak near 700 mb heights. Also shown on these sections are the extent of lower (heavy dashed lines) and high (heavy solid lines) clouds, as determined from GOES W enhanced infrared imagery (prepared by F. P. Robertson of Marshall Space Flight Center, NASA). Due to design and to unanticipated problems, the ECMWF analysis depends only on surface data and model initalizations based on these data. Thus, both here (Fig. 2a) and in Table 1, the moisture analysis is independent of satellite observations and sounding data.

There is good qualitative consistency between the three data portrayals and the cloud imagery. Though not perfect, ECMWF data identify both moisture bursts and the dry core on the 25th. The highest relative humidity values are unambiguously associated with the deepest clouds. There is a modest tendency for relative humidities to be elevated on the west side of the burst axes.

The satellite moisture signal (Fig. 2b) also identifies two moisture bursts. However, the highest moisture signal is not nearly so well associated with the deep convection. Generally, the wettest air lies east of the burst. It is not clear which of these moisture evaluations correctly position the moist air. The microwave signal (Fig. 2c) indicates that the burst region appears to be cold in the middle troposphere. However, the "bull's eyes" are probably heavy precipitation regions which are affecting the microwave signal. These regions agree well in position with the high cloud regions. Outside the burst region, almost no variation is picked up at this latitude, a result consistent with Fig. 1b.

3. EVALUATION

Although not specifically about phenomena, this paper identifies interesting synoptic behavior. There is considerable thermal and moisture variability in the region of, but not limited to, the burst origin. There are also unexplained moisture variations along the burst axis, whereas temperature variability is much smaller and more uncertain.

Conclusions on measurement capability are:

a. Satellite data, both visual and quantitative, contain important temporal and spatial variability not currently identified in analysis schemes.

b. The ECMWF model is remarkably able to anticipate upper level moisture fields, given the actual lack of observations in the area.

c. Point comparisons outside of the active burst regions show systematic overpredictions of mean relative humidity and underpredictions of temporal variability by ECMWF analysis with respect to observations.

d. Uninverted channel radiance data exhibit detail not available in operational temperature retrievals.

4. ACKNOWLEDGEMENT: The authors acknowledge the support of NASA's George C. Marshall Space Flight Center under contract No. NAS8-35182.

5. REFERENCES

McGuirk, J. P., and A. H. Thompson, 1984: Transient tropical disturbances within the Pacific Hadley cell, Postprints of the 15th Conference on Hurricanes and Tropical Meteorology, Miami, 249-255.

Extended Abstracts Volume: 16th Conf. on Hurricanes & Tropical Meteorology, May 14-17, 1985, Houston, Texas. Published by American Meteorological Society, Boston, Mass. USA

TWO MODES IN THE PACIFIC HADLEY CELL

James P. McGuirk and Aylmer H. Thompson

Texas A&M University

College Station, Texas 77843-3146

1. TROPICAL CIRCULATION

A moisture burst is defined as a common synoptic-scale system developing along the ITCZ and penetrating into midlatitudes. It is characterized by northeastward moving cloud masses, and virtually always occurs in conjunction with a deep tropospheric trough and with exceedingly large northward fluxes of westerly monentum. It plays a major role in the temporal and zonal mean behavior of the Pacific Hadley cell (McGuirk et al., 1984, Smith et al., 1985).

Two different mechanisms of tropical mean meridional circulation (MMC) are described herein. The annual cycle and longer term secular variation of MMC strength is reviewed. Climatological variations of moisture burst frequency are then described as they relate to these variations of the MMC. Finally, the contributions of moisture bursts to the MMC are elucidated through three case studies (two in January and one in May, 1979).

Variations in MMC are described in meridional cross sections at 80°W, 150°W, and 150°E by Newell et al. (1972); Janowiak et al. (1985) used satellite data to summarize MMC variations throughout the Pacific. Based on these data, the ITCZ in the mid Pacific is strongest in July and weakest in January. The South Pacific Convergence Zone is most intense in the central Pacific in July. The meridional sections show a reversed MMC at 150°W with actual tropical subsidence, apparently induced by meridional confluence at 150 mb; in summer, this pattern reverses, at least over the ITCZ region, with difluence at 150 mb and weak boundary layer confluence. At 80°W the situation reverses with a MMC extending to the tropopause in winter and a more complicated pattern in summer dominated by a shallow MMC below 500 mb. At 150°E a weak MMC appears which becomes weaker and shallower in summer.

The most significant variation in strength of the Pacific ITCZ occurs with the massive intensification associated with El Niño; this variation overwhelms the annual cycle to give the strongest observed Pacific ITCZ in (NH) winters of El Niño.

2. MOISTURE BURST BEHAVIOR

The frequency of moisture bursts varies systematically in time and space with the strengths of the ITCZ and the MMC (McGuirk et al. 1984). Generally, where the ITCZ is weakest, moisture bursts are most common: in the winter in the central Pacific where about 11 occur per month and a burst is active at least 75% of the time; in the vicinity of the dateline and close to Central America in late spring when the MMC weakens in these regions, and about 70% of the wintertime frequency is observed; in these same regions at the end of El Niño, but even less frequently. Bursts seldom occur in the central Pacific in summer; they do not occur at all in the active El Niño regions.

Fig. 1 shows the time mean behavior of the meridional winds between 180° and 110°W for two 9-day periods in January and May, 1979 (based on ECMWF analyzed winds). These figures depart from their counterparts by Newell et al. (1972). One reason is the much larger data base available for the ECMWF analysis. More important, three moisture bursts (two in January) appear in these time means.

Before the bursts develop (Fig. 2a and 3a), the MMC is similar to Newell's climatology. As bursts evolve (b), the zonally averaged MMC strengthens; and, by the termination of the bursts (c), the MMC assumes the shape of most classical representations of the tropical meridional winds. A second interesting feature of the sections is the shallow MMC which generally appears below 500 mb before and during the early portions of the bursts' evolution.

One additional feature of the Hadley cell is the strong northward transport of westerly momentum. Moisture bursts account for a large portion of this flux, at least when they are present. At jetstream level, (uv) averaged over the Pacific sector increases from 5 to 8 times as a typical burst evolves. Tropospheric averages across 30°N are shown in fig. 4. Moisture bursts are easy to identify in these time series.

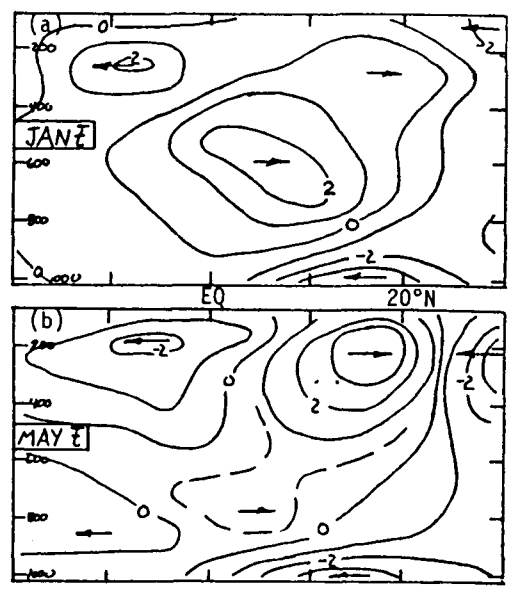

Fig. 1. Time averaged cross-sections of meridional winds, for Pacific sector for January and May 1979 case studies. Units of m/sec.

C-2

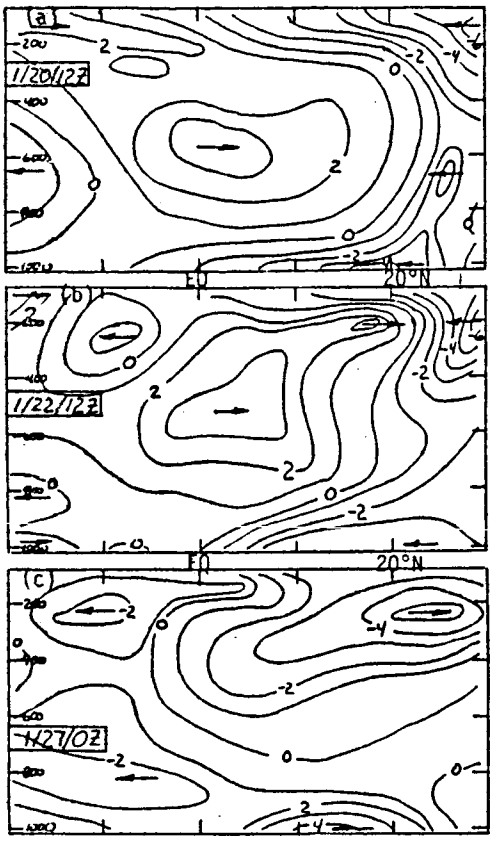

Fig. 2. As in Fig. 1, except for individual time periods in January.

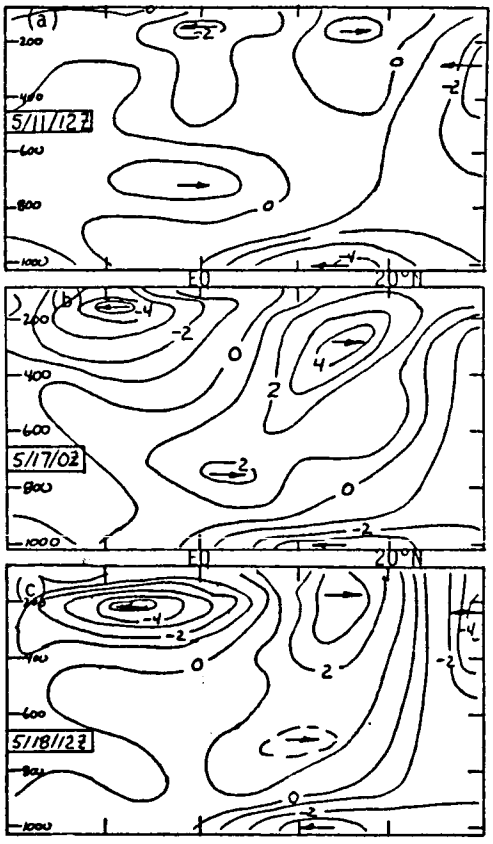

Fig. 3. As in Fig. 1, except for individual time periods in May.

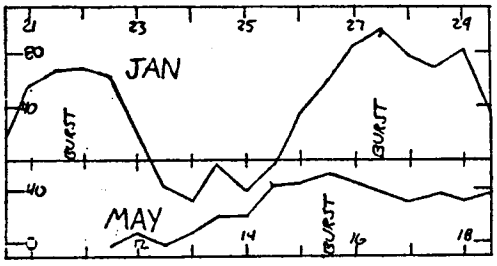

Fig. 4. Vertically-integrated zonal momentum flux across 30°N for Pacific sector. Units of m^2/sec^2.

3. INTERPRETATION

Based on these data, a hypothesis is suggested. The strength of the Hadley cell is controlled by some zonally symmetric forcing. Where this forcing is strong, synoptic disturbances do not occur along the ITCZ, as during El Niño, or to a lesser extent, in summer. Where and when this forcing is weaker, a shallower, or even a reversed, MMC results in the lower troposphere. In this environment, synoptic moisture bursts develop and the statistical mean behavior resembles that of a zonally symmetric, thermally direct MMC.

Perhaps the most interesting aspect of this interpretation is that the zonally symmetric form of the circulation does not substantially influence mid-latitude weather, whereas the synoptic moisture bursts commonly appear as, or with, midlatitude weather systems.

4. ACKNOWLEDGEMENT: The authors acknowledge the support of NASA's George C. Marshall Space Flight Center under contract No. NAS8-35182.

5. REFERENCES

Janowiak, J. E., A. F. Krueger, P. A. Arkin, and A. Gruber, 1985: Atlas of Outgoing Longwave Radiation, NOAA Atlas No. 6, 44 pp.

McGuirk, J. P., and A. H. Thompson, 1984: Transient tropical disturbances within the Pacific Hadley cell, Postprints of the 15th Conference on Hurricanes and Tropical Meteorology, Miami, 249-255.

Newell, R. E., J. W. Kidson, D. G. Vincent and G. J. Boer, 1972: The General Circulation of the Tropical Atmosphere, MIT Press, Cambridge.

Smith, N. R., J. R. Schaefer, J. P. McGuirk, and A. H. Thompson, 1985: The synoptic structure of tropical Pacific moisture bursts, presented at the AMS 16th Conference on Hurricanes and Tropical Meteorology, Houston, May.

14.3

Extended Abstracts Volume: 16th Conf. on Hurricanes & Tropical Meteorology, May 14-17, 1985, Houston, Texas. Published by American Meteorological Society, Boston, Mass. USA

THE SYNOPTIC STRUCTURE OF TROPICAL PACIFIC MOISTURE BURSTS

N. R. Smith, J. P. McGuirk and A. H. Thompson

Meteorology Department, Texas A&M University
College Station, TX 77843-3146

1. INTRODUCTION

McGuirk and Thompson (1984) described the synoptic climatology of the occurrence of moisture bursts - synoptic scale cloud bands which move northeastward out of the ITCZ into middle latitudes. The origins of these systems are linked to locally enhanced Hadley cell overturning and have appearances typical of tropical disturbances. The midlatitude extension is commonly related to the subtropical jet stream, midlatitude troughs and downstream cyclogenesis (Thepenier and Cruette, 1981).

2. UPPER LEVEL PATTERN

Fig. 1 typifies both the burst development conditions and its evolution; this burst occurred between 17 and 22 January 1982.

The climatology of the 200-mb flow is consistent throughout all observed events. In nearly every burst, an extratropical trough extends into the tropics before or as the burst develops on the ITCZ. The trough often extends across the equator (Fig. 6), leading to significant interhemispheric momentum and moisture exchanges. The burst generally develops in the ITCZ region within 1,000 km, and to the east, of the 200-mb trough. For the burst in Fig. 1, the cloud origin region remained consistently within 200 km of the trough axis. Bursts move slowly eastward with the trough; westward propogation is observed only occasionally in intensifying bursts.

Detailed wind analyses of three 1979 bursts show strong meridional overturning circulations in the burst region and associated acceleration of the zonal winds. Jet wind speeds at and downstream of the burst origin in Fig. 1 accelerated from 35 m/sec on the 17th to over 80 m/sec over the central United States on the 21st. Some bursts are observed to develop with weak upper winds over the origin.

Significant moisture fluctuations appear along the burst, but only small temperature changes occur; temperature is more variable in the trough to the northwest of a typical burst. As the leading edge of a burst crosses the North American coast, the horizontal temperature contrast across the burst intensifies. This intensification is anticipated as the geostrophic constraint becomes more dominant and the upper level winds strengthen. No strong or consistent temperature signal has been detected in the origin region in the early stages of a burst. However, several strong bursts have been detected in the region of intersection of the ITCZ with a polar front associated with southward displaced cyclones. These bursts may not develop immediately as the front reaches the ITCZ.

3. LOW LEVEL PATTERN

The low level flow in the burst origin region is not nearly as consistent as is the upper level flow. Although a col often appears (56% of the time) as the burst develops, other low level wind patterns are common. These other patterns primarily include cusps or weaker waves which resemble cusps, but bursts also occur within unclassifiable wind fields. Typical phenomena most commonly associated with burst development are: 1) Fronts penetrating into the deep tropics; 2) Easterly waves of either tropical or subtropical origin; and, 3) Southern hemisphere anticyclones which cross the equator. The common link is that bursts develop in regions in which the climatological easterly flow assumes a southerly component.

Fig. 1 represents a typical col case. A weak wind field exists as the burst develops (on the 17th). Still, a col is apparent in the winds away from the originating cloud mass. The col is more apparent on the 19th. The precise position of the burst origin varies within the col. It almost invariably appears somewhere in the anticyclonically curving flow east of the col center (as in Fig. 1b) with the southern edge of the clouds commonly south of the col's neutral point. In col cases, the confluence axis normally aligns itself with the burst axis and the winds under the clouds blow parallel to the burst. In the non-col cases, no uniform wind direction exists under the clouds. The region directly east of the burst origin has been typified as one of relative dryness, low variability and anticyclonic circulation.

As bursts develop, northwesterly flow often appears to the northwest of the origin, particularly in col cases. These northwesterlies, particularly strong in Fig. 1 b and c, are typically cold, and most probably modified polar air; on the 17th, the leading edge of this air is some 2000 km from the burst origin. Other case studies show strong low level westerlies and northwesterlies to the west of the origin, even before the burst develops; although climatologically unexpected, these winds may often exist and go undetected under the ITCZ cloud mass which is often present to the west of the burst origin.

4. SUMMARY

Many features observed in moisture bursts are observed in midlatitude jet stream regions and in tropical waves. These two events are connected in moisture bursts, as is further downstream midlatitude synoptic development. The jet stream can occasionally be traced back to the tropical wave and across the equator into the southern hemisphere.

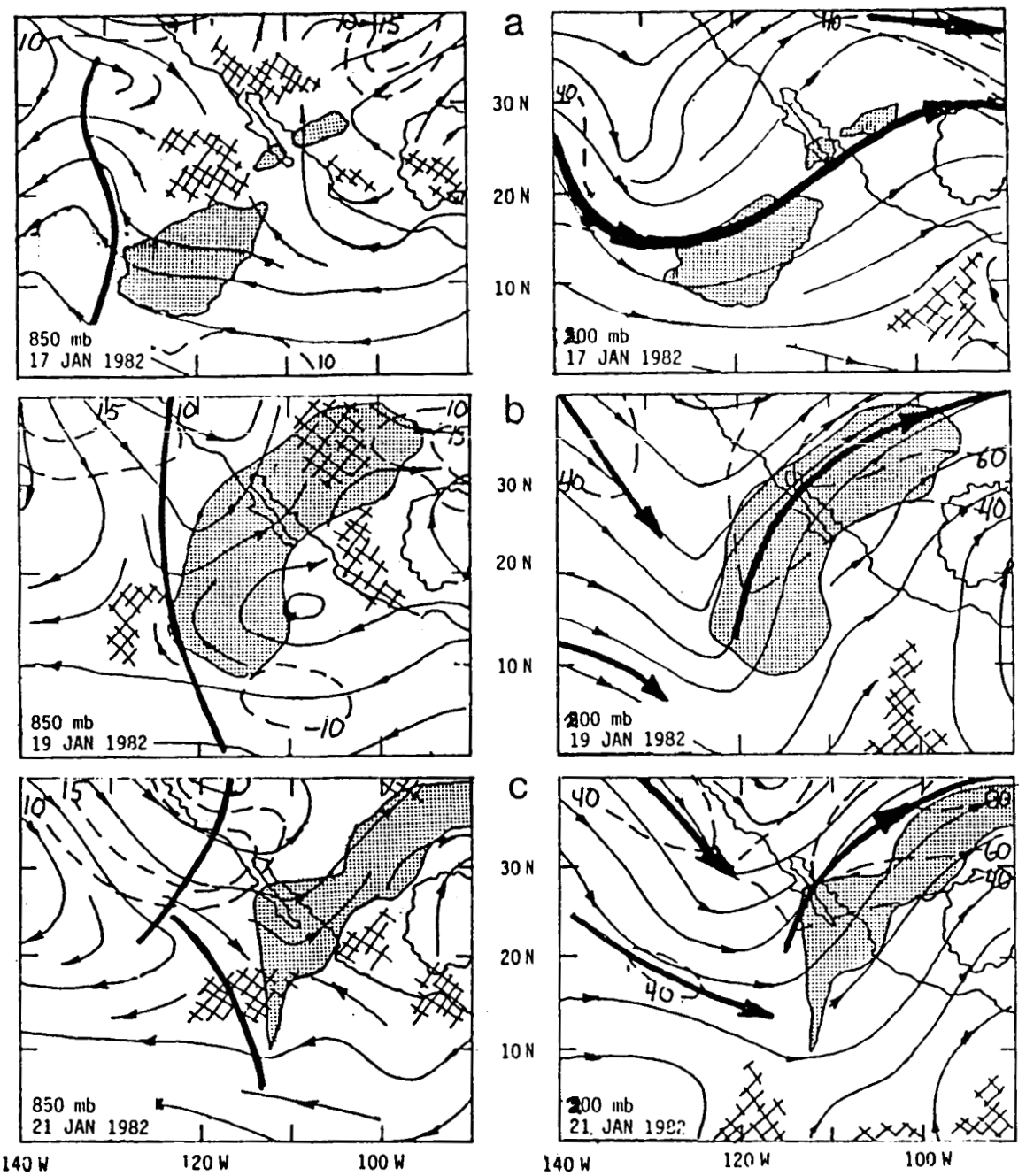

Fig. 1. Streamline charts at 850 mb and 200 mb for 17, 19 and 21 January 1982. Areas of weak and variable winds are cross hatched. The cloud masses of the moisture burst are stippled. The heavy lines on the 850 mb chart are positions of the 200 mb trough. The isotachs (dashed lines) are labeled in m/sec.

Bursts develop as midlatitude troughs interact with low level tropical disturbances in the easterlies. Frequently, low level flow conducive to burst development exists and no bursts result. Whereas fronts are often found near burst origins, they are not essential components of burst initiation.

5. ACKNOWLEDGEMENT

The authors acknowledge the support of the George C. Marshall Space Flight Center, NASA, under Contract No. NAS8-35182.

6. REFERENCES

McGuirk, J., and A. Thompson, 1984: Transient tropical disturbances within the Pacific Hadley cell, Postprints, 15th Conf. on Hurricanes and Tropical Meteorology, Amer. Meteor. Soc., Miami, FL, 249-255.

Thepenier, R.-M., and D. Cruette, 1981: Formation of cloud bands associated with the American subtropical jet stream and their interaction with midlatitude synoptic disturbances reaching Europe. Mon. Wea. Rev., 109, 2209-2220.

PREPRINT VOLUME
NATIONAL CONFERENCE ON SCIENTIFIC
RESULTS OF THE FIRST GARP GLOBAL
EXPERIMENT. Jan. 13-17, 1986, Miami,
FL. Amer. Meteor. Soc. Pp. 40-43.

COMPARISONS OF FGGE IIb AND IIIb WINDS IN A TROPICAL SYNOPTIC SYSTEM

J. P. McGuirk, A. H. Thompson and B. A. Snyder

Texas A&M University
College Station, TX 77843-3146

1. INTRODUCTION

Wind analysis over the tropical Pacific Ocean is subject to a number of uncertainties. Correlation of observational errors, dependence of observational characteristics on the synoptic systems themselves, limitations on the information content of observations, and problems with extrapolation into data void regions all act to limit the effectiveness of sophisticated analysis procedures. Finally, the physics of the tropics itself acts to decouple the divergent and rotational wind components and to render divergence estimates uncertain. Optimal interpolation (OI) cannot overcome data sparsity and the lack of geostrophic control. This paper examines these issues based on FGGE data and ECMWF analyses for a nine-day period in January 1979. The investigation is centered on a synoptic system, called a moisture burst, over the data-sparse tropical northeast Pacific Ocean. About 10 of these systems per month develop in this region (Smith et al., 1985).

2. DATA AVAILABILITY

2.1 Synoptic Organization

The classic problem of data sparsity occurring in the vicinity of ocean storms has changed somewhat. Cloud drift winds now provide observations in synoptically active regions, but are still restricted: high clouds preclude low level observations. McGuirk et al. (1985) showed that nearly the entire synoptically-active moisture burst region was devoid of both ship and low level cloud drift wind observations. Nevertheless, EMCWF analyses detected synoptic variations, presumably through an adequate initialization based on upper level observations. Fig. 1 summarizes the low level (850-1000 mb) equatorial wind shear associated with a moisture burst. The burst is in Region III in the inset to Fig. 1. The data points demark the shear near the equator from the dateline to about 110°W. These shears fall into four groups, which are stratified geographically as well. Region I consists of equatorial westerlies to the west of the moisture burst; the shear is westerly, implying strengthening winds with height. Region II shows easterly trades becoming stronger with height to the south of the burst. Region III is the burst, with surface northeasterlies giving way to southerlies with height. Surface easterlies becoming westerly with height occur in Region IV. The conclusions are threefold: i) With a moisture burst developing every few days, synoptic scale wind variability may be larger than generally thought in the tropics; ii) Large organized differences in boundary layer structure exist on the synoptic scale; iii) Vertical structure functions currently in use in OI schemes do not allow for complex boundary layer structure; thus extrapolation of cloud drift winds downward or surface observations upward may lead to large errors.

2.2 Horizontal Correlation

One of the problems specifically treated by OI is the correlation between observational errors. It occurs with synoptically biased

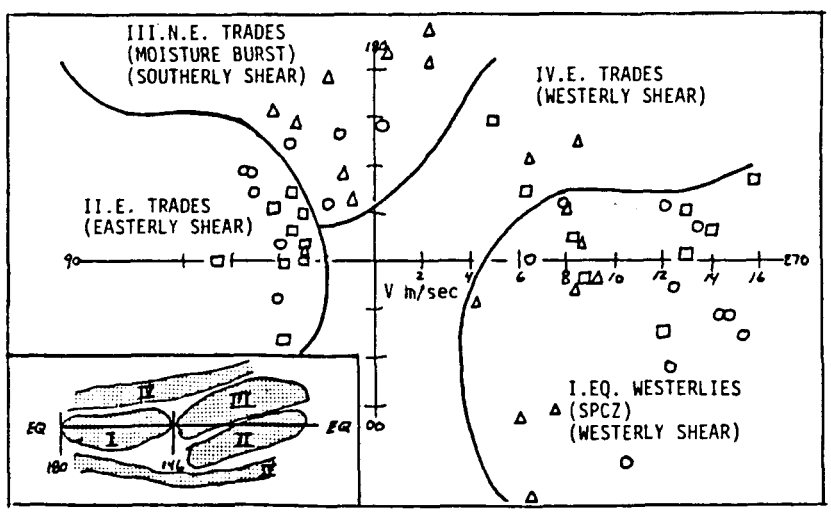

Fig. 1. 850-1000 mb shear in the equatorial region from ECMWF wind analysis. Data points locate the point of the shear vector, anchored at the origin. Clustered groups correspond to geographical regions denoted in the inset.

observations and particularly with cloud drift winds. For example, if one low level cloud drift wind is placed at an improper elevation, the entire fleet of winds in the region will be improperly located. It was found (figures not shown) that vector differences between cloud drift winds and 850 mb winds at co-located grid points are spatially coherent on scales ranging between 800 and 3000 km. Within these regions the wind direction of the vector differences were the same within ± 20°. The OI scheme interpreted this coherent structure as observational error. In the absence of other data, it might be better for the OI scheme to interpret observations more flexibly.

2.3 Vertical Correlation

When data, such as the cloud drift winds discussed above, are used for analysis at different, but nearby, elevations, OI invokes vertical structure functions. Winds are extrapolated upward from the surface or downward from cloud level by adjusting their speed but not their direction. According to data of Kantor and Cole (1980), this procedure may not be adequate. They show that the correlation between 1000 and 850 mb rawinsonde winds in the deep tropics can be nearly zero and is usually less than 0.4. Fig. 2 shows the 850-1000 mb shear vectors for wind soundings launched from ships between 3°S and 9°N and east of 150°W. Speed shear varies between 1 and 15 m/sec and the directional shear at individual ships usually spans 180°. The shear direction over this equatorial strip is randomly distributed.

2.4 Temporal Correlation

Fig. 1 indicated that the ECMWF analysis can identify low level shear patterns. Fig. 3 shows Hovmöller diagrams (time vs. longitude) of winds at 1000 and 850 mb along 3.75°N. The "streamlines" do not indicate local parcel trajectories, but the temporal change of wind direction at fixed points. The active moisture burst region lies between 130 and 160°W. Outside of this region, the directional shear between 850 and 1000 mb is small. Large temporal changes and differences between 1000 and 850 mb wind direction appear in the burst region. Most of the large directional changes occur in those regions where sounding data are available; however, correspondence between the analyzed streamlines and these dropsonde wind directions is poor, even in regions of no other data. Few cloud drift winds were available in the burst region; where they did exist, they often possessed large discrepancies with the analysis if rawinsonde data were present. The obvious question is whether or not the data void regions are equally as variable as the burst region.

3. WIND INFORMATION CONTENT

3.1 Wind Accuracy

OI attempts to overcome imperfect observations. What must be defined, and has not, is the information content of a data set. Whitney (1984) has documented low level rms cloud drift wind errors to be nearly 5 m/sec. Traditionally, this number has been compared to mean low level winds. The appropriate number, however, should be the rms variation of the wind about its climatological mean. If this variation is smaller, there will

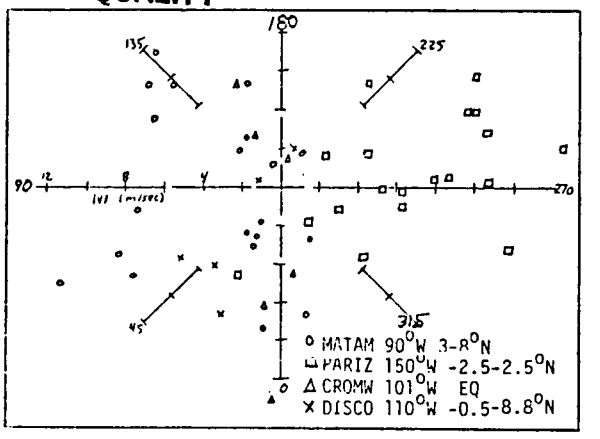

Fig. 2. 850-1000 mb wind shear, observed from radiosondes launched from four ships between 150 and 90°W and equatorward of 10° for a nine-day period in January 1979.

not be a great deal of information in cloud drift winds not contained already in simple climatology. A test was executed to evaluate this information content over the tropical east Pacific. The vector wind difference was calculated between low level cloud drift winds and 850 mb ECMWF analyzed winds at nearby gridpoints. No attempt was made to interpolate the gridded data horizontally or vertically to the exact position of the observation. The histogram of these "observational errors" is given in Fig. 4a. The rms difference between observations and analysis is about 3.6 m/sec. The discrepancy with Whitney's value occurs because the observations are compared with analysis in Fig. 4. A second set of cloud drift winds, observed from GOES (Indian Ocean), was superimposed over the Eastern Pacific domain, simply by reflecting the observations about the dateline. The rms differences were computed using these "random" observations; their histogram appears as Fig. 4b. If a few large errors are ignored, an rms "observational error" of 4.2 m/sec results. The implication is that the information content of cloud drift winds over climatology may be as little as 0.6 m/sec in an rms sense. Great care must be taken in utilizing these observations and in analysis over data sparse regions.

3.2 The Divergent Component

Divergence in the tropics is especially difficult to estimate, not only because of the limited information content of observations, but also because of the lack of geostrophic balance and because of the major divergent forcing by diabatic processes (Julian, 1984). OI schemes underestimate divergence, particularly on synoptic, and smaller, scales. To examine the problem of linking divergent and non-divergent wind fields, we decomposed the ECMWF windfields into non-divergent and irrotational components, increased the divergence uniformly by a constant factor, and reconstructed the two dimensional streamlines, using the enhanced divergent winds. Although the resulting divergence is not an improved estimate, it still can be used to test the effect of larger divergence on the streamline field. Typical results appear in Fig. 5, in which the non-divergent stream function (a) is compared with streamlines (b) reconstructed using 4 times

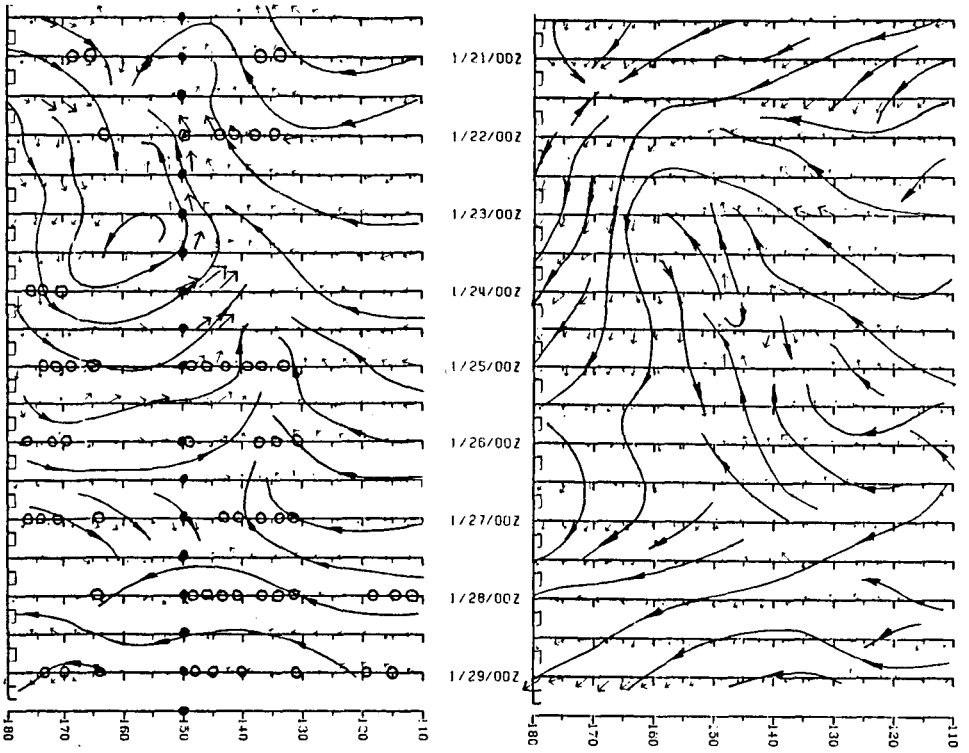

Fig. 3. "Streamline" patterns at 1000 mb (right) and 850 mb (left) along 3.75°N between 180 and 110°W. Time increased downward. Circles at 850 mb give approximate dropsonde locations and circles at 150°W give tropical shipsonde location.

the divergent wind. The patterns are similar, with major changes restricted to the proximity of velocity potential extrema. Even in these areas, the changes are restricted to the downwind (non-divergent) side of the extremum. The reasons are twofold: i) At low levels, the divergent wind is usually smaller than the non-divergent wind, so large increases are necessary before divergence influences the overall pattern; ii) A comparison of these two analyses shows that the divergent wind points in the same direction as the non-divergent wind; thus, changes in magnitude of the divergent wind will not change the streamline pattern. Since the non-divergent wind dominates at 200 mb, divergence fields have almost no effect on the 200 mb streamline pattern. In fact, the only significant change at 200 mb occurs over the SPCZ.

If the ECMWF analysis correctly simulates tropical divergence behavior, two conclusions are clear: i) Divergence at 200 mb will be more difficult to estimate than at 850 mb; ii) Divergence is so poorly related to streamline patterns that dynamical or kinematic procedures are not likely to result in improved divergence estimates.

4. CONCLUSION

The material of Section 3 suggests that it is extremely important to maximize wind accuracy. At the same time, more credibility should be given to the few observations available in data sparse areas. New procedures for linking divergence to synoptic activity (as suggested by Julian, 1984) and other wind features should be explored. More innovative OI schemes should be developed, allowing more divergence (Daley, 1985), or keying structure functions to the synoptic system. Methods of incorporating satellite imagery and other quantitative data into the initialization or data correction step should be developed.

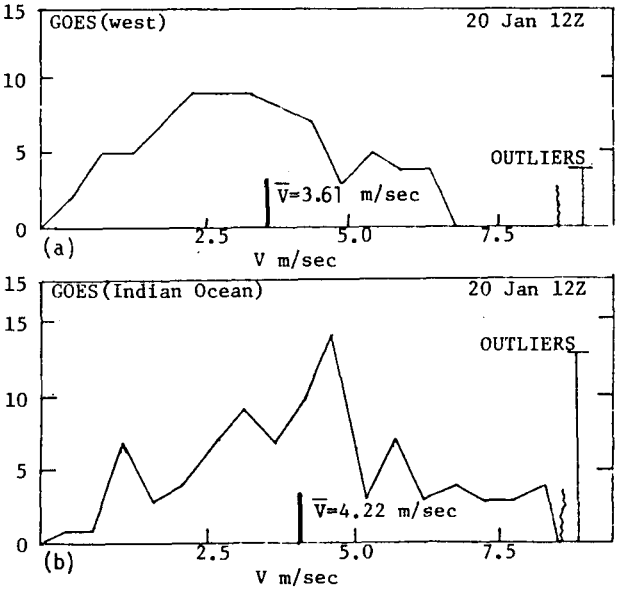

Fig. 4. a) Histogram of 850 mb "observational" errors with respect to cloud drift winds. b) As in (a), except for randomized cloud drift winds, observed by GOES (Indian Ocean) over the Bay of Bengal and Western Pacific, and superimposed over the Eastern Pacific.

5. ACKNOWLEDGEMENTS

The authors acknowledge the support of the George C. Marshall Space Flight Center, NASA, under Contract No. NAS8-35182.

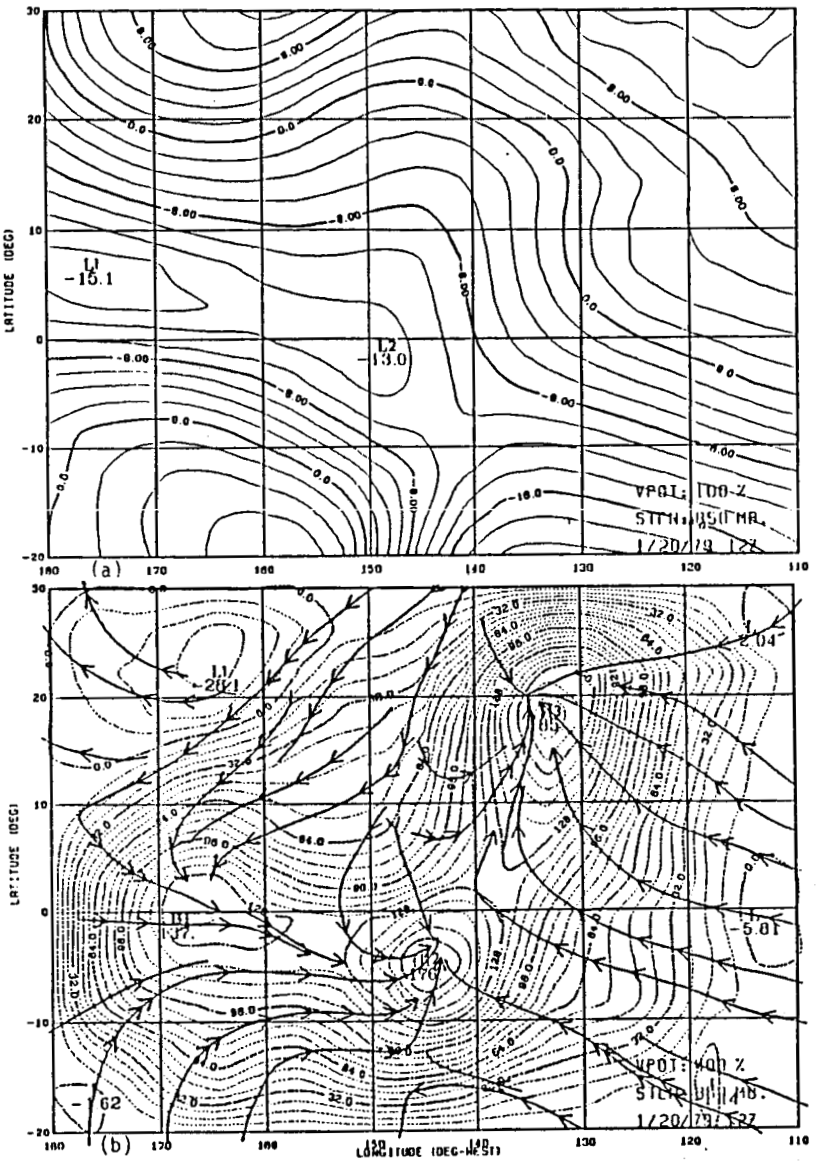

Fig. 5. a) 850 mb stream function derived from ECMWF analysed winds. b) Streamline analysis resulting from adding the divergent winds (arbitrarily increased by a factor of four) to the analysis in (a); dashed lines give the modified velocity potential field.

6. REFERENCES

Daley, R., 1985: The analysis of synoptic scale divergence by a statistical interpolation procedure. Mon. Wea. Rev., 113, 1066-1079.

Julian, P. R., 1984: Objective analysis in the tropics: A proposed scheme. Mon. Wea. Rev., 112, 1752-1767.

Kantor, A. J., and A. E. Cole, 1980: Wind distributions and interlevel correlations, surface to 60 km. AFGL-TR-80-0242, Hanscom AFB, MA 01731, 115 pp.

McGuirk, J. P., A. H. Thompson, and N. R. Smith, 1985: Observing the eastern Pacific Hadley circulation. Proceedings of the Annual Climate Diagnostics Workshop, Oregon State Univ., Corvallis, OR, 429-436. [NTIS PB85-183911].

Smith, N. R., A. H. Thompson and J. P. McGuirk, 1985: Moisture bursts over the tropical Pacific Ocean. Submitted to Mon. Wea. Rev.

Whitney, L. F., 1984: Satellite-derived products, winds, NESDIS. A CGMS XIII working paper for April, 1984, Geneva, available from NOAA/NESDIS/ASB(E/RA11), Suitland Professional Cntr, Washington 20233.

PREPRINT VOLUME
NATIONAL CONFERENCE ON SCIENTIFIC RESULTS OF THE FIRST GARP GLOBAL EXPERIMENT. Jan. 13-17, 1986. Miami, FL. Amer. Meteor. Soc. Pp. 44-47.

WINTERTIME DISTURBANCES IN THE TROPICAL PACIFIC: FGGE IIIb AND SATELLITE COMPARISONS

J. P. McGuirk, A. H. Thompson and L. L. Anderson, Jr.

Texas A&M University
College Station, TX 77843-3146

1. BACKGROUND

Data sparsity and flaws in the special observing network in operation during the FGGE first special observing period make the unambiguous interpretation of tropical synoptic systems nearly impossible. Smith et al. (1985) described the appearance of moisture bursts occurring in the tropical northeast Pacific Ocean as seen by European Center (EC) wind analyses. Thompson et al. (1984) gave examples of how these systems appear in TIROS individual channel brightness temperatures, interpolated and analyzed to an appropriate grid. Thompson et al. (1985) made an intercomparison of moisture distributions, as described by radiosonde and satellite observations, with the EC moisture analyses. Although there was considerable pattern similarity, correspondence between variables was poor near the equator and in dry regions. When compared with independent observations, the EC analysis appeared more realistic than would have been supposed based on data availability and analysis procedures. We extend these efforts by describing the synoptic development of moisture fields associated with moisture bursts near the ITCZ.

2. ITCZ DISTURBANCES

2.1 Sounding Data

Fig. 1 presents a radiosonde time section from ship Pariz near the equator and 150°W. A moisture burst developed during this period; development began about 06 GMT 21 January. The section demarks a number of moist layers before and after the burst event, with near saturation below

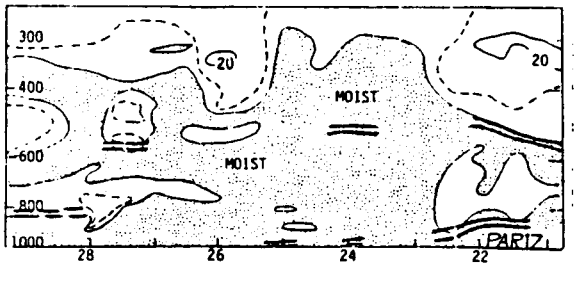

Fig. 1. Time section of radiosonde data from ship Pariz (Eq. and 150°W) between 21 and 29 January, 1979. Isopleths give dew point depression in °C, with shaded regions less than 5°C. Heavy lines show inversions and stable layers.

300 mb throughout the active phase of the burst. Although the burst developed to the west of Pariz, the section suggests that the burst involved the equatorial region only after 24 to 36 hours of development. Cloud imagery confirm that burst clouds link up with SPCZ cloud mass along and south of the equator only after the initial development period. Prior to burst development, a low level inversion was overlain by a 200 mb thick layer of drier air. After the burst, the dry air and stable layer returned. Appearing intermittently is an inversion at about 550 mb, often suggestive of subsidence given the relative dryness aloft. This inversion is a nearly ubiquitous feature of soundings over the tropical and subtropical north Pacific during this time period. Although time sections at nearby dropsonde sites look somewhat different than Fig. 1, it is curiously observed that the time section of radiosonde data at Isla Socorro, 4500 km to the northeast, mirrors the pattern in Fig. 1 closely, but delayed in time about 36 hours. The moisture burst crossed Socorro as it streamed northeastward.

Although severe data gaps occurred in both satellite and sounding data during the burst's early development stage, a full range of observations was available by the 23rd. Fig. 2a shows the distribution of moisture (dew point depression) as obtained from a series of dropsonde observations made along the southern edge of the ITCZ. The dropsondes were launched between 12 and 23 GMT, 23 January along 4°N from 150 to 130°W; the sounding near 160°W is Fanning Island where the section turns northward (the figure should be folded at a right angle) and the two leftmost soundings are Hawaiian stations located 1500 km to the north. The deep layer of moisture, noted in Fig. 1, is centered at 135°W at this latitude. The dryness north and east of the burst is apparent. The extremely rapid disappearance of clouds to the north, viewed in GOES enhanced imagery, confirms subsidence extending throughout the depth of the troposphere.

2.2 Satellite Data

The curves below this sounding section present a number of satellite observations and their variability along 4°N. Fig. 2b depicts the approximate cloud heights (as determined from color-enhanced GOES infrared imagery at 00 GMT, 24 January). Agreement is good, with the highest and convectively appearing cloud close to, but slightly west of, the deep moist layer. The deep upper layer of moisture at the eastern edge of the section is not associated with high clouds. The abrupt drying at Fanning is coupled with

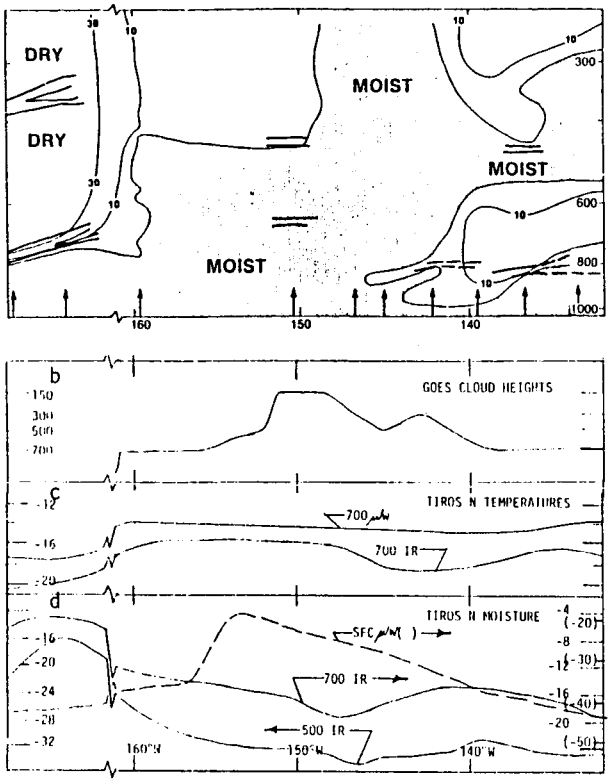

Fig. 2. Sections of meteorological data east of 160°W at 4°N. Data to the left of 160°W lie along a line from Fanning Island to Hawaii at 20°N. a) As in Fig. 1, except dropsonde data, with arrows giving sounding locations. b) Cloud heights determined from color enhanced GOES imagery. c) TIROS N brightness temperatures for microwave and infrared channels peaking at 700 mb. d) Moisture channels peaking at 700 and 500 mb and a microwave channel peaking close to the surface.

disappearance of clouds above the surface layer. Discrepancies are explained in part by the difference in time of the observations. It is disappointing that the cloud imagery is unable to differentiate between the moisture structure to the east and that to the west of the burst.

Fig. 2c depicts thermal signals, nominally in a layer centered at 700 mb. The north-south temperature difference (on the left side of the figure) is easily seen. The microwave signal is nearly flat, with only a broad minimum (0.5°C in brightness temperature) centered over the moist region. The 2.5°C decrease in brightness temperature in the infrared signal perhaps is caused by cloud contamination. Although processing procedures are supposed to eliminate cloud-contaminated observations, they are apparently not entirely successful.

Fig. 2d depicts TIROS infrared moisture channels for layers centered on the 700 and 500 mb surfaces and the microwave channel peaking near the surface. The wettest areas (cold infrared) agree well with the deep layer of moisture detected by dropsondes at 145°W, and noted by the deep cloud in Fig. 2b. The signal is stronger in the lower channel. It is surprising that, despite the cloud cover (noted as contamination of the thermal signal), both moisture channels recognize the drier air east of the moist region. The peak in the microwave signal corresponds to the high convective clouds slightly west of the moist region. The decrease from this peak follows the trend in cloud height closely. This peak probably is due to absorption by heavy precipitation and re-emission in the rain shaft; this re-emission will appear warm because the low emissivity of the ocean surface makes the background radiation appear to be coming from a colder source.

2.3 EC Analysis

These observations can be compared with EC analysis along the ITCZ. Fig. 3a shows the vertical section of analyzed relative humidity, comparable to Fig. 2a. In spite of the very low variability of EC analyzed moisture in this region, significant synoptic variation occurs along the section. The moist region, which peaks at 500 mb, corresponds to that in Fig. 2a, although the analysis places it about 5° too far to the east. Detail outside this wet region is lacking, although there is some hint of 850 mb dryness at about 137°W. The upper level dry regions are not well simulated. (Thompson et al., 1985, showed that the EC analysis has difficulty with tropical dry regions.) Fig. 3b locates the equatorial section with squares; it also demarks locations of vertical sections perpendicular to the ITCZ. These sections are shown in Fig. 4. The extreme upper tropospheric dryness north of the ITCZ (Fig. 2b) is well simulated in Section 1. The four sections show that the mid-tropospheric moisture maximum actually crosses the equator (it is centered at 3.5°S in Section 2) and moves through the ITCZ latitudes (to 12°N in Section 4) and even to 20°N further to the east. On the extreme west side of Fig. 3, the moist region is drier and shallower, with relative humidity in excess of 70% limited to the surface layer south of the equator (Section 1 in Fig. 4). Subsequent moisture sections, however, show that this equatorial drying to the west of the moisture burst is only a temporary event.

3. ON BURST DYNAMICS

Most of the analyzed data (soundings, mappings of satellite channel data, satellite imagery and EC analysis) suggest that the moisture burst develops along the north side of the ITCZ and only later becomes linked to northern subtropical and midlatitude disturbances, and also to cross-equatorial circulations. Divergence estimates based on EC wind analysis at single levels fail to confirm this initial isolation from the southern hemisphere. These analyses uniformly show this moisture burst developing directly out of a convergence/divergence center, located several degrees south of the equator at about 160°W, and associated with a local perturbation of the SPCZ. To test this aspect of the EC analyses, as well as to examine the motion fields in conjunction with the satellite data, we prepared two estimates of vertically integrated divergence. A sample of each is shown in Fig. 5. The first is the 24 hour change in total mass field sensed by changes in sea level pressure. The second is the vertically-integrated mass divergence determined kinematically and converted to surface pressure change, assuming that omega is zero at 100 mb. The differences are

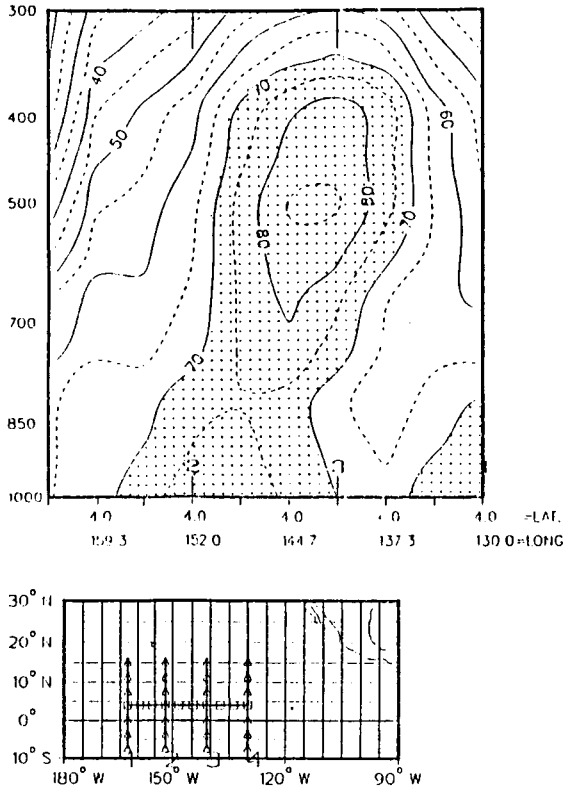

Fig. 3. a) Vertical cross section of analyzed relative humidity corresponding to Fig. 2. Relative humidity greater than 70% is shaded. b) Location of section in (a) (squares) and of cross-sections in Fig. 4 (triangles).

striking.

The extrema of pressure change observed in Fig. 5a follow the burst axis delineated by cloud imagery rather closely. Two peaks of pressure increase are observed, one at 10°S, 155°W and the other about 2000 km to the northeast. Generally, pressure falls occur to the west of the burst. At no time during the burst development do strong pressure falls occur in the burst origin region. Where the burst crossed the American coast, large pressure falls are associated with large areas of deep clouds. The reason for pressure increases along the convective cloud axis is uncertain. Although there is no requirement for falling surface pressure, rising motion is usually coupled with falling pressure. If the observations are correct, they imply simply that convergence at lower levels is stronger than divergence at upper levels.

The kinematically-inferred surface pressure change pattern (Fig. 5b) shows almost no similarity to the observed pressure change. Strong pressure falls are estimated immediately southeast of Hawaii, but no pattern aligns itself along the burst axis. More puzzling is the near disappearance of vertically-integrated divergence south of 12°N; this pattern is maintained over the entire 9 day study period and must be considered a spurious property of the analysis. Although a number of authors have discussed the shortcomings of tropical divergence schemes, and in particular those procedures utilized by EC, this property of nearly precise vertical compensation of convergence and divergence which switches on impulsively south of 12°N, has not previously been discussed.

Although the patterns of surface pressure change are inconsistent and not always well-correlated to the satellite cloud imagery and channel data, patterns like that of Fig. 5a suggest that cross-equatorial connections are potentially very strong. Because of the inconsistency of patterns, no conclusions can be reached regarding burst initiation regions.

4. SUMMARY

Important synoptic variations occur along the winter ITCZ in the North Pacific. Operational satellite data and special FGGE data describe subtle detail of this variation. Although EC analysis cannot be expected to reproduce this detail precisely, it is still surprisingly realistic, surprising in view of the excessive sparsity of data for model initialization. Discrepancies occur in the individual satellite observations, most of

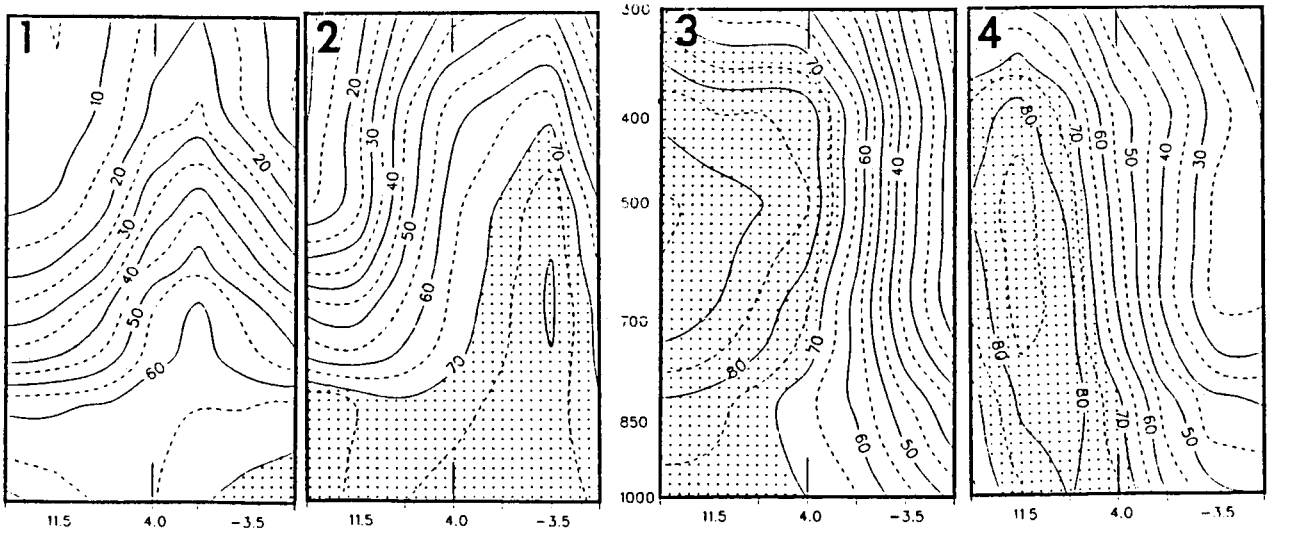

Fig. 4. Cross sections of relative humidity, locations as in Fig. 3b.

which have reasonable physical explanations. When different channels are viewed simultaneously these discrepancies can yield added signal--the existence of heavy precipitation cores, cloudy data in supposedly clear sky retrievals, and so forth. Unraveling synoptic development associated with vertical motion is still a thorny problem. While satellite data reveal important evolution patterns, in both space and time, linking these patterns to motion fields and other dynamic variables remains obstinately unsolved.

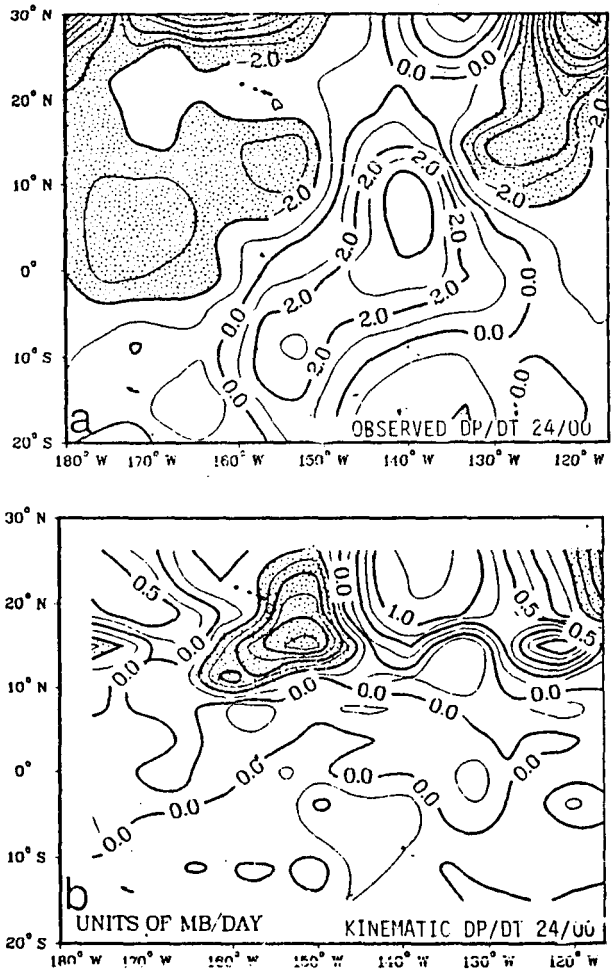

Fig. 5. Sea level pressure change in units of mb/day: a) Observations, with falls greater than 2mb/day shaded; b) Derived data from vertically integrated divergence, with falls greater than 0.5mb/day shaded.

5. ACKNOWLEDGEMENTS

The authors acknowledge the support of the George C. Marshall Space Flight Center, NASA, under Contract No. NAS8-35182.

6. REFERENCES

Smith, N. R., J. P. McGuirk and A. H. Thompson, 1985: The synoptic structure of tropical Pacific moisture bursts. Extended Abstracts, 16th Conference on Hurricanes and Tropical Meteorology, Houston, TX, May 14-17, Amer. Meteor. Soc., 192-193.

Thompson, A. H., J. P. McGuirk and L. L. Anderson, Jr., 1985: Comparisons between tropical synoptic moisture fields as determined from analysis and from observations. Op. cit., 54-55.

_____, _____, _____ and N. R. Smith, 1984: Analysis of tropical synoptic disturbances using satellite-derived soundings and radiance data from selected channels. Preprints, Conference on Satellite/Remote Sensing and Applications, Clearwater Beach, FL, June 25-29, Amer. Meteor. Soc., 135-142.

PREPRINT VOLUME
NATIONAL CONFERENCE ON SCIENTIFIC
RESULTS OF THE FIRST GARP GLOBAL
EXPERIMENT. Jan. 13-17, 1986. Miami,
FL. Amer. Meteoro. Soc., Pp. 212-215.

MOISTURE TRANSPORTS AND BUDGETS OF "MOISTURE BURSTS"

A. H. Thompson and J. P. McGuirk

Texas A&M University
College Station, TX.77843-3146

1. INTRODUCTION

An understanding of the water vapor fluxes and water vapor budgets of all areas of the Earth is desirable and for some problems essential. However, for most areas, particularly the oceanic areas of tropical and subtropical latitudes, data routinely available are inadequate to allow determination of the fluxes and budgets. Recently, the tasks of the Global Atmospheric Research Program (GARP) have included gathering data more adequate for such evaluations. This paper describes the results of calculations of moisture fluxes made using data obtained during the first Special Observing Period (SOP-1) of the First GARP Global Experiment (FGGE). The area examined was over the deep tropical eastern Pacific Ocean north of the equator. The area specifically examined extended from the equator to latitude 20°N and from longitude 180° to 100°W, but with concentration on the region south and southeast of the Hawaiian Islands. The specific synoptic feature to which the transport and budgets were related was a pair of "moisture bursts": the development of an extrusion of cloudiness and accompanying moisture from the convergence zone of the equatorial North Pacific north-eastward toward North America (Smith et al., 1985; Thompson et al., 1984).

2. DATA

Normally, the only upper air reports from the area of interest are the radiosonde reports from the Hawaiian Islands and pilot reports from commercial and military aircraft. Surface reports also are scarce except in Hawaii and the shipping lanes because of the few islands other than the Hawaiian group. During the FGGE SOP-1, special observations were made. These included reconnaissance flights with dropwindsonde capability and some weather ships with rawinsonce equipment. While the data density remained low compared to some land areas, it was much better than ever before for the area. The data became part of the so-called FGGE II-b data set and make up the basic data for this study.

2.1 The Dropsonde Data

Reconnaissance aircraft were used to fly missions from the west coast of North America and from Oahu. Tracks usually were flown diagonally toward the equator, then along a latitude circle near the equator for about 2,000 km, then northward a few hundred km, then along a latitude circle in a direction opposite to that of the second leg, and finally back to home base. Flight levels usually were near 10,000 m or a little higher. On the optimum days, one flight was made from the west coast and two from Oahu, one to the southeast and the other to the southwest. The flights usually were made close enough to the same time that they were considered as synoptic. The second leg of the flight southeast of Oahu was usually close to 4°N, while one of the east-west legs of each of the other flights was also close to this latitude; by displacing the dropsonde positions for each of these legs to a common latitude (4°N), a zonal section from about the date line (lat. 180°) to 110°W could be prepared on most days. Also, combining dropwindsonde data from two of the flights (or in some cases using only a single flight) allowed making computations for a volume.

Flights were made on only seven of the ten days investigated (20-29 January 1979), and on some of those days at least one of the reconnaissance flights never started or was aborted.

There is definite indication that the winds obtained by use of the dropwindsondes contain significant inaccuracies; however, so far there has been no attempt to adjust the calculations reported in this paper; this will be considered again later.

2.2 The FGGE III-b Data

The FGGE II-b data have been analyzed by the European Center for Medium Range Weather Forecasting (ECMWF) and produced as a set of gridded data with a grid spacing of 1.875°. These are referred to as the FGGE III-b data set. These data were used to produce moisture fluxes for the same section (along 4°N) and volumes as those used with the dropwindsonde data.

3. CALCULATION PROCEDURES

3.1 Horizontal Flux Calculations

The calculation procedures used for the results presented here are essentially the same as used by several other investigators. Among them are Saha and Bavadekar (1973), Cadet (1983), Rowland and Sikdar (1983) and Khatep et al. (1984). All determined the fluxes across a vertical surface or across the vertical walls of an atmospheric volume by using the expression

$$F = \frac{1}{g}\int_{P_t}^{P_b}\int_{0}^{L} V(p,l)q(p,l)\,dl\,dp$$

where F is net flux of water vapor across a boundary wall,
l is horizontal length along the boundary wall,
L is the total length of the boundary wall,
V is the component of the wind normal to the boundary wall,

and the other symbols have their usual meteorological or mathematical meanings. V and q may be expressed as instantaneous values, as mean values, or as mean plus eddy values, as appropriate for the particular problem being examined. For this paper, instantaneous values are used; the values are determined from the dropwindsonde data or from the FGGE III-b data and applied to a boundary wall along latitude 4°N or to the vertical walls of the volumes designated by the reconnaissance flight tracks. It should be noted that the volumes vary somewhat from one flight to another.

3.2 Moisture Budget

The usual assumption in determining moisture budgets is to neglect any moisture above some upper boundary, say the 30 kPa surface. This is close to the reconnaissance flight level.

The difficult task in this study is the determination of the vertical flux of moisture across the sea surface. It does not seem proper to use the lowest level reported by dropwindsonde to represent the air at 10 m above the ocean. Also, no sea-surface temperature value is available from the aircraft report. Further, no research ships were on the periphery of the selected volume. Probably good mean values of the sea-air differences may be determined, allowing conventional bulk transfer estimates of flux, but such values would give no added information on variability beyond that provided by the day-to-day values of the fluxes through the vertical walls. Thus, an attempt to compute volume budgets has not been made as yet.

3.3 Period Studied

The dates selected for evaluation are between 21 and 29 January 1979, a period when two moisture bursts evolved over the area described above. This examination of the moisture transfers is a part of an investigation of the moisture bursts (McGuirk et al., 1985).

4. RESULTS

4.1 Flux Across Latitude 4°N

Moisture transport across latitude 4°N is examined first. The first calculation was for the last few hours of the 20th, thus a few hours before the initiation of a moisture burst early on the 21st (all times refer to GMT). This particular line extends only from 170°W to 110°W, as indicated in Fig. 1. The arrows normal to the line represent water vapor flux across a unit length of the section, with the length proportional to the flux magnitude in accord with the scale on the figure. The flow across any segment of the long section is given by the product of the flux of that section and the length of that segment, positive for flows to the north; the net flow (upper left corner of the figure) is the length-weighted sum of the flows across each segment. The average moisture flux is obtained by dividing the net flow by the total length of the section. The moisture burst was initiated near 150°W. To the east of this point the flux was northward for some 2,000 km, while it was southward further west. East of about 130°W the flux was weaker, though mostly to the north. The average flux and total water vapor flow are

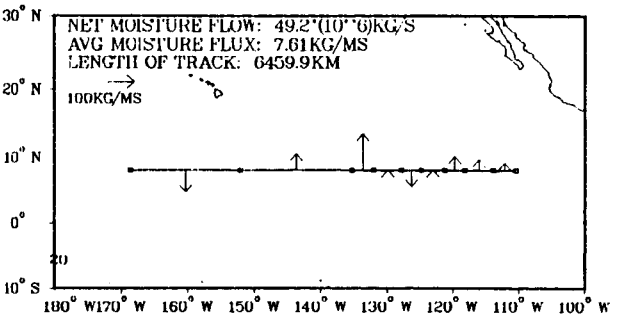

Fig. 1. Meridional component of water vapor flux across 4°N on 20 January 1979 about 21 GMT, computed using dropwindsonde data. Line segments with arrowheads, directed normal to the latitude line are the fluxes, positive to the north, with the segment length proportional to the flux across a 1 meter portion of the latitude circle. Note the inserted flux scale.

toward the north.

The second moisture burst was initiated the morning of the 25th near 140°W. The water vapor flows across 4°N several hours before the initiation are given in Fig. 2. The flows were either near zero (true for most of the line) or toward the south near the point of initiation and even more strongly toward the south at the west end of the section.

A day later, on the afternoon of the 25th, by which time the moisture burst was well established, the moisture transports (Fig. 3) had changed significantly. While the fluxes were small for most of the section, the places of large flow had shifted position and direction radically. Flux in the vicinity of the burst was toward the north, thus changing direction 180°, while the southerly flux had disappeared at the west end of the section and had established itself at the east end.

Still another day later (on the 26th), the flow of moisture in the longitudes of the moisture burst was still from the south (not illustrated), with a flux across a unit width of the section roughly twice that of a day earlier. Flow to the south had been reestablished at the west end (west of 170°W), with near-zero flow between 170 and 145°W and east of 110°W.

By the 28th (Fig. 4), west of 140°W the flow was to the south; east of 140°W there was

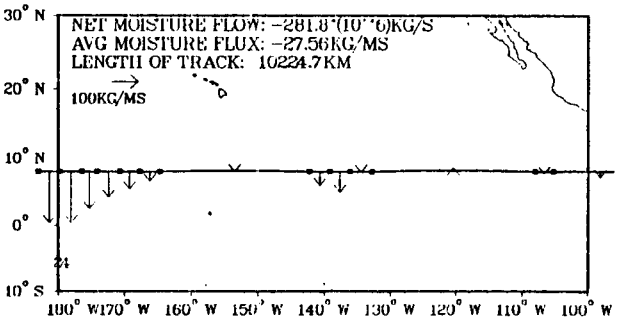

Fig. 2. Same as Fig. 1, but for 24 January 1979 about 21 GMT.

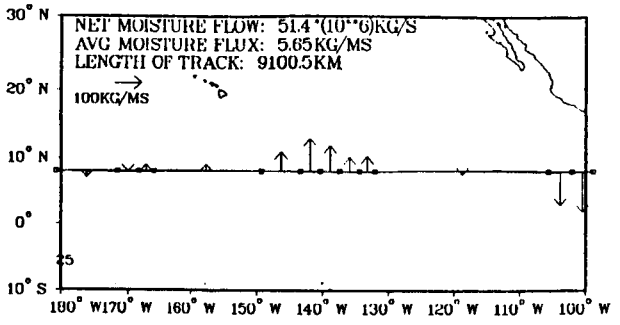

Fig. 3. Same as Fig. 1, but for 25 January 1979 about 21 GMT.

nearly equal flow to the north. The total (net) flow was an order of magnitude less than on the other days.

The water vapor fluxes across 4°N were also calculated based on the analyzed FGGE III-b data. Values of the mapped variables along 4°N (actually 3.75°N) were inserted into the water vapor flux equation. This calculation allowed an estimate of the flux for each map time. The results of calculations for four map times are shown in Fig. 5. The horizontal lines represent distance along 4°N (actually 3.75°N), while the vertical line segments are proportional to the flux across a unit length of the latitude circle.

The top line gives the fluxes for 21 January, 1979; the time corresponds approximately to that of Fig. 1. The fluxes calculated from the III-b analyses were toward the north between 155°W and 130°W, thus about the longitude of the developing moisture burst. West of 155°W they were toward the south. Weak fluxes were present east of 130°W. This pattern is in phase with the fluxes based on the dropwindsonde data (Fig. 1), though the magnitudes do not agree.

By the 25th (Fig. 5b), the fluxes east of 130°W were definitely from the south, while the fluxes near 140°W and near 160°W had dropped to near zero. Other sectors were similar to those of the 21st. Comparison with Fig. 2 shows good agreement west of about 160°W, fluxes of opposite sign near 140°W, and differences of magnitude east of 130°W. Agreement between the two methods is less satisfactory than on the 21st.

Twenty four hours later (Fig. 5c), about the time of the second burst, the fluxes were small west of 150°W and from the south but variable in magnitude east of 150°W. This behavior corresponds

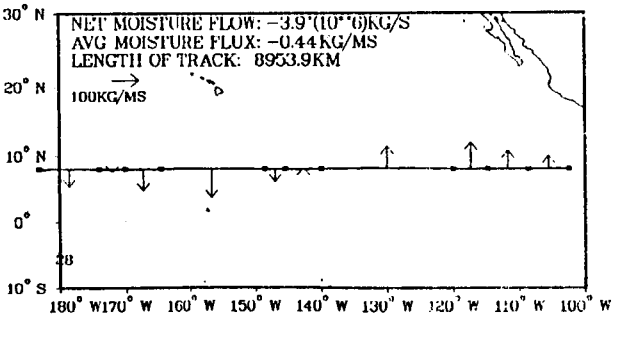

Fig. 4. Same as Fig. 1, but for 28 January 1979 about 21 GMT.

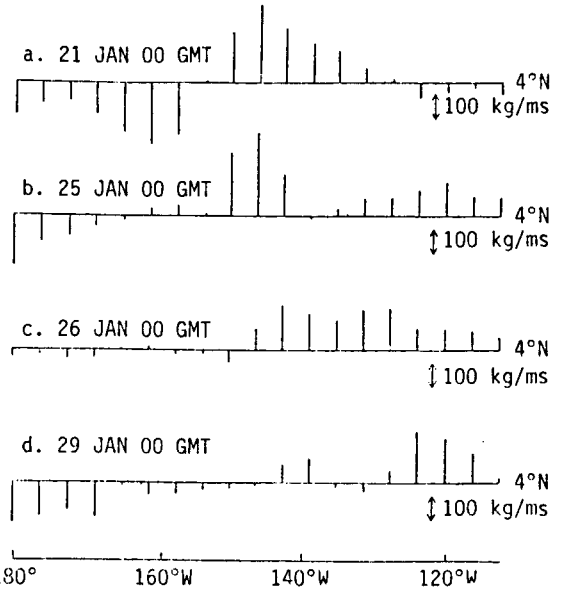

Fig. 5. Meridional component of water vapor flux across 4°N lat. on four days in January 1979, computed using FGGE III-b analyses. Line segments running upward from the base line are fluxes to the north, with the segment length proportional to the flux across a 1 meter portion of the latitude circle. Note the inserted flux scale.

favorably with that determined from the dropwindsonde data (Fig. 3); note though that the calculations represented in Fig. 3 extend significantly east of those represented in Fig. 5.

By the time of the conclusion of the second burst on the 29th (Fig. 5d), fluxes toward the south had increased west of 165°W and fluxes toward the north had increased east of 126°W; the fluxes between tended to be significantly weaker and more variable in direction. By then the moisture burst was dissipating.

4.2 The Lateral Flow from Volumes

Only two examples of the computation of water vapor flow out of volumes are presented. The first is for the afternoon of the 20th (Fig. 6). The moisture burst occurred near the center of the area (or volume) enclosed by the dropwindsonde reports. The representation is the same as

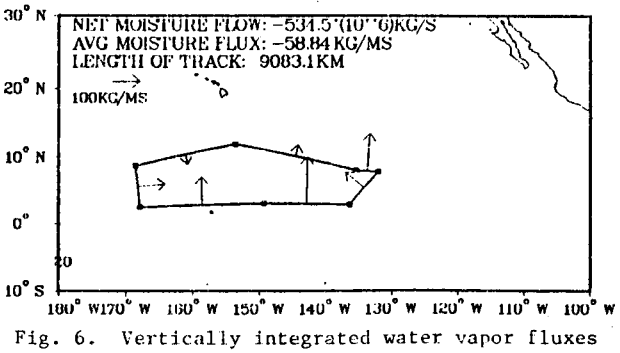

Fig. 6. Vertically integrated water vapor fluxes and net flow across the vertical surfaces of a volume delineated by dropwindsonde observations near 21 GMT on 20 January 1979. The vectors represent the water vapor flux, with magnitude given by the scale at the upper left.

that in earlier figures, except that the direction of the arrow indicates whether the flux is outward (designated as positive) from the volume or inward. An outward net flow is also indicated as positive. The net moisture inflow of 5.3 x 10^8 kg/s probably is related to the convergence of moisture and of mass as the burst undergoes initial development. Computation of the net moisture flow for the same volume, but based on the FGGE III-b data resulted in an inflow of 1.3 x 10^8 kg/s, determined from the 24-h changes in relative humidity over the period from 12 GMT on the 20th to 12 GMT on the 21st. The same computation carried out for a 12-h period ending at 00 GMT on the 21st resulted in an outflow (moisture divergence) of 6.0 x 10^8 kg/s, the same magnitude as, but of opposite sign from the value obtained from the dropwindsonde data.

On the 25th the dropwindsonde positions defined a volume a little smaller than, but in about the same position as on the 20th (Fig. 7). The longitude of the origin of the second moisture burst was near the center of the volume. Despite strong fluxes across short segments of the north boundary surface, the net outflow of 1.0 x 10^6 kg/s was two orders of magnitude less than the inflow on the 20th. Calculations of the volume outflow made using the FGGE III-b data again led to conflicting results: an inflow of 1.1 x 10^8 kg/s when computed over a 24-h period and 2.1 x 10^7 kg/s over a 12-h period, both beginning at 12 GMT on the 25th.

Calculations for other volumes and times show similar inconsistencies when results based on the dropwindsonde data are compared with those based on the FGGE III-b analyses, whether calculated over 12-h or 24-h periods.

5. SUMMARY AND COMMENTS

This paper outlines the results of an attempt to determine moisture fluxes and budgets associated with moisture bursts of the eastern North Pacific Ocean area. The FGGE II-b and III-b data sets provide the basic information. A calculation based on dropwindsonde data and a second result based on FGGE III-b data (the analyses) are discussed and compared. Several conclusions follow:

1. Calculations of water vapor flow across latitude lines probably provide a fair representation of reality, especially when based on the dropwindsonde data. The fluxes across various segments of the latitude circle usually match what would be expected from the synoptic behavior of the atmosphere at the moisture burst.

2. Water vapor flow out of small volumes is not well represented by results from either form of data. The FGGE III-b analyses likely are the poorer data form when synoptic investigations are being undertaken because the numerical analysis procedures utilized tend to be biased toward the climatological structure when data are scarce, as is always the case in the area being investigated.

3. The results also may be biased because of the questionable accuracy of the initial data.

This paper reports a first step of an ongoing study. Our goal is to use moisture data derived from satellite-borne instruments together with the conventional data to improve estimates of water vapor flux and budgets.

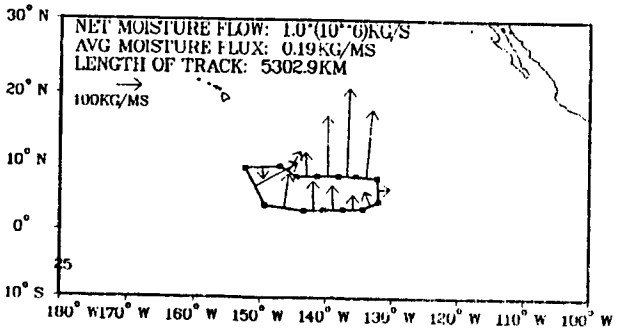

Fig. 7. Same as Fig. 6 but for 16 GMT on 25 January 1979.

6. ACKNOWLEDGEMENTS

Paul Dirmeyer and Lauren Murphy carried out the calculations and designed the figures. The research reported here has been supported by the George C. Marshall Space Flight Center, NASA, under Contract No. NAS8-35182.

7. REFERENCES

Cadet, D., 1983: Mean fields of precipitable water over the Indian Ocean during the 1979 summer monsoon from TIROS-N soundings and FGGE data. Tellus, 35B, 329-345.

Howland, M., and D. Sikdar, 1983: The moisture budget over the northeastern Arabian Sea during premonsoon and monsoon onset, 1979. Mon. Wea. Rev. 111, 2255-2268.

Khalep, M., B. Fitzharris and W. Bardsley, 1984: Water vapor transfer over the southwest Pacific: Mean patterns and variations during wet and dry periods. Mon. Wea. Rev., 112, 1960-1975.

McGuirk, J., L. Anderson and A. Thompson, 1985: Satellite-derived synoptic climatology in data-sparse regions. Avd. Space Res., 5, No. 6, 45-48.

Saha, S., and S. Bavadekar, 1973: Water vapour budget and precipitation over the Arabian Sea during the northern summer. Quart. J. Roy. Meteor. Soc., 99, 273-278.

Smith, N., A. Thompson and J. McGuirk, 1985: Moisture bursts over the tropical Pacific Ocean. Submitted to Mon. Wea. Rev.

Thompson, A., J. McGuirk, L. Anderson and N. Smith, 1984: Analysis of tropical synoptic disturbances using satellite-derived soundings and radiance data from selected channels. Preprints, Conf. on Satellite/Remote Sensing and Applications, Clearwater Beach, FL, Amer. Meteor. Soc., 137-142.

Reprinted from Preprint Volume, Second Conference on Satellite Meteorology/Remote Sensing and Applications, May 13-16, 1986, Williamsburg, VA. Amer. Meteor. Soc. P. 118-122.

TROPICAL SYNOPTIC INTERPRETATION OF INTER-CHANNEL CORRELATIONS FROM TIROS N

J. P. McGuirk, L. L. Anderson, Jr., and A. H. Thompson

Department of Meteorology, Texas A&M University
College Station, TX 77843-3146

1. INTRODUCTION

In the tropical northeast Pacific, a synoptic event, called a "moisture burst," occurs commonly (Smith et al., 1986; McGuirk and Thompson, 1984). The data-sparse nature of the region precludes accurate diagnoses of the structure of these events. The most appropriate data set for the study of these systems is quantitative satellite data, particularly individual channel brightness temperatures. This data format is preferable to the reconstructed temperature and moisture profiles because the reconstructions have a tendency to smooth in both the horizontal and the vertical.

This paper describes synoptic variability contained in a set of TIROS N brightness temperatures for a nine-day period during January 1979, between the dateline and 90°W and between 30°N and 20°S. The spatial coherence of each channel is described as functions of interchannel differences and geographic and synoptic variations. Second, horizontal and vertical patterns of individual channels are examined through empirical orthogonal functional (EOF) decomposition. Finally, response surface regression models are developed to predict missing TIROS N channels from available TIROS N and NOAA-5 data.

All three analyses present considerable organized synoptic variability in tropical systems for which the synoptic thermodynamic signal is normally weak.

2. SPATIAL COHERENCE

To examine the spatial coherence of the brightness temperatures in a given channel, the correlation coefficient was calculated for each observation with respect to all other observations during the same synoptic time and throughout the domain. The correlations were stratified by horizontal separation distance between pairs of observations. Separation distances ranged between zero and 2500 km, in 250 km increments. For nearly all channels and nearly all separation distances, at least 150 pairs of observations contributed to the correlation coefficient for a given time period, yielding a 95% confidence estimate of ±0.1 for the amplitude of the correlation coefficient at any specific separation distance.

2.1 Inter-Channel Differences

A single time period, 24 January 1979 at 12 GMT, was selected to examine the differences in horizontal coherence between the different TIROS N channels. The channels were divided into six groups, based on the absorbing characteristics at the specific wavelength of the channel, as well as the shape of the channel weighting function. The channels of a given group possessed similar coherence properties. See Table 1 for these groups and Smith et al. (1979) for a detailed description of channel characteristics.

Table 1

Channel groupings for spatial correlations.

Emission source	Channel numbers
Tropospheric (thermal)	13, 14, 15, 16
Tropospheric (thermal, H_2O sensitive)	4, 5, 6, 7
Water vapor	10, 11, 12
Stratospheric	1, 2, 3
Surface (window, boundary layer)	8, 13, 14, 18, 19
Microwave (MSU 1, 2, 3, 4) noted as	21, 22, 23, 24

By way of example, Fig. 1a shows the correlation coefficient as a function of separation for the two tropospheric thermal groups. For zero separation, the correlation is 1.0; observations correlate perfectly with themselves. As the separation distance increases, the channel observations become less correlated, as expected. For distances greater than 750 km, the correlation in channels more sensitive to water vapor falls off much more rapidly. These correlation profiles are compared most easily through the integral length scale (the area under the correlation curve to the left of the first zero crossing). This scale provides a single number estimating the mean correlation distance; it should be related to the length scale of atmospheric variation. The maximum difference in integral length scales in Fig. 1a (between Channels 4 and 14) is 650 km (1820 km vs. 1170 km; these are the approximate distances at which two observations in the same channel will become uncorrelated).

Correlations for a typical channel from each of the six groups of Table 1 are shown in Fig. 1b. Prior to interpreting this figure, some exceptions are first noted. The stratospheric channels varied widely in length scale, from about 900 km to well over 2000 km, exceeding the detectable length scale within the observation domain. The same was true of the microwave channels, in

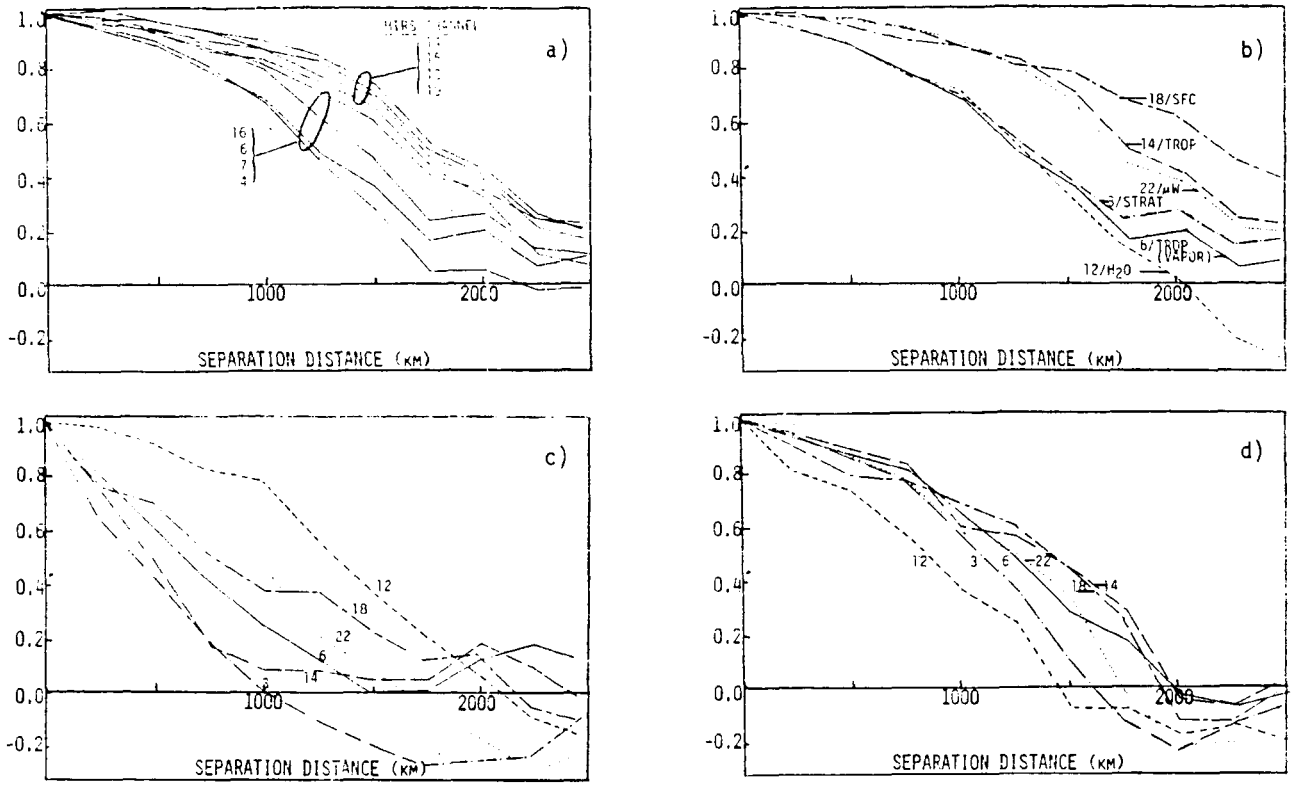

Fig. 1. Individual channel brightness temperature correlation (ordinate) as a function of separation distance between pairs of observations (abscissa). a) For all tropospheric infrared signals and for the entire region. b) For six representative channels and for the entire region. c) As in (b), but for an equatorial strip. d) As in (b), but for a subtropical strip. See text for details and see Table 1 for an explanation of the numbers labeling the several curves.

which unrealistically small length scales occurred in the window and tropopause channels.

Three behaviors appear in Fig. 1b. The highest spatial coherence occurs in surface channels with length scales exceeding 2000 km. Tropospheric signals, insensitive to moisture, possess length scales of about 1800 km, but are nearly identical with surface correlations at distances less than 1300 km. Finally, the stratospheric and moisture sensitive tropospheric channels are similar, with length scales of about 1000 km.

The implication of the first two results is that the scale of the atmospheric system is somewhat larger than the scale of imposed sea surface temperature variation within this part of the tropics. It is likely then that sea surface patterns do not drive directly the most active synoptic systems over the eastern Pacific Ocean.

Connecting the second two results leads to the implication that temperature and humidity variations occur on two diverse scales over the tropical eastern Pacific.

2.2 Geographic Differences

The correlations for each channel were recomputed for two zonal bands, one between 10°S and 15°N (the equatorial section), and the other between 15°N and 30°N (the subtropical section). These subsets, shown in Figs. 1c and 1d, minimize the meridional temperature gradient in two ways: the first separates the tropics from the subtropics, while the second aliases out the north-south separations at scales larger than about 1000 km for each subset. (The distance between 15°N and 30°N is only about 1600 km, so most of the longer separation distances for observations contributing to the correlation coefficient tend to be oriented east-west).

Comparison of Figs. 1b, c and d allow latitudinal differences to be identified. Except for water vapor channels, the apparent scale of tropical systems is reduced in the zonal strips. The integral length scales of the equatorial strip are about 40% of the scales for the entire region. Scales for the subtropical strip are about 75% of scales in Fig. 1b. Thus, for the five channels associated with temperature variation, the dominant variation appears to be associated with the mean meridional temperature gradient. In the equatorial region the integral length scale for tropospheric disturbances is about 600 km. Length scales at the surface are longer, about 850 km. The infrared water vapor channel possesses an integral scale of 1300 km in the equatorial belt, the same as its scale throughout the region. Not only is moisture's coherence about twice as large as that for temperature along the equator, it is not sensitive to meridional variation. In the subtropics, however, the scale of moisture variation is about 750 km, much smaller than equatorial variation. Finally, the scatter in correlation behavior for individual channels within each group is much greater in the equatorial zone than in the other zones.

The first conclusion is that moisture variations are synoptic in nature, and not a result of a mean meridional gradient in moisture. The scale of moisture variation is dominated by

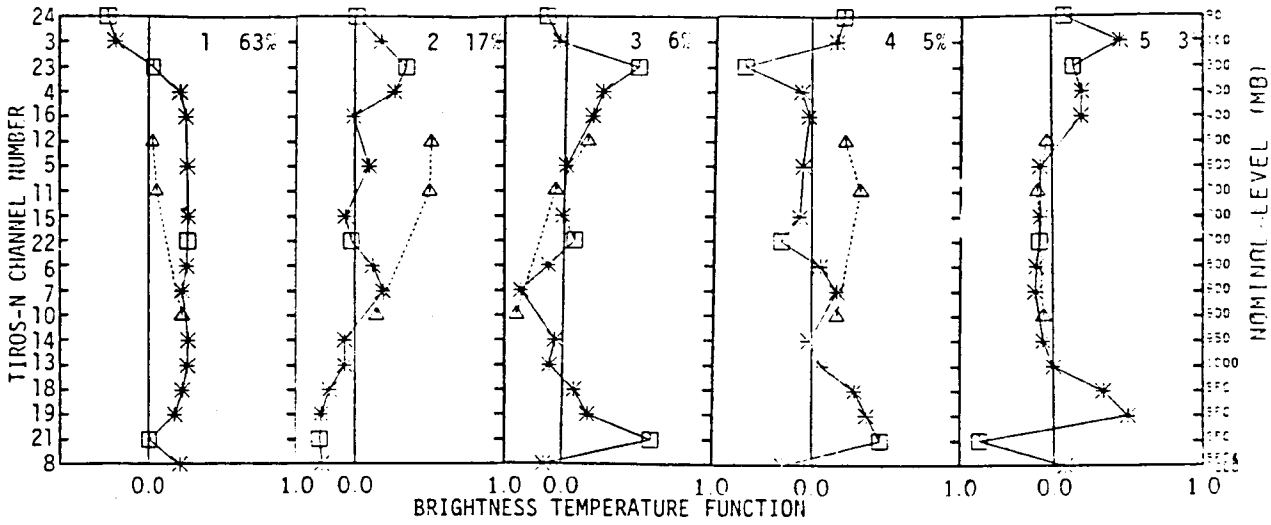

Fig. 2. Eigenvectors of channel brightness temperatures for 23 January 1979 at 00 GMT. The vertical scales are channel number (left) and approximate peak in mb of the weighting function (right). The first eigenvector is at the left and the fifth is at the right. Asterisks are infrared thermal channels, triangles are moisture channels, and squares are microwave channels. The explained variance appears in the upper right hand corner of each individual diagram.

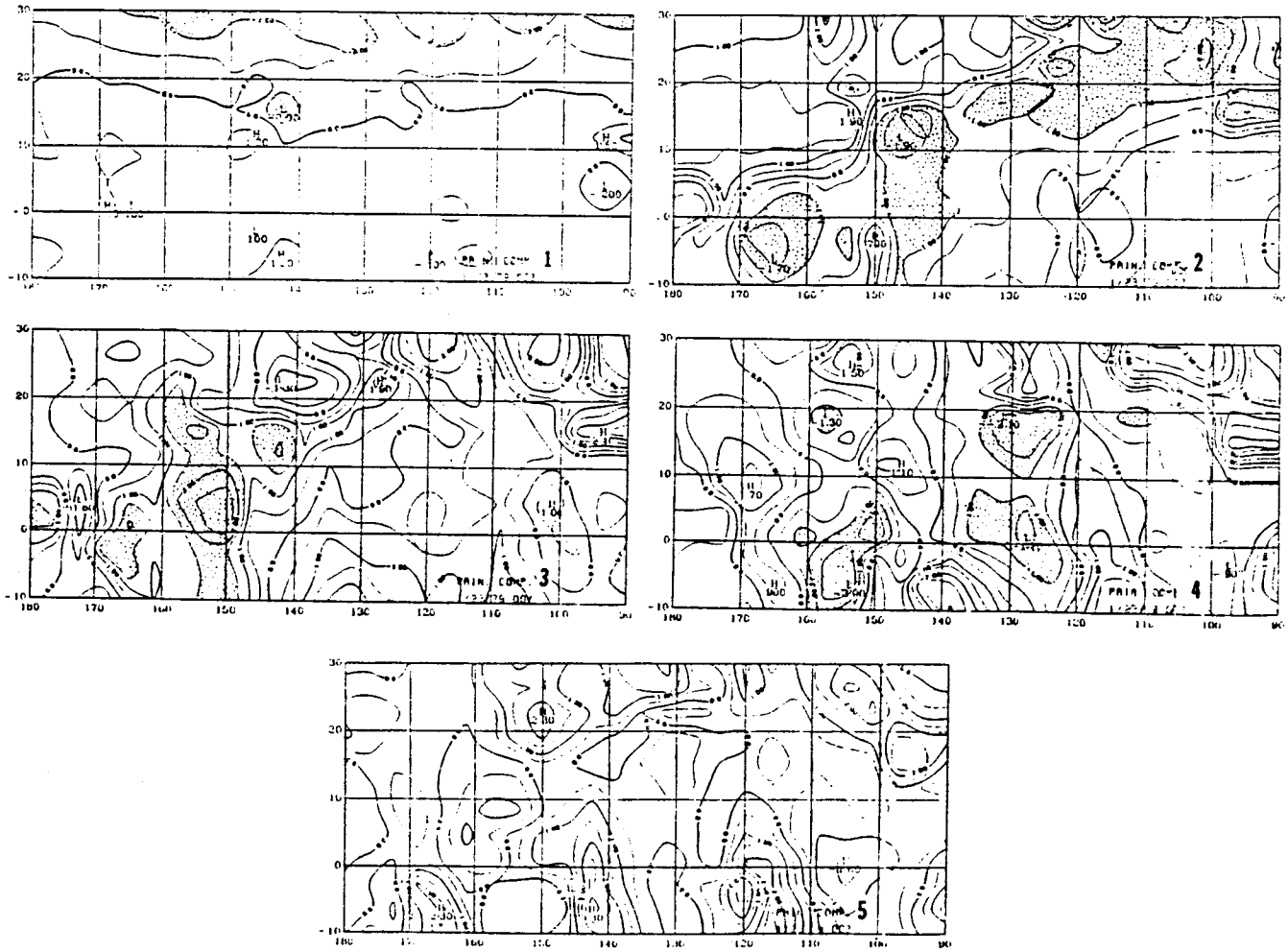

Fig. 3. EOF's, or spatial patterns, for the eigenvectors shown in Fig. 2. Areas shaded for emphasis are explained in the text. The coordinates are latitude (from 10°S to 30°N) and longitude (from 180° to 90°W).

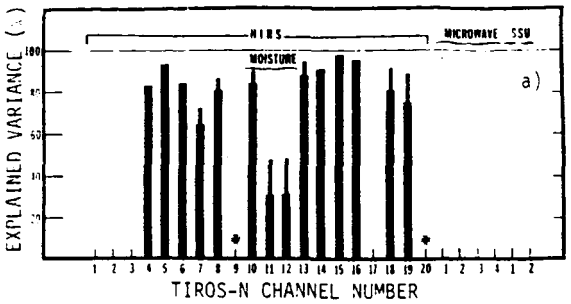

Fig. 4a. Percent variance explained for each TIROS N channel from microwave and stratospheric channels for the same satellite sounding. Heavy lines for linear regression terms; light lines for quadratic regression terms. (not predicted.)*

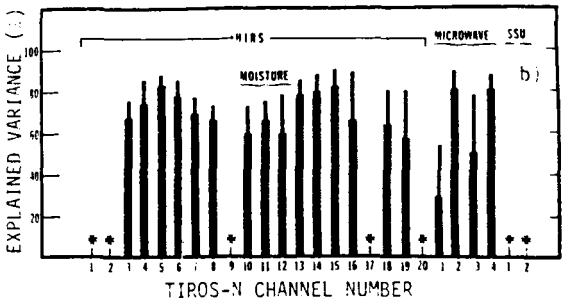

Fig. 4b. As in Fig. 4a, except for prediction from co-located NOAA-6 HIRP channels.

equatorial variation, not by that of the subtropics. On the other hand, temperature variation is controlled strongly by the mean meridional temperature contrast. This contrast occurs primarily in the northern portion of the domain. Equatorial thermal coherance is very small. Finally, the TIROS N moisture channels are truly sensing moisture signals, which vary distinctly from thermal signals, even in the equatorial and subtropical regions.

2.3 Synoptic Differences

Finally correlations were computed for a central Pacific sector between longitudes 140°W and 180° for two different days separated by five days. One day experienced heavy convection along the equatorial section and in the northwest corner of the region. The second day was relatively cloud- and convection-free. In all channels, integral length scales were less for the day with weak synoptic activity, approximately 25% or about 400 km less for the four tropospheric channels of Fig. 1b, including moisture. (The correlation figures are not shown.) The decreases in scale for the surface and stratospheric channels were not significant. The conclusion is that synoptic activity makes the horizontal patterns more coherent and the satellite can detect this organization. The stratosphere and surface do not appear to vary importantly on time scales of a few days.

3. SPATIAL PATTERNS

The horizontal and vertical synoptic patterns in the TIROS channel data were examined through EOF analysis. For a given synoptic time, all the satellite observations over the tropical Pacific region were merged into eigenvectors (vertically-oriented channel brightness temperature patterns) and EOFs (horizontal amplitude patterns of the eigenvectors). EOFs are alternatively called "principal components." This decomposition was done for each synoptic time and the first five eigenvectors for a typical time period appear as Fig. 2. Eigenvector Numbers 3, 4 and 5 varied from day to day, but Eigenvector Numbers 1 and 2 remained stable. Due to a retrival error, the "900 mb moisture signal" is actually a low level thermal signal. Thus, the first eigenvector is unambiguously a mean tropospheric temperature signal, with near zero weight given to the surface microwave signal and the moisture signals. It typically accounts for 60% of the spatial variability of the entire satellite channel data set. The second eigenvector is primarily a moisture signal, accompanied by a weak surface thermal signal; the signs are such that when the troposphere is moist, the boundary layer is warmer than normal. This signal typically explains 15% of the variability. The next three eigenvectors are more complex and less physically interpretable, but typically include large moisture, microwave and surface signals. They can be linked to moisture, cloud, precipitation and surface effects, and typically explain about 5% of the variability each. Thus, the first five EOFs explain over 90% of the variability.

The five EOFs, or principal components, associated with eigenvectors in Fig. 2 are shown in Fig. 3. EOF 1 shows the meridional temperature gradient north of 10°N and the cold trough (cold is shaded) associated with a moisture burst between 150°W and 120°W. EOF 2 shows the moist axis corresponding to the moisture burst (with the wettest areas shaded) and the strong moisture gradient on the northwest flank. Highs in EOF 3 (shaded) generally show contamination by heavy precipitation cores or a warm tropopause. Over land areas surface emissivity dominates the signal. This pattern does not always correspond to cold cloud top temperatures from GOES imagery, suggesting that the GOES signal is not always a good precipitation indicator. EOFs 4 and 5 are more difficult to interpret. They carry a non-meteorological signal along the satellite track in channels MSU 1 and 3, particularly along the equator. This signal has not been discussed in the literature. EOF 4 shows several minima along the burst (shaded), adjusting observations in wet areas which do not have a warm boundary layer. EOF 5, with a warm tropopause and surface, shows a weak maximum along the burst axis.

Most EOF analyses of geophysical data exhibit a gradually decreasing scale in spatial patterns. Except for the first amplitude pattern of mean temperature, the TIROS N data set does not follow this trend. Starting with the moisture pattern, the spatial patterns show a surprising complexity, a result of the atmospheric structure of this portion of the tropics. It is not surprising, then, that the integral length scales of the preceeding section exhibited so much variation or signal.

4. INTERCHANNEL COMPARISONS

Because of regions of missing satellite observations, attempts were made to reconstruct

"bogus" TIROS N channel brightness temperatures from two sources: NOAA-5 (VTPR) observations where no TIROS N observations were available; and TIROS N microwave and stratospheric channels for cloudy/overcast conditions where tropospheric infrared channels were not available. The procedure was statistical, involving a full quadratic response surface regression model.

For the bogus data generated from TIROS N data in cloudy regions, the tropospheric IR channels were predicted by regression, using the available TIROS data (MSU 1, 2, 3, 4; SSU 1, 2; HIRS 1, 2, 3, 17). The model was constructed using over 2500 complete soundings available in clear sky conditions. The model was then applied to overcast regions.

In an analogous model, NOAA-5 VTPR channel data were regressed to predict TIROS N channel brightness temperature. The model was constructed with clear sky TIROS and NOAA soundings colocated within 500 km in space, and 3 hours in time; only 300 colocated soundings were available for model construction.

Figs. 4a and b depict the percentage variance predicted in each channel from the TIROS N microwave and stratospheric channels, and from the NOAA-5 channels, respectively. The heavy lines show the linear terms; the light lines give the improvement by including quadratic terms. Improvements by quadratic terms in excess of 10% were limited to only a few channels in the NOAA-5 model. NOAA-5 predictions were only slightly less accurate due primarily to time and space extrapolation and to the degraded observing capability of the deteriorating NOAA satellite. Generally speaking, about 85% of the variance in each channel can be predicted for the TIROS model, excepting the two tropospheric moisture channels, where prediction is less successful. About 80% of the variance is recovered by the NOAA model, except for the microwave window channel. Because NOAA-5 infrared channels are sensitive to water vapor, their prediction of moisture in clear sky conditions was more successful; since they are, however, all infrared, they will provide no new moisture information in cloudy regions.

5. SUMMARY

Individual channels of TIROS N vary on their own integral length scales. The variation is sensitive to absorber (particularly water vapor and precipitation), to mean meridional atmospheric gradients, and to synoptic signal. This length scale variation, and the strong channel interdependence allow TIROS N channel brightness temperatures to be merged into a few vertical/horizontal structures through EOF analysis. The vertical eigenfunctions and horizontal EOFs can be interpreted synoptically. Finally, the strong channel inter-dependence allows "bogus" channel data to be constructed from partial channel soundings or from different satellites carrying different instruments; however, water vapor channels will remain poorly predicted in cloudy regions.

6. ACKNOWLEDGEMENTS

Paul Dirmeyer, Donna Woolley and Mark Chambers prepared data and figures. The research reported here is supported by the George C. Marshall Space Flight Center, NASA, under Contract No. NAS8-35182.

7. REFERENCES

McGuirk, J. P., and A. H. Thompson, 1984: Transient tropical disturbances within the Pacific Hadley cell. Postprints, 15th Conf. Hurricanes and Tropical Meteor. Miami, Amer. Meteor. Soc., 249-254.

Smith, N. R., A. H. Thompson and J. P. McGuirk, 1986: Moisture bursts over the tropical Pacific Ocean. Paper submitted to Mon. Wea. Rev.

Smith, W. L., H. M. Woolf, C. M. Hayden, D. Q. Wark and L. M. McMillin, 1979: The TIROS-N operational vertical sounder. Bull. Amer. Meteor. Soc., 60, 1177-1187.

1. REPORT NO.	2. GOVERNMENT ACCESSION NO.	3. RECIPIENT'S CATALOG NO.
NASA CR-4092		

4. TITLE AND SUBTITLE	5. REPORT DATE
Application of Satellite Data to Tropic/Subtropic Moisture Coupling	September 1987
	6. PERFORMING ORGANIZATION CODE
7. AUTHOR(S)	8. PERFORMING ORGANIZATION REPORT #
Aylmer H. Thompson and James P. McGuirk	
9. PERFORMING ORGANIZATION NAME AND ADDRESS	10. WORK UNIT NO.
Texas A&M University College of Geosciences College Station, Texas 77843-3146	M-569
	11. CONTRACT OR GRANT NO.
	NAS8-35182
12. SPONSORING AGENCY NAME AND ADDRESS	13. TYPE OF REPORT & PERIOD COVERED
National Aeronautics and Space Administration Washington, D.C. 20546	Final Contractor Report April 1983 - July 1987
	14. SPONSORING AGENCY CODE

15. SUPPLEMENTARY NOTES

Contract Monitor: John W. Kaufman, Earth Sciences And Application Division, Structures and Dynamics Laboratory, Science and Engineering, Marshall Space Flight Center, Alabama 35812

16. ABSTRACT

Common tropical synoptic events, called moisture bursts, have been defined in terms of their appearance in infrared satellite imagery. Their synoptic and climatological behavior over the tropical North Pacific Ocean has been described, using data over four cool seasons including the 1982-83 El Nino winter, and during the FGGE Special Observing Periods of January and May 1979. Moisture bursts act as transient amplifications of the Hadley cell, and are infrequent when the ITCZ is active; many synoptic features--midlatitude troughs, the subtropical jetstream, tropical waves--are linked to moisture bursts. Because of a severe lack of data, the information content of TIROS N channel radiance data were evaluated and implemented in the synoptic study. Numerous comparisons with in situ observations qualified the satellite data as equivalent to, but different from, classifical observations; the satellite data were then used to verify the quality of gridded analyses, particularly moisture fields, which were almost entirely model generated output. Eigenfunction decomposition of TIROS radiance profiles resulted in identifying five meaningful vertical patterns: the first two (accounting for 80% of the variance) describe tropospheric mean temperature and tropospheric moisture content; the remaining three relate to cloud/hydrometeor effects. Statistical regression from NOAA 5 and partial TIROS soundings allowed the construction of radiance fields in some cloudy and otherwise data void regions. These techniques and data allowed the detection of much synoptic detail of moisture bursts.

17. KEY WORDS	18. DISTRIBUTION STATEMENT
Moisture Bursts Tropical Moisture Satellite Moisture Observations Tropospheric Moisture Content NOAA 5 and TIROS Data	Unclassified - Unlimited Subject Category: 47

19. SECURITY CLASSIF. (of this report)	20. SECURITY CLASSIF. (of this page)	21. NO. OF PAGES	22. PRICE
Unclassified	Unclassified	118	A06

MSFC - Form 3292 (Rev. December 1972)

For sale by National Technical Information Service, Springfield, Virginia 22161

NASA-Langley, 1987